

**CORROSION INHIBITION EFFECT OF SOME NATURAL  
PRODUCTS ON MILD STEEL IN ACIDIC MEDIUM**

A

Thesis

Submitted to



For the award of

**DOCTOR OF PHILOSOPHY (Ph.D.)**

in

**CHEMISTRY**

By

**AKHIL SAXENA**

**11512280**

Supervised By

**Dr. DWARIKA PRASAD**

**LOVELY FACULTY OF TECHNOLOGY AND SCIENCES**

**LOVELY PROFESSIONAL UNIVERSITY**

**PUNJAB**

**2018**

## DECLARATION

I hereby declare that this Ph.D. thesis entitled “**Corrosion Inhibition Effect of Some Natural Products on Mild steel in Acidic Medium**” was carried out by me for the degree of Doctor of Philosophy in Chemistry under the guidance of Dr. Dwarika Prasad, Associate Professor, Department of Chemistry, Lovely Professional University Punjab, India.

I declare that this thesis has been composed solely by me and that it has not been submitted in whole or part in any previous application for a degree.

Date:

Akhil Saxena

Place:

Reg. No.: 11512280

## CERTIFICATE

This is to certify that the thesis entitled “**Corrosion Inhibition Effect of Some Natural Products on Mild steel in Acidic Medium**” submitted for the award of the degree of **Doctor of Philosophy in Chemistry** to Lovely Professional University Punjab, India is a record of bonafide research work carried out by **Mr. Akhil Saxena** under my guidance. To the best of my knowledge, the thesis has not been previously submitted elsewhere for the award of any other degree, diploma or distinction of any kind anywhere before.

Dr. Dwarika Prasad

Department of Chemistry

Lovely Professional University Punjab, India

## ABSTRACT

The thesis entitled “**Corrosion Inhibition Effect of Some Natural Products on Mild Steel in Acidic Medium**” deals with the study of efficient corrosion inhibitors and their testing on mild steel in 0.5 M H<sub>2</sub>SO<sub>4</sub> solution by using different techniques. Corrosion is an irreversible interfacial reaction of the material with its environment, which results in consumption or dissolution of the material. Corrosion is basically an economic problem associated closely with the loss of capital assets and business profits. Corrosion control should, therefore, provide the most advantageous course of avoiding such losses.

Most broadly utilized alloy in the modern process, creation and development is mild steel because of its skillful mechanical competency, simple accessibility and the most vital its low generation cost. Acid assault on steel surface prompts corrosion issues. To reduce the aggressive corrosion of mild steel, inhibitors are added to the acid solution. The effective corrosion inhibitors that are usually found in commercial formulations are acetylenic alcohols, alkenyl phenones, aromatic aldehydes and condensation products of carbonyls and amines. These inhibitors are very costly, effective only at high concentrations and they are harmful to the environment, so it is important to search for new low cost, eco-friendly and effective corrosion inhibitors for mild steel.

Plant extract, a sort of natural products, constitute an extensive class of corrosion inhibitors since they are effectively accessible and non-lethal. The phytochemical constituents like phenolic compounds, flavonoids and polysaccharide, enrich plant extract with the capability of repressing the corrosion procedure of mild steel. Most by far of the natural products containing functional groups like NH<sub>2</sub>, CO and CHO are known to be effective inhibitors. These compounds get adsorbed on the metal surface to form a protective layer. The flowers, leaves, seeds and roots of different plants have been examined by a few researchers as corrosion inhibitors.

The purpose of the present study is to investigate the corrosion behavior of mild steel in 0.5 M H<sub>2</sub>SO<sub>4</sub> solution in the absence and presence of different inhibitors of plant extracts at different concentrations and temperatures. To understand the inhibition mechanism,

Langmuir adsorption isotherm was evaluated for tested inhibitors on the basis of weight loss measurements. Potentiodynamic polarization experiments were carried out to investigate the preferential activeness of the inhibitors towards cathodic and anodic areas of the metal surface. Electrochemical impedance spectroscopy (EIS) was used to calculate the charge transfer resistance. Surface morphology of the exposed metal surface was analyzed by scanning electron microscopy (SEM) and atomic force microscopy (AFM) techniques. DFT method was employed for quantum chemical calculations. The thesis comprises of **four chapters**.

## **Chapter 1**

In chapter 1, some fundamental aspects of corrosion and corrosion prevention, an economic impact of corrosion and a comprehensive review of literature to the utilization of different inhibitors for corrosion of mild steel in different acid medium has been described. This chapter also presents methods of corrosion control, the importance of inhibitors, mechanistic views of corrosion inhibition, parameters affecting corrosion inhibition efficiency such as inhibitors concentration and temperature and objectives of the present study.

## **Chapter 2**

Chapter 2 describes the experimental procedures as well as techniques used for corrosion study of mild steel in 0.5 M H<sub>2</sub>SO<sub>4</sub> solution. The weight loss experiments were carried out in the temperature range of 298 K-318 K for different inhibitor concentrations. The experimental setup for potentiodynamic polarization measurements and electrochemical impedance spectroscopy studies of the mild steel in 0.5 M H<sub>2</sub>SO<sub>4</sub> solution in the absence and presence of inhibitors were described. The corrosion current density was calculated by using Tafel extrapolation method. In electrochemical impedance spectroscopy studies, Nyquist plots and Bode plots were discussed and impedance data such as charge transfer resistance ( $R_{ct}$ ) and constant phase element (CPE) were obtained. FTIR study was used to confirm the presence of heteroatoms. SEM and AFM techniques have been described to

analyze the inhibitor film formed on the metal surface. DFT is used to calculate the quantum chemical parameters such as energies of the highest occupied and lowest unoccupied molecular orbitals ( $E_{\text{HOMO}}$  and  $E_{\text{LUMO}}$ ) and the energy gap ( $\Delta E$ ), to discuss the mechanism of corrosion inhibition of mild steel in 0.5 M  $\text{H}_2\text{SO}_4$  solution.

### **Chapter 3**

Chapter 3 has been divided into seven parts (3.1 to 3.7). This chapter presents the corrosion inhibition studies of selected plants namely *Saraca ashoka*, *Cuscuta reflexa*, *Achyranthes aspera*, *Piper nigrum*, *Trachyspermum ammi*, *Syzygium aromaticum* and *Asparagus racemosus* on mild steel in 0.5 M  $\text{H}_2\text{SO}_4$  solution.

### **Chapter 4**

Summary and Conclusions: This chapter consists of the salient features, the main findings, the important conclusions and the comparative analysis during the present investigation.

## **ACKNOWLEDGEMENT**

I would like to express my deepest gratitude and respect to my guide Dr. Dwarika Prasad, Associate Professor, Department of Chemistry, Lovely Professional University, Punjab. Without his exceptional guidance, constant support and valuable suggestions and supervision this research could have been completed. He always extended me a helping hand in all phases of my work even at odd hours despite his other important preoccupations. Working under his supervision has been a real journey towards enlightenment.

I would like to express my sincere thanks to Prof. Gurmeet Singh Ex. Head, Department of Chemistry, University of Delhi, for his open-handed generous help, all providing me necessary experimental facilities during the progress of my research work. I would like to express my sincere thanks to all my colleague research scholars.

Lastly and most importantly, I would like to thank my parents and family members for their love, support, encouragement and care.

Akhil Saxena

## Table of Contents

S. No.	Title	Page No.
1.	Declaration	i
2.	Certificate	ii
3.	Abstract	iii
4.	Acknowledgement	vi
5.	Table of Contents	vii
6.	List of Tables	ix-xi
7.	List of Figures	xii-xv
8.	List of Appendices	xvi
Chapter 1		1-13
Introduction and Review of Literature		
Objectives		13
References		14-19
Chapter 2		20-28
Materials and Methods		
References		29-32
Chapter 3		
Results and Discussion		
Section 1	Corrosion inhibition and adsorption activities of <i>Saraca ashoka</i> extract.	34-44



Section 2	Corrosion inhibition and adsorption activities of <i>Cuscuta reflexa</i> extract.	45-55
Section 3	Corrosion inhibition and adsorption activities of <i>Achyranthes aspera</i> extract.	56-66
Section 4	Corrosion inhibition and adsorption activities of <i>Piper nigrum</i> extract.	67-77
Section 5	Corrosion inhibition and adsorption activities of <i>Trachyspermum ammi</i> extract.	78-88
Section 6	Corrosion inhibition and adsorption activities of <i>Syzygium aromaticum</i> extract.	89-99
Section 7	Corrosion inhibition and adsorption activities of <i>Asparagus racemosus</i> extract.	100-110
References		111-112
Summary and Conclusions		114-115
List of Publications		116

### List of Tables

Table No.	Title	Page No.
3.1.1	The data of weight loss for mild steel in 0.5 M H <sub>2</sub> SO <sub>4</sub> without and with different concentrations of <i>Saraca ashoka</i> extract.	35
3.1.2	Adsorption parameters for mild steel in 0.5 M H <sub>2</sub> SO <sub>4</sub> at optimum concentration of <i>Saraca ashoka</i> inhibitor.	36
3.1.3	Polarization parameters for mild steel in 0.5 M H <sub>2</sub> SO <sub>4</sub> without and with different concentrations of <i>Saraca ashoka</i> extract.	38
3.1.4	EIS parameters for mild steel in 0.5 M H <sub>2</sub> SO <sub>4</sub> without and with different concentrations of <i>Saraca ashoka</i> extract.	41
3.1.5	Quantum chemical parameters of Epicatechin calculated with DFT method.	44
3.2.1	The data of weight loss for mild steel in 0.5 M H <sub>2</sub> SO <sub>4</sub> without and with different concentrations of <i>Cuscuta reflexa</i> extract.	46
3.2.2	Adsorption parameters for mild steel in 0.5 M H <sub>2</sub> SO <sub>4</sub> at optimum concentration of <i>Cuscuta reflexa</i> inhibitor.	46
3.2.3	Polarization parameters for mild steel in 0.5 M H <sub>2</sub> SO <sub>4</sub> without and with different concentrations of <i>Cuscuta reflexa</i> extract.	49
3.2.4	EIS parameters for mild steel in 0.5 M H <sub>2</sub> SO <sub>4</sub> without and with different concentrations of <i>Cuscuta reflexa</i> extract.	51
3.2.5	Quantum chemical parameters of 3-methoxy-3,4,5,7 tetrahydroxy flavone calculated with DFT method.	55
3.3.1	The data of weight loss for mild steel in 0.5 M H <sub>2</sub> SO <sub>4</sub> without and with different concentrations of <i>Achyranthes aspera</i> extract.	57
3.3.2	Adsorption parameters for mild steel in 0.5 M H <sub>2</sub> SO <sub>4</sub> at optimum concentration of <i>Achyranthes aspera</i> inhibitor.	58

3.3.3	Polarization parameters for mild steel in 0.5 M H <sub>2</sub> SO <sub>4</sub> without and with different concentrations of <i>Achyranthes aspera</i> extract.	60
3.3.4	EIS parameters for mild steel in 0.5 M H <sub>2</sub> SO <sub>4</sub> without and with different concentrations of <i>Achyranthes aspera</i> extract.	62
3.3.5	Quantum chemical parameters of Oleanolic acid calculated with DFT method.	66
3.4.1	The data of weight loss for mild steel in 0.5 M H <sub>2</sub> SO <sub>4</sub> without and with different concentrations of <i>Piper nigrum</i> extract.	68
3.4.2	Adsorption parameters for mild steel in 0.5 M H <sub>2</sub> SO <sub>4</sub> at optimum concentration of <i>Piper nigrum</i> inhibitor.	69
3.4.3	Polarization parameters for mild steel in 0.5 M H <sub>2</sub> SO <sub>4</sub> without and with different concentrations of <i>Piper nigrum</i> extract.	71
3.4.4	EIS parameters for mild steel in 0.5 M H <sub>2</sub> SO <sub>4</sub> without and with different concentrations of <i>Piper nigrum</i> extract.	73
3.4.5	Quantum chemical parameters of Retrofractamide A and Dehydropiperonaline calculated with DFT method.	77
3.5.1	The data of weight loss for mild steel in 0.5 M H <sub>2</sub> SO <sub>4</sub> without and with different concentrations of <i>Trachyspermum ammi</i> extract.	79
3.5.2	Adsorption parameters for mild steel in 0.5 M H <sub>2</sub> SO <sub>4</sub> at optimum concentration of <i>Trachyspermum ammi</i> inhibitor.	80
3.5.3	Polarization parameters for mild steel in 0.5 M H <sub>2</sub> SO <sub>4</sub> without and with different concentrations of <i>Trachyspermum ammi</i> extract.	82
3.5.4	EIS parameters for mild steel in 0.5 M H <sub>2</sub> SO <sub>4</sub> without and with different concentrations of <i>Trachyspermum ammi</i> extract.	84
3.5.5	Quantum chemical parameters of Thymol and $\alpha$ Terpineol calculated with DFT method.	88

3.6.1	The data of weight loss for mild steel in 0.5 M H <sub>2</sub> SO <sub>4</sub> without and with different concentrations of <i>Syzygium aromaticum</i> extract.	90
3.6.2	Adsorption parameters for mild steel in 0.5 M H <sub>2</sub> SO <sub>4</sub> at optimum concentration of <i>Syzygium aromaticum</i> inhibitor.	91
3.6.3	Polarization parameters for mild steel in 0.5 M H <sub>2</sub> SO <sub>4</sub> without and with different concentrations of <i>Syzygium aromaticum</i> extract.	93
3.6.4	EIS parameters for mild steel in 0.5 M H <sub>2</sub> SO <sub>4</sub> without and with different concentrations of <i>Syzygium aromaticum</i> extract.	95
3.6.5	Quantum chemical parameters of Eugenol and Eugenol acetate calculated with DFT method.	99
3.7.1	The data of weight loss for mild steel in 0.5 M H <sub>2</sub> SO <sub>4</sub> without and with different concentrations of <i>Asparagus racemosus</i> extract.	101
3.7.2	Adsorption parameters for mild steel in 0.5 M H <sub>2</sub> SO <sub>4</sub> at optimum concentration of <i>Asparagus racemosus</i> inhibitor.	102
3.7.3	Polarization parameters for mild steel in 0.5 M H <sub>2</sub> SO <sub>4</sub> without and with different concentrations of <i>Asparagus racemosus</i> extract.	104
3.7.4	EIS parameters for mild steel in 0.5 M H <sub>2</sub> SO <sub>4</sub> without and with different concentrations of <i>Asparagus racemosus</i> extract.	106
3.7.5	Quantum chemical parameters of Sarsasapogenin calculated with DFT method.	110

## List of Figures

Figure No.	Title	Page No.
2.1	A Typical plot of $C/\theta$ against C	23
2.2	Equivalent circuit of constant phase element	25
2.3	SEM and AFM images of abraded mild steel and mild steel immersed in 0.5 M H <sub>2</sub> SO <sub>4</sub>	26-27
3.1	Chemical structure of Epicatechin	34
3.1.1	Langmuir adsorption isotherm for <i>Saraca ashoka</i> extract on mild steel in 0.5 M H <sub>2</sub> SO <sub>4</sub>	36
3.1.2	Tafel polarization curves for mild steel in 0.5 M H <sub>2</sub> SO <sub>4</sub> without and with different concentrations of <i>Saraca ashoka</i> extract	37
3.1.3	Nyquist and Bode plots for mild steel in 0.5 M H <sub>2</sub> SO <sub>4</sub> without and with different concentrations of <i>Saraca ashoka</i> extract	39-40
3.1.4	FTIR spectrum of <i>Saraca ashoka</i> extract	42
3.1.5	UV spectra of <i>Saraca ashoka</i> extract before and after the corrosion test	43
3.1.6	SEM and AFM images of mild steel immersed in 0.5 M H <sub>2</sub> SO <sub>4</sub> in the presence of <i>Saraca ashoka</i> extract	44
3.1.7	The optimized structure, HOMO and LUMO distribution for Epicatechin	44
3.2	Chemical structure of 3-methoxy-3,4,5,7 tetrahydroxy flavone	45
3.2.1	Langmuir adsorption isotherm for <i>Cuscuta reflexa</i> extract on mild steel in 0.5 M H <sub>2</sub> SO <sub>4</sub>	47
3.2.2	Tafel polarization curves for mild steel in 0.5 M H <sub>2</sub> SO <sub>4</sub> without and with different concentrations of <i>Cuscuta reflexa</i> extract	48

3.2.3	Nyquist and Bode plots for mild steel in 0.5 M H <sub>2</sub> SO <sub>4</sub> without and with different concentrations of <i>Cuscuta reflexa</i> extract	50-51
3.2.4	FTIR spectrum of <i>Cuscuta reflexa</i> extract	52
3.2.5	UV spectra of <i>Cuscuta reflexa</i> extract before and after the corrosion test	53
3.2.6	SEM and AFM images of mild steel immersed in 0.5 M H <sub>2</sub> SO <sub>4</sub> in the presence of <i>Cuscuta reflexa</i> extract	54
3.2.7	The optimized structure, HOMO and LUMO distribution for 3-methoxy-3,4,5,7 tetrahydroxy flavone	54
3.3	Chemical structure of Oleanolic acid	56
3.3.1	Langmuir adsorption isotherm for <i>Achyranthes aspera</i> extract on mild steel in 0.5 M H <sub>2</sub> SO <sub>4</sub>	58
3.3.2	Tafel polarization curves for mild steel in 0.5 M H <sub>2</sub> SO <sub>4</sub> without and with different concentrations of <i>Achyranthes aspera</i> extract	59
3.3.3	Nyquist and Bode plots for mild steel in 0.5 M H <sub>2</sub> SO <sub>4</sub> without and with different concentrations of <i>Achyranthes aspera</i> extract	61-62
3.3.4	FTIR spectrum of <i>Achyranthes aspera</i> extract	63
3.3.5	UV spectra of <i>Achyranthes aspera</i> extract before and after the corrosion test	64
3.3.6	SEM and AFM images of mild steel immersed in 0.5 M H <sub>2</sub> SO <sub>4</sub> in the presence of <i>Achyranthes aspera</i> extract	65
3.3.7	The optimized structure, HOMO and LUMO distribution for Oleanolic acid	65
3.4	Chemical structure of Retrofractamide A and Dehydropiperonaline.	67
3.4.1	Langmuir adsorption isotherm for <i>Piper nigrum</i> extract on mild steel in 0.5 M H <sub>2</sub> SO <sub>4</sub>	69

3.4.2	Tafel polarization curves for mild steel in 0.5 M H <sub>2</sub> SO <sub>4</sub> without and with different concentrations of <i>Piper nigrum</i> extract	70
3.4.3	Nyquist and Bode plots for mild steel in 0.5 M H <sub>2</sub> SO <sub>4</sub> without and with different concentrations of <i>Piper nigrum</i> extract	72-73
3.4.4	FTIR spectrum of <i>Piper nigrum</i> extract	74
3.4.5	UV spectra of <i>Piper nigrum</i> extract before and after the corrosion test	75
3.4.6	SEM and AFM images of mild steel immersed in 0.5 M H <sub>2</sub> SO <sub>4</sub> in the presence of <i>Piper nigrum</i> extract	76
3.4.7	The optimized structure, HOMO and LUMO distribution for Retrofractamide A and Dehydropiperonaline.	76-77
3.5	Chemical structures of Thymol and $\alpha$ Terpineol.	78
3.5.1	Langmuir adsorption isotherm for <i>Trachyspermum ammi</i> extract on mild steel in 0.5 M H <sub>2</sub> SO <sub>4</sub>	80
3.5.2	Tafel polarization curves for mild steel in 0.5 M H <sub>2</sub> SO <sub>4</sub> without and with different concentrations of <i>Trachyspermum ammi</i> extract	81
3.5.3	Nyquist and Bode plots for mild steel in 0.5 M H <sub>2</sub> SO <sub>4</sub> without and with different concentrations of <i>Trachyspermum ammi</i> extract	83-84
3.5.4	FTIR spectrum of <i>Trachyspermum ammi</i> extract	85
3.5.5	UV spectra of <i>Trachyspermum ammi</i> extract before and after the corrosion test	86
3.5.6	SEM and AFM images of mild steel immersed in 0.5 M H <sub>2</sub> SO <sub>4</sub> in the presence of <i>Trachyspermum ammi</i> extract	87
3.5.7	The optimized structure, HOMO and LUMO distribution for Thymol and $\alpha$ Terpineol.	87-88
3.6	Chemical structures of Eugenol and Eugenol acetate	89

3.6.1	Langmuir adsorption isotherm for <i>Syzygium aromaticum</i> extract on mild steel in 0.5 M H <sub>2</sub> SO <sub>4</sub>	91
3.6.2	Tafel polarization curves for mild steel in 0.5 M H <sub>2</sub> SO <sub>4</sub> without and with different concentrations of <i>Syzygium aromaticum</i> extract	92
3.6.3	Nyquist and Bode plots for mild steel in 0.5 M H <sub>2</sub> SO <sub>4</sub> without and with different concentrations of <i>Syzygium aromaticum</i> extract	94-95
3.6.4	FTIR spectrum of <i>Syzygium aromaticum</i> extract	96
3.6.5	UV spectra of <i>Syzygium aromaticum</i> extract before and after the corrosion test	97
3.6.6	SEM and AFM images of mild steel immersed in 0.5 M H <sub>2</sub> SO <sub>4</sub> in the presence of <i>Syzygium aromaticum</i> extract	98
3.6.7	The optimized structure, HOMO and LUMO distribution for Eugenol and Eugenol acetate	98-99
3.7	Chemical structures of Sarsasapogenin	100
3.7.1	Langmuir adsorption isotherm for <i>Asparagus racemosus</i> extract on mild steel in 0.5 M H <sub>2</sub> SO <sub>4</sub>	102
3.7.2	Tafel polarization curves for mild steel in 0.5 M H <sub>2</sub> SO <sub>4</sub> without and with different concentrations of <i>Asparagus racemosus</i> extract	103
3.7.3	Nyquist and Bode plots for mild steel in 0.5 M H <sub>2</sub> SO <sub>4</sub> without and with different concentrations of <i>Asparagus racemosus</i> extract	105-106
3.7.4	FTIR spectrum of <i>Asparagus racemosus</i> extract	107
3.7.5	UV spectra of <i>Asparagus racemosus</i> extract before and after the corrosion test	108
3.7.6	SEM and AFM images of mild steel immersed in 0.5 M H <sub>2</sub> SO <sub>4</sub> in the presence of <i>Asparagus racemosus</i> extract	109
3.7.7	The optimized structure, HOMO and LUMO distribution for Sarsasapogenin	109



## List of Appendices

CR	- Corrosion rate
$\Theta$	- Surface coverage
$\eta$	- Efficiency
c	- Concentration
$K_{\text{ads}}$	- Adsorption equilibrium constant
$E_{\text{corr}}$	- Corrosion potential
$I_{\text{corr}}$	- Corrosion current density
$\beta_a$	- Anodic Tafel slope
$\beta_c$	- Cathodic Tafel slope
$R_{\text{ct}}$	- Charge transfer resistance
CPE	- Capacitance
$\Delta E$	- Energy gap between HOMO and LUMO

**Chapter 1**  
**Introduction**

## **1.1 Introduction to corrosion**

Corrosion is an unwanted phenomenon that destroys the brightness and perfection of the materials and diminishes their life. Corrosion is the deterioration of metals arising from the interaction of metals with their surroundings. It is a consistent issue, often can't be discarded completely. Prevention is more sensible and achievable than complete disposal [1].

Corrosion is not always simply restricted to metals; it could likewise occur on distinct materials, for instance, polymers and plastic manufacturing. Amongst many metals, corrosion is experienced firmly in iron and steel. The formation of oxides in the process of oxidation does no longer hold immovably to the surface of metal, as a result it gets off the metal effortlessly. Corrosion is an irreversible interfacial response of a material with its surroundings or its disintegration into the segments as the material can't be come back to its most thermodynamically steady state. It consists of an electrochemical procedure which depends on vital environmental factors like pH, temperature, pressure etc. [2].

Mild steel is applied to make a substantial range of metal systems due to its easy availability and remarkable mechanical quality. The corrosion of mild steel can be understood as a stepwise electrochemical procedure. Initially, the attack takes place at anodic sites of the surface that prompts to the migration of ferrous particles into the solution. Discharged electrons from the anode lead their way to cathodic sites, thereby reacting with  $O_2$  and  $H_2O$  forming hydroxyl particles. The hydroxyl particles so formed, react with ferrous particles forming ferrous oxide which on oxidation is converted in ferric oxide i.e. rust.

## **1.2 Economic impact of corrosion**

Using metals mainly steel has expanded exponentially through the years with the increase in industrialization which results a significant increase in the cost of metal. In various industrially dependent countries like Australia, Great Britain, Japan etc. the cost of corrosion is approximately 3-4% loss of Gross National Product.

The predominant problems brought on due to corrosion are-

- Industrial shutdown: The substitute of a corroded tube in an oil refinery may cost a few hundred dollars but shut down of the unit while maintenance is under-way may cost dollar 50,000 or more per hour in lost production. In addition, the substitute of a corroded boiler or condenser in a large plant may additionally require dollar 1,000,000 or more for energy bought from inter linked electric power systems to supply customers while the boiler is down. Losses of this type cost the electric utilities in United States tens of millions of dollars annually [3].
- The mechanical excellence of metal gets faded, leading to the damage or overall breakdown of the whole metal.
- Dangers or wounds to human beings resulting from structural damage or breakdown (e.g. spans, vehicles, flying machine).
- Loss of timely availability of modern equipments, decreased estimation of stock and contamination of fluids in metal compartments.
- Corrosion additionally leads to mechanical loss to metals, blockage of tunnels and pipes by expanding the frictional properties of a metal.

### **1.3 Mechanistic approach to corrosion**

At the initial stage, the process of corrosion was explained by Evans, Wagner and Traud based on local cell model and corrosion potential model [3-4]. According to electrochemical theory of corrosion, on immersing a metal or alloy in corrosive medium different potential zones are developed because of the destruction of its crystalline lattices by means of corrosion. Because of this potential difference anodic and cathodic areas are formed on the surface of metal where oxidation and reduction take place respectively. Generally, the corrosion of a metal can be explained by considering the local electrochemical cells that are formed over the surface of metal during metal dissolution. Some part of surface acts as anode and other as cathode.

Two partial reactions, oxidation and reduction take place at the same time on the surface of metal. The reactions for the corrosion of iron are given below-

Anodic reaction



Cathodic reaction



Overall reaction



#### **1.4 Factors affecting metallic corrosion**

For the most part all metals and alloys show a crystalline structure. The crystals or grains of a metal are comprised of these unit cells repeated in a three-dimensional arrangement. The crystalline nature of metals is not promptly clear in light of the fact that the metal surface are generally fits with the shape in which it has been formed. Corrosion cells are made on the surface of metal in contact with an electrolyte as a result of energy differences between the metal and the electrolyte. Diverse regions on the metal surface could likewise have distinct potentials for the electrolytes. These variations are due to metallurgical factors, i.e. differences in their composition of microstructures, manufacture process, field establishment and environmental factors. Corrosion is primarily influenced and relies upon the primary and secondary factors. Generally, the primary factors are specifically connected with the metal or alloy while secondary factors are related with specific environment.

#### **1.5 Methods of corrosion control**

The significance of corrosion prevention might be perceived in perspective of vast financial losses endured because of metallic corrosion in all spheres of life and especially by

industries. The need to utilize constructional material security cost adequately and with due consideration towards the rivalries emerging from their corrosion is an essential concern in numerous industries. From the view purpose of country's economy, it is extremely important to receive proper ways and intends to lessen the misfortunes due to corrosion. With increasing development in technology and industries the utilization of metals and alloys is expanded quickly and any progression in the heading of avoiding corrosion would be an incredible help. Corrosion scientific experts and technologists trust that around one third of misfortunes because of corrosion can be spared by applying anticipation technique. From the attacks of corrosion can be accomplished by numerous conceivable choices. The most essential among them are-

- Modification of materials by additionally alloying or de-alloying.
- Adjustment in the corrosive environments.
- Utilization of defensive coatings.
- Cathodic and anodic protection.
- Utilization of corrosion inhibitors.

Prevention of corrosion by applying inhibitors is one of the most convenient way. In the present study corrosion inhibition has been considered by utilizing corrosion inhibitors, in this manner an itemized discussion on corrosion inhibitors and their applications has been done.

## **1.6 Corrosion inhibitors**

Corrosion inhibitors are those substances which reduce the corrosion of metal without influencing the environment, when they are added in small amount to a corrosive environment. The inhibitors utilized as a part of corrosive environment basically functions by creating a layer on the surface of metal [5-7].

Different compounds are there that are considered in the form of appropriate inhibitors [8-11]. They ordinarily have N, O and conjugated systems and strong capacity of being

adsorbed on the surface [12]. The most imperative disadvantage relative with the greater part of them is their high cost and non-eco-friendly character. Along these lines the investigation of most recent low harmful inhibitors is essential to discard this disadvantage. Nowadays inhibitors are being developed by using various parts of plants as they can be accessed easily and they are sustainable. The presence of different compounds like polyphenols, polysaccharides etc. increases the capability of such inhibitors (plant extract) to restrain the procedure of corrosion [13]. The viability of inhibitors is reliant on different factors. Some of them are given below-

#### **a)- Effect of inhibitor concentration**

The relationship between corrosion inhibition and inhibitor concentration has been examined by other researchers. It was discovered that the rate of corrosion decreases with the increase in inhibitor concentration and trend to approach a most extreme effectiveness at a certain concentration past which no critical increment in efficiency is observed [14-16]. This is known as the optimum concentration and the maximum surface area of metal is covered at this concentration [17-19].

#### **b)- Effect of temperature**

The corrosion rate straightly increases with increase in temperature. The metal dissolution reaction is complex at an elevated temperature and causes the accompanying changes-

- Desorption of pre adsorbed inhibitor molecules take place from the metal surface.
- The active area of metal surface changes on account of fast scratching.
- Decomposition and rearrangement of some inhibitor molecules may take place.

### **1.7 Review of Literature**

Earlier studies related to corrosion inhibition of mild steel by using plant extracts as corrosion inhibitors are discussed here-

El Etre et. al studied the corrosion restraining performance of Lawsonia extract utilizing the potentiodynamic polarization. The outcomes demonstrated that the Lawsonia extract provides good corrosion hindrance impact on mild steel corrosion and the efficiency of inhibitor was found to be increased with increasing concentration of inhibitor [20].

Emeka E. Oguzie investigated the corrosion inhibition action of *Occimum viridis* in acidic environments. The comparative study in two different acidic mediums suggests that the cause of restraining capability of extract is the existence of various organic species. The efficiency of inhibitor was found to be decreased with increase in temperature [21].

A. Y. El Etre demonstrated the corrosion hindrance impact of *Ammi visnaga* extract for SX 316 steel in 2 M HCl with the utilization of weight loss method and potentiostatic technique. In this study he found that some of the furanochromes got adsorbed on the surface which indicates the restraining properties of inhibitor [22].

L. Chauhan et. al investigated the corrosion hindrance activities of *Zenthoxylum alatum* extract in acidic environment. The inhibitory performance was checked for different concentrations and temperatures. Adsorption studies were also carried out by using SEM, XPS and FTIR techniques. GC-MS analysis of the extract was carried out for studying the composition of extract [23].

A. A. Rahim et.al studied the corrosion inhibition performance of *Rhizophora apiculata* in acidic environment. Computational studies were also carried out for studying the adsorption behavior of extract on the mild steel surface. The electrochemical examination has demonstrated that *Rhizophora apiculata* extract behaves like an excellent inhibitor [24].

A. Gaber et. al examined the plant extract of *Lupinuous albus* as a corrosion inhibitor in two different acidic environments and compared the results in both acidic conditions. In this study he suggested that the inhibitor was of mixed sort [25].



P. C. Okafor et al. explored the corrosion restraint effect of *Phyllanthus amarus* extract on mild steel corrosion in two different acidic environments and compared the results for both acidic solutions. Favorable results were obtained in both acidic mediums. Adsorption of inhibitor was found to obey Temkin isotherm [26].

Emeka E. Oguzie examined the leaves and seeds extract of selected plant materials to study their corrosion restraint performances in various acidic environments. Relative examination on the inhibitor adsorption conduct in both corrosive environments and the impact of temperature recommend that both protonated species could be in charge of the inhibition performance of extracts [27].

A. Y. El Etre examined the root extract of *Ferula harmonis* to study its corrosion inhibitory action in acidic environment. It was investigated that the increment in inhibitor concentration makes the process of corrosion slow and increases the corrosion restraint effectiveness of extract. The inhibitive impact of extract was talked about in perspective of adsorption of its ingredients on the steel surface. The corrosion restraint effectiveness of the extract diminishes as the temperature is expanded [28].

A. K. Satapathy et al. investigated the leaves extract of *Justicia gendarussa* as a good corrosion inhibitor in acidic environment. The adsorption of extract on the mild steel surface was studied with atomic force microscope. The corrosion restraint effectiveness was examined as far as adsorption and defensive film formation [29].

M. A. Quraishi et al. studied the corrosion restraint effectiveness of *Murraya koenigii* extract in two different acidic environments and compared the results for both mediums. The corrosion restraint effectiveness was found to be increased on increasing the inhibitor concentration. The impact of temperature, immersion time and inhibitor concentration were likewise examined in both corrosive medias. The inhibition was accepted to happen by means of adsorption of inhibitor molecules on the surface of metal [30].

Emeka E. Oguzie et al. explored the inhibition effect of *Dacryodis edulis* leaves extract for corrosion of low carbon steel in two different acidic environments and compared the results in both mediums. The adsorption activities, as approximated by Langmuir adsorption isotherm, indicates particular disparities going from lower to higher inhibitor concentrations which were related with a change from physisorption at lower concentrations and to chemisorption at adequately higher concentrations [31].

E. A. Noor investigated the *Radish* seeds extract as an effective material that could be utilized as corrosion inhibitor. The exploratory outcomes recommend that the hindrance productivity increases as the inhibitor concentration is increased and the adsorption follows Temkin adsorption isotherm [32].

M. Hussain and M. Kassim studied the inhibitive and adsorptive activities of *Uncaria gambir* extract in acidic environment. The potentiodynamic polarization comes about demonstrated that the examined inhibitor goes about as mixed sort [33].

K. V. Kumar et al. examined the corrosion restraint effectiveness of seeds extract of *Psidium guajava* for C-steel corrosion in 5% HCl. The inhibition performance has been described by polarization measurements. The estimations demonstrated that corrosion inhibition productivity increases with expanding concentration [34].

M. Lebrini et al. inspected the corrosion hindrance action of *Oxandra asbeckii* extract in acidic environment. In order to comprehend the mechanism of hindrance, Langmuir adsorption isotherm was tried. The reviews demonstrated that the corrosion restraint effectiveness relies on concentration of inhibitor. Electrochemical reviews demonstrated that the inhibitor carry on as mixed type [35].

A. Lecante et al. investigated the corrosion restraint effectiveness of leaves extract of *S. tinctoria* and bark extract of *G. ouregou* on low carbon steel in acidic environment. The test comes about uncover that both the studied inhibitors are proficient mixed type of

corrosion inhibitors and their corrosion restraint efficiencies increase with expanding inhibitor concentration [36].

M. Behpour et al. examined the plant extract of *Punica granatum* as a good corrosion inhibitor in two different acidic environments. The outcomes demonstrated that the corrosion rate was likewise figured hypothetically as far as mm every year utilizing current density estimations of mild steel. It was found that the inhibitor has striking corrosion hindrance productivity [37].

S. Deng et al. examined the corrosion restraint effectiveness of *Ginkgo* extract on cold rolled steel in two different acidic environments and compared the results in both mediums. The reviews were completed at distinctive concentrations. The outcomes demonstrated that the performance of inhibitor was extremely good even at low concentrations [38].

U. Eduok et al. studied the corrosion inhibition behavior *Sida acuta* in acidic environment by utilizing weight loss as well as hydrogen evolution methods. The outcomes demonstrated that the *Sida acuta* extract is an effective mixed type of corrosion inhibitor and the corrosion hindrance execution expanded with the increase in inhibitor concentration [39].

X. Li demonstrated the corrosion hindrance impact of leaves extract of *Dendrocalmus sinicus* in two distinct acidic environments and compared the results for both mediums. The corrosion restraint effectiveness was contemplated by polarization technique and EIS technique. AFM study was utilized to portray steel surface. The thermodynamic parameters were also computed and examined [40].

N. Egbedi et al. explored the corrosion restraint ability of leaves extract of *Spondias mombin* in 0.5 M H<sub>2</sub>SO<sub>4</sub> for aluminium corrosion. A preparatory screening of hindrance effect was completed utilizing weight loss estimations. The impact of temperature on the corrosion of aluminium was contemplated in the temperature go from 30°C- 60°C. The adsorption procedure obeyed Langmuir isotherm [41].

L. Li et al. demonstrated the corrosion hindrance performance of leaves extract of *Osmanthus fragran* in acidic environment. The outcomes demonstrated that the considered inhibitor goes about as mixed sort. In order to comprehend the mechanism of hindrance, Langmuir adsorption isotherm was tried. The results also demonstrated that the corrosion restraint effectiveness relies on concentration of inhibitor [42].

S. Garai et al. studied the plant extract of *Artemisia pallens* as an effective corrosion inhibitor in acidic environment. The exploratory outcomes recommended this plant extract as a proficient corrosion inhibitor and the hindrance productivity increases as the inhibitor concentration is increased [43].

N. Soltani et al. investigated the corrosion restraint effectiveness of leaves extract of *Salvia officinalis* in acidic environment utilizing weight loss as well as electrochemical systems. The outcomes demonstrated that the extract is an effective mixed type of corrosion inhibitor. The related initiation parameters and thermodynamic information of adsorption were accessed and talked about [44].

M. Otaibi et al. examined the corrosion hindrance action of various plant extracts on the corrosion of mild steel in 0.5 M HCl utilizing electrochemical analysis. The estimations demonstrated that the corrosion hindrance productivity increases with expanding inhibitor concentration and all of them were found to be of mixed sort [45].

X. Li et al. studied the corrosion restraint performance of *Dendrocalamus brandisii* extract in acidic environment. The reviews demonstrated that the corrosion restraint effectiveness relies on the concentration of inhibitor and temperature estimations. Electrochemical reviews demonstrated that the inhibitor carry on as mixed type [46].

I. Uwah et al. learned the corrosion restraint capacity of leaves, bark and roots extract of *Nauclea latifolia* in acidic medium utilizing weight reduction and electrochemical systems. Corrosion hindrance productivity increases with an expansion in inhibitor concentration and reduces with an expansion in temperature [47].

P. Raja et al. analyzed the leaves and bark extract of *Neolamarckia cadamba* as an effective inhibitor in acidic medium utilizing weight reduction. The experimental results recommended the extract as a mixed sort inhibitor and the corrosion restraint efficiency increases with expanding inhibitor concentration [48].

A. Bribri et al. demonstrated the restraint performance of *Euphorbia falcata* extract in acidic environment. The corrosion of C-steel has been considered by weight reduction, electrochemical estimations. The corrosion rate was likewise figured hypothetically as far as mm every year utilizing current density estimations of mild steel in 1 M HCl medium. It was observed that the studied inhibitor has striking corrosion hindrance productivity [49].

A. Hamdy et. al explored the corrosion restraint effectiveness of *henna* extract in acidic environment utilizing weight reduction and polarization studies. The experimental results showed that the studied extract acted as an efficient inhibitor against the C-steel corrosion and the corrosion restraint effectiveness relies on the concentration of inhibitor [50].

N. Odewunmi investigated the corrosion restraint effectiveness of *watermelon* rind extract in two different acidic environments and compared the results for both mediums. Corrosion hindrance of studied extract towards mild steel in both corrosive mediums was explored by utilizing electrochemical estimations (EIS and Tafel plots) and SEM analysis. The outcomes demonstrated that the inhibitor is an effective mixed type corrosion inhibitor and its corrosion hindrance execution expanded with the increase of inhibitor concentration [51].

K. Shalabi et al. examined the corrosion restraint performance of plant extract of *Atropa belladonna* in acidic environment utilizing the routine electrochemical estimations (EIS and Tafel plots). The outcomes demonstrated that the extract provides a good corrosion hindrance impact towards C-steel corrosion [52].

N. Soltani et al. investigated the corrosion hindrance activities of leaves extract of *Silybum marianum* for corrosion of 304 stainless steel in 1 M HCl by using electrochemical

impedance spectroscopy and Tafel polarization estimations. Polarization studies recommended the inhibitor as a mixed sort inhibitor and the corrosion hindrance effectiveness increments with expanding concentration of inhibitor [53].

V. Rajeswari et al. investigated the corrosion hindrance properties of leaves extract of different plant extracts in acidic environment. A preparatory screening of hindrance effectiveness was completed utilizing weight reduction estimation. The experimental results recommended all the extracts as mixed sort inhibitors [54].

M. Mehdipour et al. determined the corrosion hindrance impact of *Aloe* extract in acidic environment utilizing weight reduction and electrochemical procedures. The potentiodynamic polarization results are in favor of mixed sort behavior of the extract. The adsorbed film shaped on the metal surface was described by SEM [55].

M. Faustin et al. examined the corrosion restraint effectiveness of leaves extract of *Geissospermum* in acidic environment by using electrochemical estimations (EIS and Tafel studies). The considered inhibitor takes after Langmuir adsorption isotherm. Potentiodynamic polarization information proposed mix type of corrosion hindrance [56].

J. Bhawsar et al. explored the corrosion restraint behavior of *Nicotiana tabacum* extract in acidic environment utilizing weight reduction process. The exploratory outcomes recommend that the studied plant extract is a proficient inhibitor and the hindrance productivity relies on the concentration of inhibitor [57].

K. Anupama et al. investigated the corrosion restraint impact of leaves extract of *Pimenta dioica* in two different acidic environments and compared the results for both mediums, utilizing various techniques for example, electrochemical impedance spectroscopy and Tafel studies. The potentiodynamic polarization comes about demonstrated that the examined inhibitor goes about as mixed sort. The related initiation parameters and thermodynamic information of adsorption was accessed and talked about [58].

M. Prabakaran et al. investigated the corrosion restraint performance of *Ligularia fischeri* extract for corrosion of mild steel in 1 M HCl. The hindrance action was examined utilizing weight reduction, electrochemical studies and surface analysis. All estimations demonstrated that corrosion hindrance productivity increases with expanding concentration [59].

### **1.8 The extension and significance of corrosion inhibitor technology**

The significant ventures utilizing corrosion inhibitors are the oil and gas investigation and creation industry, the oil refining industry, the chemical industry and the overwhelming mechanical assembling industry. Corrosion inhibitors are also additionally utilized as a part of numerous frameworks including cleaning pads, cooling frameworks, pipelines, chemical operations and numerous items that are showcased to the overall population. One of the striking highlights of corrosion inhibitors is non-disturbance of the procedure. Inhibitors are mostly utilized for their adequacy in protecting the particular metal or mix of metals.

### **1.9 The objectives of current study**

The objectives of the present study are:

- To investigate the inhibitive and adsorptive properties of selected plants for the corrosion of mild steel in acidic medium by using weight loss measurements.
- To study the mechanism of adsorption of inhibitors on the surface of mild steel by using UV, IR, SEM, AFM and Quantum chemical calculations.
- To determine the corrosion rate of mild steel and corrosion inhibition efficiency of different inhibitors by using Electrochemical Measurements.
- To find green corrosion inhibitors having higher inhibition efficiency at lower concentration of inhibitor.

## References

1. M. Acharya, J. Chauhan, A. Dixit and D. Gupta, "Green Inhibitors for Prevention of Metal and Alloys Corrosion" An Overview *Chemistry and materials research*, 6 (2013) 2224-3224.
2. N. Kairi and J. Kassim, "The Effect of Temperature on the Corrosion Inhibition of Mild Steel in 1 M HCl Solution by *Curcuma Longa* Extract", *Int. J. Electrochem. Sci*, 8 (2013) 7138 – 7155.
3. B. Kermani and M. Harrop, "The impact of corrosion on the oil and gas industry" *SPE Prod. Oper*, 11 (1996) 186-190.
4. R. Revie and H. Uhlig, "Corrosion and corrosion control, An Introduction to Corrosion Science and Engineering", *Corrosion and corrosion control*, New Jersey, 2008.
5. C. Wagner and W. Traud, "On the Interpretation of Corrosion Processes Through the Superposition of Electrochemical Partial Processes and on the Potential of Mixed Electrodes", *Zeitschrift fur Electrochemie und Angew. Phys. Chemie*.44 (1938) 391-402.
6. M. Pourbaix, "Atlas of electrochemical equilibria in aqueous solutions", Pergamon Press, Oxford, 1966.
7. S. Zhang, Z. Tao, W. Li and B. Hou, "The effect of some triazole derivatives as inhibitors for the corrosion of mild steel in 1 M hydrochloric acid", *Appl. Surf. Sci.*, 255 (2009) 6757-6763.
8. M. Wahadan, A. Hermas and M. Morad, "Corrosion inhibition of carbon-steels by propargyl triphenyl phosphonium bromide in H<sub>2</sub>SO<sub>4</sub> solution", *Mater. Chem. Phys.*, 76 (2002) 111-118.
9. K. Sapre, S. Seal, P. Jepson, H. Wang, Z. Rahman and T. Smith, "Investigation into the evolution of corrosion product layer (CPL) of 1018 C-steel exposed to multiphase environment using FIB and EIS techniques", *Corros. Sci.*, 45 (2003) 59-80.



10. A. Shafei, M. Moussa, A. Far, "The corrosion inhibition character of thiosemicarbazide and its derivatives for C-steel in hydrochloric acid solution", *Mater. Chem. Phys.*, 70 (2001) 175-180.
11. E. Oguzie, *Mater. Letters*, "Corrosion inhibition of mild steel in hydrochloric acid solution by methylene blue dye", 59 (2005) 1076-1079.
12. E. Oguzie, *Corros. Sci.*, "Evaluation of the inhibitive effect of some plant extracts on the acid corrosion of mild steel", 50 (2008) 2993-2998.
13. S. Martinez and I. Stern, "Inhibitory mechanism of mimosa tannin using molecular modeling and substitutional adsorption isotherms", *Mater. Chem. Phys.*, 77 (2003) 97-102.
14. D. Yadav, D. Chauhan, I. Ahmad and M. Quraishi, "Electrochemical behavior of steel/acid interface: adsorption and inhibition effect of oligomeric aniline", *RSC Adv.*, 3 (2013) 632-646.
15. S. Banerjee, A. Mishra, M. Singh, B. Maiti, B. Ray and P. Maiti, "Highly efficient polyurethane ionomer corrosion inhibitor: the effect of chain structure" *RSC Adv.*, 1 (2011) 199.
16. M. Gopiraman, C. Sathya, S. Vivekananthan, D. Kesavan and N. Sulochana, "Influence of 2,3-Dihydroxyflavanone on Corrosion Inhibition of Mild Steel in Acidic Medium", *J. Mater. Eng. Perform.* 21 (2011) 240-246.
17. J. Saranya, P. Sounthari, K. Parmeswari and S. Chitra, "Acenaphtho[1,2-b]quinoxaline and Acenaphtho[1,2-b]pyrazine as corrosion inhibitors for mild steel in acid medium", *Meas. J. Int. Meas. Confed.*, 77 (2016) 175-185.
18. F. Bentiss, M. Traisnel and M. Lagrenee, "The substituted 1,3,4-oxadiazoles: a new class of corrosion inhibitors of mild steel in acidic media", *Corros. Sci.*, 42 (2000) 127-146.
19. F. Ansari and M. Quraishi, "Inhibitive Effect of Some Gemini Surfactants as Corrosion Inhibitors for Mild Steel in Acetic Acid Media", *Arab. J. Sci. Eng.*, 36 (2011) 11-20.

20. A. Etre, M. Abdallah and Z. Tantawy, "Corrosion inhibition of some metals using *lawsonia* extract", *Corros. Sci.* 47 (2005) 385-395.
21. E. Oguzie, "Studies on the inhibitive effect of *Occimum viridis* extract on the acid corrosion of mild steel", *Mater. Chem. Phys.*, 99 (2006) 441-446.
22. A. Etre. "*Khillah* extract as inhibitor for acid corrosion of SX 316 steel", *Appl. Surf. Sci.*, 252 (2006) 8521-8525.
23. L. Chauhan and G. Gunasekaran, "Corrosion inhibition of mild steel by plant extract in dilute HCl medium", *Corros. Sci.* 49 (2007) 1143-1161.
24. A. Rahim, E. Rocca, J. Steinmetz, M. Kassim, R. Adnan, M. Ibrahim, "*Mangrove* tannins and their flavonoid monomers as alternative steel corrosion inhibitors in acidic medium", *Corros. Sci.* 49 (2007) 402-417.
25. A. Gaber, B. Nabey and M. Saadawy, "The role of acid anion on the inhibition of the acidic corrosion of steel by *lupine* extract", *Corros. Sci.*, 51 (2009) 1038-1042.
26. P. Okafor, M. Ikpi, I. Uwah, E. Ebenso, U. Ekpe and S. Umoren, "Inhibitory action of *Phyllanthus amarus* extracts on the corrosion of mild steel in acidic media", *Corros. Sci.* 50 (2008) 2310-2317.
27. E. Oguzie, "Evaluation of the inhibitive effect of some plant extracts on the acid corrosion of mild steel", *Corros. Sci.* 50 (2008) 2993-2998.
28. A. Etre, "Inhibition of C-steel corrosion in acidic solution using the aqueous extract of *zallouh* root", *Mater. Chem. Phys.* 108 (2008) 278-282.
29. A. Satapathy, G. Gunasekaran, S. Sahoo, A. Kumar and P. Rodrigues, "Corrosion inhibition by *Justicia gendarussa* plant extract in hydrochloric acid solution", *Corros. Sci.* 51 (2009) 2848-2856.
30. M. Quraishi, A. Singh, V. Singh, D. Yadav and A. Singh, "Green approach to corrosion inhibition of mild steel in hydrochloric acid and sulphuric acid solutions by the extract of *Murraya koenigii* leaves", *Mater. Chem. Phys.* 122 (2010) 114-122.
31. E. Oguzie, C. Enenebeaku, C. Akalezi, S. Okoro, A. Ayuk and E. Ejike, "Adsorption and corrosion-inhibiting effect of *Dacryodis edulis* extract on low-

- carbon-steel corrosion in acidic media”, *J. Colloid Interface Sci.*, 349 (2010) 283-292.
32. E. Noor, “The impact of some factors on the inhibitory action of *Radish* seeds aqueous extract for mild steel corrosion in 1 M H<sub>2</sub>SO<sub>4</sub> solution”, *Mater. Chem. Phys.* 131 (2011) 160-169.
33. M. Hussain and M. Kassim, “The corrosion inhibition and adsorption behavior of *Uncaria gambir* extract on mild steel in 1 M HCl”, *Mater. Chem. Phys.* 125 (2011) 461-468.
34. K. Kumar, M. Pillai, G. Thusnavis, “Seed Extract of *Psidium guajava* as Ecofriendly Corrosion Inhibitor for Carbon Steel in Hydrochloric Acid Medium”, *J. Mater. Sci. Technol.*, 27 (2011) 1143-1149.
35. M. Lebrini, F. Robert, A. Lecante, C. Roos, “Corrosion inhibition of C38 steel in 1 M hydrochloric acid medium by alkaloids extract from *Oxandra asbeckii* plant”, *Corros. Sci.* 53 (2011) 687-695.
36. A. Lecante, F. Robert, P. Blandinières and C. Roos, “Anti-corrosive properties of *S. tinctoria* and *G. ouregou* alkaloid extracts on low carbon steel”, *Curr. Appl. Phys.*, 11 (2011) 714-724.
37. M. Behpour, S. Ghoreishi, M. Khayatkashani and N. Soltani, “Green approach to corrosion inhibition of mild steel in two acidic solutions by the extract of *Punica granatum* peel and main constituents”, *Mater. Chem. Phys.*, 131 (2012) 621-633.
38. S. Deng and X. Li, “Inhibition by *Ginkgo* leaves extract of the corrosion of steel in HCl and H<sub>2</sub>SO<sub>4</sub> solutions”, *Corros. Sci.* 55 (2012) 407-415.
39. U. Eduok, S. Umoren and A. Udoh, “Synergistic inhibition effects between leaves and stem extracts of *Sida acuta* and iodide ion for mild steel corrosion in 1 M H<sub>2</sub>SO<sub>4</sub> solutions”, *Arab. J. Chem.* 5 (2012) 325-337.
40. X. Li, S. Deng and H. Fu, “Inhibition of the corrosion of steel in HCl, H<sub>2</sub>SO<sub>4</sub> solutions by *bamboo* leaf extract”, *Corros. Sci.* 62 (2012) 163-175.
41. N. Egbedi, I. Obot and S. Umoren, “*Spondias mombin* L. as a green corrosion inhibitor for aluminium in sulphuric acid: Correlation between inhibitive effect and

- electronic properties of extracts main constituents using density functional theory”, *Arab. J. Chem.* 5 (2012) 361-373.
42. L. Li, X. Zhang, J. Lei, J. He, S. Zhang and F. Pan, “Adsorption and corrosion inhibition of *Osmanthus fragran* leaves extract on carbon steel”, *Corros. Sci.* 63 (2012) 82-90.
43. S. Garai, S. Garai, P. Jaisankar, J. Singh and A. Elango, “A comprehensive study on crude methanolic extract of *Artemisia pallens* (Asteraceae) and its active component as effective corrosion inhibitors of mild steel in acid solution”, *Corros. Sci.* 60 (2012) 193-204.
44. N. Soltani, N. Tavakkoli, M. Khayatkashani, M. Jalali, A. Mosavizade, “Green approach to corrosion inhibition of 304 stainless steel in hydrochloric acid solution by the extract of *Salvia officinalis* leaves”, *Corros. Sci.* 62 (2012) 122-135.
45. M. Otaibi, A. Mayouf, M. Khan, A. Mousa, S. Mazroa and H. Alkhathlan, “Corrosion inhibitory action of some plant extracts on the corrosion of mild steel in acidic media”, *Arab. J. Chem.* 7 (2012) 340-346.
46. X. Li and S. Deng, “Inhibition effect of *Dendrocalamus brandisii* leaves extract on aluminum in HCl, H<sub>3</sub>PO<sub>4</sub> solutions”, *Corros. Sci.* 65 (2012) 299-308.
47. I. Uwah, P. Okafor and V. Ebiekpe, “Inhibitive action of ethanol extracts from *Nauclea latifolia* on the corrosion of mild steel in H<sub>2</sub>SO<sub>4</sub> solutions and their adsorption characteristics”, *Arab. J. Chem.* 6 (2013) 285-293.
48. P. Raja, A. Qureshi, A. Rahim, H. Osman and K. Awang, “*Neolamarckia cadamba* alkaloids as eco-friendly corrosion inhibitors for mild steel in 1 M HCl media”, *Corros. Sci.* 69 (2013) 292-301.
49. A. Bribri, M. Tabyaoui, B. Tabyaoui, H. Attari and F. Bentiss, “The use of *Euphorbia falcata* extract as eco-friendly corrosion inhibitor of carbon steel in hydrochloric acid solution”, *Mater. Chem. Phys.*, 141 (2013) 240-247.
50. A. Hamdy and N. Gendy, “Thermodynamic, adsorption and electrochemical studies for corrosion inhibition of carbon steel by *henna* extract in acid medium”, *Egypt. J. Petroleum*, 22 (2013) 17-25.

51. N. Odewunmi, S. Umoren and Z. Gasem, "Utilization of *watermelon* rind extract as a green corrosion inhibitor for mild steel in acidic media", *J. Ind. Eng. Chem.*, 21 (2013) 239-247.
52. K. Shalabi, Y. Abdallah, H. Hassan and A. Fouda, "Adsorption and Corrosion Inhibition of *Atropa Belladonna* Extract on Carbon Steel in 1 M HCl Solution", *Int. J. Electrochem. Sci.*, 9 (2014) 1468-1487.
53. N. Soltani, N. Tavakkoli, M. Kashani, A. Mosavizadeh, E. Oguzie and M. Jalali, "Silybum marianum extract as a natural source inhibitor for 304 stainless steel corrosion in 1.0 M HCl", *J. Ind. Eng. Chem.*, 20 (2014) 3217-3227.
54. V. Rajeswari, D. Kesavan, M. Gopiraman, P. Viswanathamurthi, K. Poonkuzhali and T. Palvannan, "Corrosion inhibition of *Eleusine aegyptiaca* and *Croton rottleri* leaves extracts on cast iron surface in 1 M HCl medium", *Appl. Surf. Sci.*, 314 (2014) 537-545.
55. M. Mehdipour, B. Ramezanzadeh and S. Arman, "Electrochemical noise investigation of *Aloe* plant extract as green inhibitor on the corrosion of stainless steel in 1 M H<sub>2</sub>SO<sub>4</sub>", *J. Ind. Eng. Chem.*, 21 (2014) 318-327.
56. M. Faustin, A. Maciuk, P. Salvin, C. Roos and M. Lebrini, "Corrosion inhibition of C38 steel by alkaloids extract of *Geissospermum* leaves in 1 M hydrochloric acid: Electrochemical and phytochemical studies", *Corros. Sci.*, 92 (2014) 287-300.
57. J. Bhawsar, P. Jain and P. Jain, "Experimental and computational studies of *Nicotiana tabacum* leaves extract as green corrosion inhibitor for mild steel in acidic medium", *Alex. Eng. J.*, 54 (2015) 769-774.
58. K. Anupama, K. Ramya, K. Shainy and A. Joseph, "Adsorption and electrochemical studies of *Pimenta dioica* leaves extracts as corrosion inhibitor for mild steel in hydrochloric acid", *Mater. Chem. Phys.* 167 (2015) 28-41.
59. M. Prabakaran, S. HyunKim, K. Kalaiselvi, V. Hemapriya and I. Chung, "Highly efficient *Ligularia fischeri* green extract for the protection against corrosion of mild steel in acidic medium: Electrochemical and spectroscopic investigations", *J. Taiw. Inst. Chem. Eng.*, 59 (2016) 559-562.

**Chapter 2**  
**Materials and Methods**

## **2.1 Introduction**

Analysis were performed to contemplate the corrosion inhibitive capacities of selected plants towards corrosion of mild steel in 0.5 M H<sub>2</sub>SO<sub>4</sub> solution at various inhibitor concentrations and temperatures. The gravimetric estimations, Potentiodynamic Polarization and Electrochemical Impedance Spectroscopy (EIS) techniques were utilized to determine the corrosion rate, corrosion hindrance effectiveness and thermodynamic parameters for the inhibitors. Surface morphology was examined utilizing Scanning Electron Microscopy (SEM) and Atomic Force Microscopy (AFM). Absorption spectroscopic techniques (FTIR and UV-Visible spectroscopy) were likewise used to clarify adsorption mechanism. Density Functional Theory (DFT) was utilized for theoretical calculations. The exploratory techniques utilized for the above investigations of corrosion inhibitors are given in this section.

## **2.2 Composition of mild steel used for the study**

Mild steel is used to make a broad assortment of equipments and metallic structures. The mild steel sheet was purchased from R. K. steel traders Jalandhar. The composition of the sample was observed to be (wt %) C, 0.083; P, 0.12; Cr, 0.45; Ni, 0.27, Cu, 0.43 and Fe balance.

## **2.3 Preparation and cleaning of metal surface**

The mild steel coupons were mechanically cut into 2.0 cm × 2.0 cm × 0.1 cm and silicon carbide papers (100-2000 grade) were utilized to scrape and polish all exposed surface of mild steel coupons for weight loss process. For electrochemical estimations the mild steel coupons were incised into 1.0 cm × 1.0 cm × 0.1 cm, rubbed and cleaned correspondingly to the previous procedure, leaving an exposed area of 1 cm<sup>2</sup>, (rest covered with araldite resin), with 3 cm long stem. Prior to each experiment, coupons were washed with distilled water, degreased in acetone and dried and stored in vacuum desiccator.

### **2.3.1 Preparation of 0.5 M H<sub>2</sub>SO<sub>4</sub> solution**

In the present examination, tests were carried out in 0.5 M H<sub>2</sub>SO<sub>4</sub> solution which was prepared in double distilled water utilizing AR grade sulphuric acid provided by Sigma chemicals. For weight loss studies, the volume of 0.5 M H<sub>2</sub>SO<sub>4</sub> was kept 500 mL and for electrochemical estimations 250 mL of 0.5 M H<sub>2</sub>SO<sub>4</sub> was utilized.

### **2.4 Selected plants for the study**

The present investigation aims to explore the corrosion hindrance viability of some plant extracts on mild steel in 0.5 M H<sub>2</sub>SO<sub>4</sub>. On the basis of literature, some plants were selected for the present study.

### **2.5 Preparation of plant extract**

The required plant material was obtained from market and after that cleaned with tap water to take out searing stays of mud, dried for two days in an oven at 60 °C and ground to powder. 100 g powdered sample was refluxed persistently with 450 cm<sup>3</sup> of suitable solvent at 75 °C for 72 h. The refluxed solution was filtered. The filter liquor was evaporated to 100 ml residue, dried in a vacuum drying oven at 60 °C for 2 days. At that point the solid deposit was gained for complete dryness and spared in a desiccator.

### **2.6 Weight loss estimations**

Mild steel coupons abraded with different grades of silicon carbide papers were weighted and immersed in 500 mL of 0.5 M H<sub>2</sub>SO<sub>4</sub> without and with various concentrations of inhibitors for 24 h [1-4]. After the predetermined time, the steel samples were taken out from the corrosive solution, washed with acetone and dried before weighing. Triplicate tests were performed for every concentration of inhibitor for reproducibility and an average value of weight loss was taken to calculate corrosion rate and corrosion hindrance



effectiveness of the inhibitors. The corrosion rate (CR), inhibition efficiency ( $\eta$  %) and surface coverage ( $\Theta$ ) were calculated by following equations-

$$CR = \frac{\Delta W}{D \times A \times T} \times 87600 \quad (1)$$

$$\Theta = \frac{w_0 - w_i}{w_0} \quad (2)$$

$$\eta\% = \frac{w_0 - w_i}{w_0} \times 100 \quad (3)$$

where, W represents weight loss (mg), A is the area of mild steel coupon (cm<sup>2</sup>), T is the immersion time (h), D is the density of mild steel (gcm<sup>-3</sup>) and  $w_0$  and  $w_i$  are the weight loss in the absence and presence of inhibitors. From weight reduction estimations an increment in inhibition efficiency happens on expanding the inhibitor concentration. This increase in inhibition efficiency esteems arises as a result of the development of a defensive layer that decreases the corrosion procedure. Keeping in mind the end goal to examine the impact of inhibitors on the inhibition efficiencies, weight loss estimations were completed in the temperature range of 298-318 K in the absence and presence of various concentrations of inhibitor. The inhibition efficiency decreases on increasing temperature which is because of desorption of adsorbed inhibitor molecules.

### 2.6.1. Adsorption isotherm

The adsorption isotherms provide the essential information on the interaction between inhibitors and the steel surface. Decrease in corrosion rate on utilization of inhibitors is either by obstructing the cathodic reaction rate or by preventing the anodic metal dissolution or both by adsorbing on the metal surface in corrosive medium [5-7]. Seiverts et al. [8] demonstrated a relationship between inhibitor concentration and inhibition efficiency and further delineated that an adsorption isotherm may give a relationship between the coverage of an interface with adsorbed species and the concentration of species in the solution. The most ordinarily utilized adsorption isotherm is Langmuir adsorption

isotherm [9]. The surface coverage ( $\Theta$ ) for various concentrations of inhibitors in 0.5 M  $H_2SO_4$  solution was tried graphically to fit a reasonable adsorption isotherm. Langmuir adsorption isotherm [10] can be written in the form-

$$\frac{C}{\theta} = \frac{1}{K_{ads}} + C \quad (4)$$

Where,  $C$  is the concentration of inhibitor and  $K_{ads}$  is the adsorption constant.

If the slope and correlation coefficient of straight line obtained by plotting  $C/\theta$  against  $C$  comes near unity, then it is considered that the inhibitors obey Langmuir adsorption isotherm. A plot of  $C/\theta$  against  $C$  for Langmuir adsorption isotherm is shown in Fig.2.1.

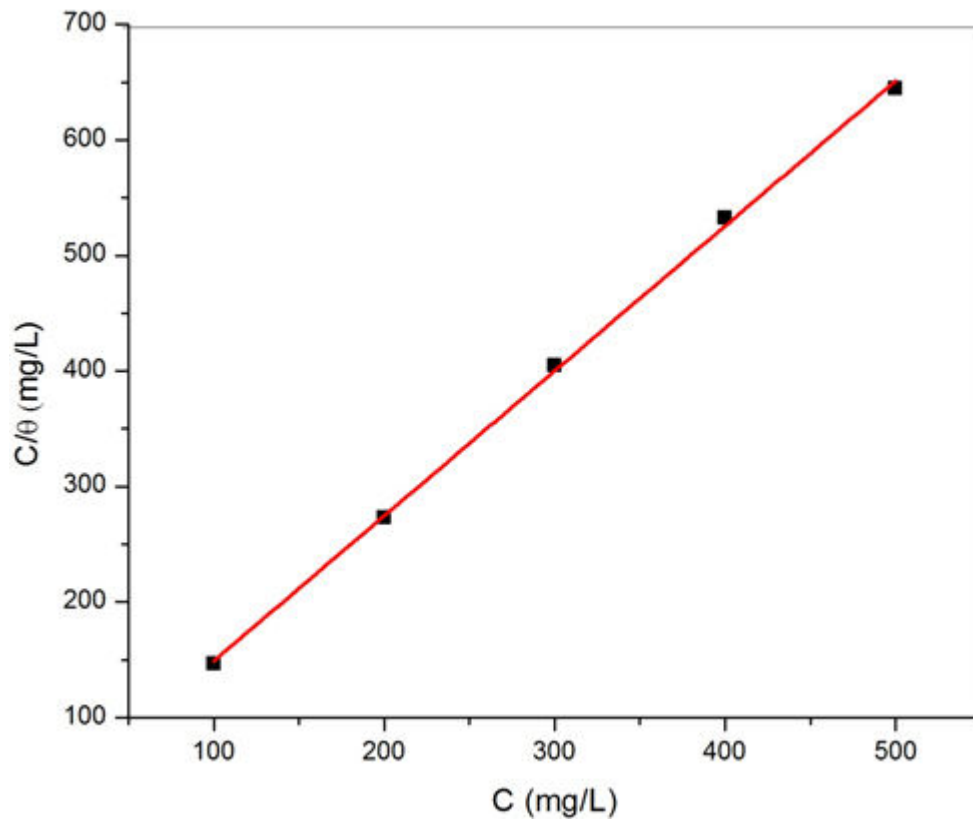


Fig. 2.1: A typical plot of  $C/\theta$  against  $C$  (Langmuir adsorption isotherm)

## 2.7 Corrosion inhibition studies by potentiodynamic polarization

Polarization estimations were completed at 298 K utilizing a three-electrode system and a glass cell containing 250 mL of corrosive solution with CH instrument electrochemical workstation. The mild steel coupons were mounted in araldite resin leaving an exposed area of 1 cm<sup>2</sup>. Toward the start of experiments, the working electrode was immersed in the test solution for 1 h to get a settled open circuit potential (OCP). Polarization plots were obtained at a scan rate of 1 mV/s between potentials of -250 mV and +250 mV. A platinum electrode was used as a counter electrode and saturated calomel electrode as the reference electrode. The corrosion current densities were computed by extrapolation of linear parts of anodic and cathodic curves to the point of convergence of the corresponding corrosion potential [11-15]. The Tafel curves suggested decrement in current densities within the presence of inhibitor. For further analysis, the parameters, including corrosion potential ( $E_{corr}$ ), corrosion current density ( $I_{corr}$ ), anodic and cathodic Tafel slopes ( $\beta_a$  and  $\beta_c$ ) and inhibition efficiency ( $\eta$  %) were ascertained by following equation [16].

$$\eta(\%) = \frac{I_{0corr} - I_{icorr}}{I_{0corr}} \times 100 \quad (6)$$

where,  $I_{0corr}$  and  $I_{icorr}$  represent the corrosion current density in the absence and presence of inhibitor respectively.

## 2.8 Corrosion inhibition studies by electrochemical impedance spectroscopy (EIS)

The same electrochemical cell and electrochemical workstation, as specified for polarization estimations, was used to carry out electrochemical impedance spectroscopy estimations in the frequency range from 100 KHz to 0.01 Hz using amplitude of 5 mV at OCP. Before to every test, the working electrode was immersed into test solution for 30 minutes at 298 K to attain the steady potential. A steady potential (vs. SCE) was readily attained, corresponding to the free  $E_{corr}$  (vs. SCE) of mild steel. The impedance information was gotten by utilizing the Nyquist and Bode plots. The EIS spectra of all tests were

dissected utilizing the parallel circuit in Figure 2.2 [17]. The inhibition efficiency was ascertained from charge transfer resistance esteems acquired from impedance estimations utilizing the accompanying relation-

$$\eta(\%) = \frac{R_{ct} - R_{ct}^0}{R_{ct}} \times 100 \quad (7)$$

where  $R_{ct}$  and  $R_{ct}^0$  represent charge transfer resistance in the presence and absence of inhibitor respectively. Increment in  $R_{ct}$  values was observed with increasing the inhibitor concentration. This incrementation in  $R_{ct}$  values is credited to the formation of a defensive film at the metal interface. The changes in  $R_{ct}$  and CPE values were caused by the substitution of water molecules by adsorption of inhibitor on the mild steel surface, decreasing the degree of metal dissolution.

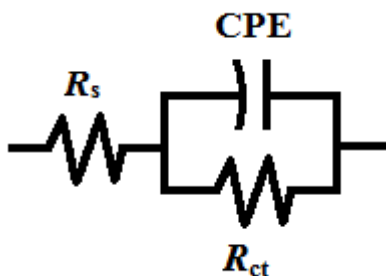


Fig.2.2: Equivalent circuit of constant phase element (CPE)

## 2.9 FT-IR spectroscopy

The Fourier transform infrared spectroscopic analysis is a standout amongst the most essential methods for elucidation of the phenomenon of adsorbed inhibitor molecules. The infrared spectral information has been considered by numerous specialists as an immediate evidence of the presence of inhibitors on the metal surface [18-20]. In the present study Fourier transform infrared spectroscopic analysis was performed to confirm the presence of heteroatoms in the extract, utilizing Shimadzu FTIR 8400S. The extract blended with

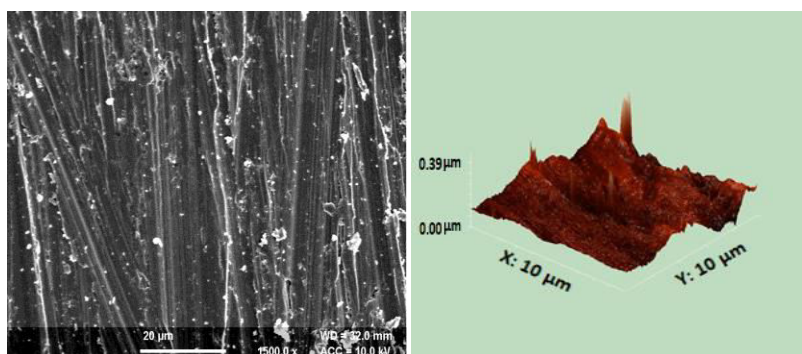
KBr powder was transferred into a pallet for FTIR characterization. The FTIR for all samples was recorded in the range 500-4000  $\text{cm}^{-1}$ .

## 2.10 UV-Visible spectroscopy

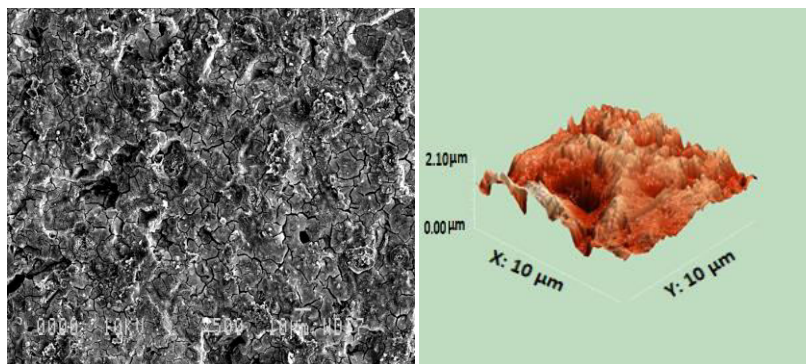
With the assistance of Shimadzu UV-1800 absorption spectrophotometer, the UV spectra of corrosive solution (before and after the corrosion test) were taken. Both these spectras were contrasted to elucidate the inhibition mechanism.

## 2.11 Surface studies

The surface morphology of the exposed metal surface has been contemplated widely by numerous specialists to comprehend the idea of surface product got in the absence and presence of inhibitors [21-24]. The mild steel coupons of size 1.0 cm  $\times$  1.0 cm  $\times$  0.1 cm were abraded with a series of emery paper (320-500-800-1200) and then washed with distilled water and acetone. After immersion in 0.5 M  $\text{H}_2\text{SO}_4$  solution in the absence and presence of optimum concentration of inhibitors for 24 h, the coupons were cleaned with distilled water, dried and afterward the SEM and AFM images were recorded utilizing LEO435BP and NT-MDT-INTEGRA respectively. The SEM and AFM images of abraded mild steel and mild steel immersed in 0.5 M  $\text{H}_2\text{SO}_4$  solution are shown in Fig.2.3. SEM of mild steel sample after 24 h immersion in 0.5 M  $\text{H}_2\text{SO}_4$  solution shows a severely harmed surface.



Abraded mild steel



Mild steel immersed in 0.5 M H<sub>2</sub>SO<sub>4</sub>

Fig.2.3: SEM and AFM images of abraded mild steel and mild steel immersed in 0.5 M H<sub>2</sub>SO<sub>4</sub>

From AFM studies, the average surface roughness for abraded mild steel is 2.099 nm and for mild steel immersed in 0.5 M H<sub>2</sub>SO<sub>4</sub>, the average surface roughness is 138.807 nm. These SEM and AFM images were compared with corresponding images after 24 h immersion of mild steel in 0.5 M H<sub>2</sub>SO<sub>4</sub> in the presence of inhibitors.

### 2.12 Quantum chemical study

The quantum chemical estimations were done utilizing Hyperchem 8.0 programming with DFT method. The reactivity of a chemical species is very much characterized as far as Frontier orbitals; the highest occupied molecular orbital (HOMO) and the lowest unoccupied molecular orbitals (LUMO) [25-26]. As indicated by Frontier sub-atomic orbital (FMO) hypothesis of chemical reactivity, the formation of a transition state is because of interaction between HOMO and LUMO of responding species. The smaller the energy gap ( $\Delta E$ ) amongst HOMO and LUMO, stronger will be the interaction between two responding species [27-28]. The quantum chemical parameters, for example, the energy of highest occupied molecular orbital ( $E_{\text{HOMO}}$ ), the energy of lowest unoccupied molecular orbital ( $E_{\text{LUMO}}$ ), and the energy gap ( $\Delta E$ ) were figured utilizing following equations [29].

$$\Delta E = E_{\text{LUMO}} - E_{\text{HOMO}} \quad (8)$$

As  $E_{\text{HOMO}}$  is frequently connected with electron donating capacity of the molecule, high values of  $E_{\text{HOMO}}$  are probably going to demonstrate an inclination of molecule to donate electrons to fitting acceptor molecules with low energy and empty molecular orbital. Similarly, the low values of energy gap  $\Delta E$  will render great inhibition efficiencies since the energy to remove an electron from last occupied orbital will be minimized. It has been reported that good inhibitors indicate higher value of  $E_{\text{HOMO}}$  and lower value of  $\Delta E$ . Therefore, DFT made it possible to corrosion scientist to accurately predict the corrosion inhibition capabilities of organic compounds based on electronic/molecular properties and reactivity indices. Previous researchers have also used the DFT study to study the interaction of inhibitor molecules with metal surface [30-33]

## References

1. A. Khadraoui, A. Khelifa, M. Hadjmeliani, R. Mehdaoui, K. Hachama, A. Tidu, Z. Azari, I. Obot and A. Zarrouk, "Extraction, characterization and anti-corrosion activity of *Mentha pulegium* oil: Weight loss, electrochemical, thermodynamic and surface studies", *J. Mol. Liq.*, 216 (2016) 724-731.
2. R. Xiao, G. Xiao, B. Huang, J. Feng and Q. Wang, "Corrosion failure cause analysis and evaluation of corrosion inhibitors of Ma Huining oil pipeline", *Eng. Fail. Anal.*, 68 (2016) 113-121.
3. P. Singh, M. Srivastava and M. Quraishi, "Novel quinoline derivatives as green corrosion inhibitors for mild steel in acidic medium: Electrochemical, SEM, AFM, and XPS studies", *J. Mol. Liq.*, 216 (2016) 164-173.
4. P. Geethamani, P. Kasthuri, M. Russel and S. Foreman, "Adsorption and corrosion inhibition of mild steel in acidic media by expired pharmaceutical drug", *Cogent Chem.*, (2015) 1-11.
5. H. Sorkhabi, and M. Haghi, "Corrosion inhibition of mild steel in hydrochloric acid by betanin as a green inhibitor", *J. Solid State Electrochem.*, 13 (2009) 1297-1301.
6. M. Hegazy and F. Altam, "Three novel *bola amphiphiles* as corrosion inhibitors for carbon steel in hydrochloric acid: Experimental and computational studies", *J. Mol. Liq.*, 218 (2016) 649-662.
7. D. Singh, S. Kumar, G. Udayabhanu, and R. John, "4(N,N-dimethylamino) benzaldehyde nicotinic hydrazone as corrosion inhibitor for mild steel in 1 M HCl solution: An experimental and theoretical study", *J. Mol. Liq.*, 216 (2016) 738-746.
8. A. Seiverts and P. Lueg, *Anog Chem.*, 126 (1923) 192.
9. S. Cheng, S. Chen, T. Liu, X. Chang and Y. Yin, "Carboxymethyl *chitosan* as an ecofriendly inhibitor for mild steel in 1 M HCl", *Mater. Lett.*, 61 (2007) 3276-3280.
10. L. Murulana, M. Kabanda and E. Ebenso, "Investigation of the adsorption characteristics of some selected sulphonamide derivatives as corrosion inhibitors at mild steel/hydrochloric acid interface: Experimental, quantum chemical and QSAR studies", *J. Mol. Liq.*, 215 (2016) 763-779.



11. K. Anupama, K. Ramya, K. Shainy and A. Joseph, "Adsorption and electrochemical studies of *Pimenta dioica* leaf extracts as corrosion inhibitor for mild steel in hydrochloric acid", *Mater. Chem Phys.* (2015) 1-14.
12. L. Liao, S. Mo, H. Luo, N. Li, "Longan seed and peel as environmentally friendly corrosion inhibitor for mild steel in acid solution: experimental and theoretical studies", *J. Colloid and interface sci.*, (2016).
13. H. Lgaz, R. Salghi, S. Jodeh, B. Hammout, "Effect of clozapine on inhibition of mild steel corrosion in 1.0 M HCl medium", *J. Mol. Liquids*, (2016).
14. P. Raja, A. Quraishi, A. Rahim, H. Osman, K. Awang, "Neolamarckia cadamba alkaloids as eco-friendly corrosion inhibitors for mild steel in 1 M HCl media", *Corrosion Science* 69 (2013) 292–301.
15. S. Nofrizal, A. Rahim, B. Saad, P. Raja, M. Shah, and S. Yahya, "Elucidation of the Corrosion Inhibition of Mild Steel in 1.0 M HCl by Catechin Monomers from Commercial Green Tea Extracts", *The Minerals, Metals & Materials Society, ASM international*, (2011).
16. S. Junaedi, A. Amiery, A. Kadhum, A. Kadhum, and A. Mohamad, "Inhibition Effects of a Synthesized Novel 4-Aminoantipyrine Derivative on the Corrosion of Mild Steel in Hydrochloric Acid Solution together with Quantum Chemical Studies", *Int. J. Mol. Sci.*, 14 (2013) 11915-11928.
17. S. Nofrizal, A. Rahim, B. Saad, P. Raja, A. Shah and S. Yahya, "Elucidation of the Corrosion Inhibition of Mild Steel in 1.0 M HCl by Catechin Monomers from Commercial Green Tea Extracts", *Metall. Mater. Trans. A Phys. Metall. Mater. Sci.*, 43 (2012) 1382-1393.
18. N. Piracha, F. Ito and T. Nakanaga, "Infrared depletion spectroscopy of aniline–toluene cluster: the investigation of the red shifts of the NH<sub>2</sub> stretching vibrations of aniline–aromatic clusters", *Chem. Phys.* 297 (2004) 133-138.
19. A. Chetouani, B. Hammouti, T. Benhadda and M. Daudi, "Inhibitive action of bipyrazolic type organic compounds towards corrosion of pure iron in acidic media", *Appl. Surf. Sci.*, 249 (2005) 375-385.

20. C. Unterberg, A. Gerlach, A. Jansen and M. Gerhards, "Structures and vibrations of neutral and cationic 3- and 4-aminophenol", *Chem. Phys.*, 304 (2004) 237-244.
21. J. Saranya, P. Sounthari, K. Parameswari and S. Chitra, "Acenaphtho[1,2-b]quinoxaline and acenaphtho[1,2-b]pyrazine as corrosion inhibitors for mild steel in acid medium", *Meas. J. Int. Meas. Confed.*, 77 (2016) 175-185.
22. B. Ramezanzadeh, H. Vakili and R. Amini, "The effects of addition of poly(vinyl) alcohol (PVA) as a green corrosion inhibitor to the phosphate conversion coating on the anticorrosion and adhesion properties of the epoxy coating on the steel substrate", *Appl. Surf. Sci.*, 327 (2015) 174-181.
23. M. Singh, K. Bhrara and G. Singh, "The Inhibitory Effect of Diethanolamine on Corrosion of Mild Steel in 0.5 M Sulphuric Acidic Medium", *Port. Electrochim. Acta*, 6 (2008) 479-492.
24. G. Achary, Y. Naik, S. Kumar, T. Venkatesha and B. Sherigara, "An electroactive co-polymer as corrosion inhibitor for steel in sulphuric acid medium", *Appl. Surf. Sci.*, 254 (2008) 5569-5573.
25. P. Singh, V. Srivastava and M. Quraishi, "Novel quinoline derivatives as green corrosion inhibitors for mild steel in acidic medium: Electrochemical, SEM, AFM, and XPS studies", *J. Mol. Liq.*, 216 (2016) 164-173.
26. J. Cruz, T. Pandiyan and E. Ochoa, "A new inhibitor for mild carbon steel: Electrochemical and DFT studies", *J. Electroanal. Chem.*, 583 (2005) 8-16.
27. H. Ju, Z. Kai and Y. Li, "Aminic nitrogen-bearing polydentate Schiff base compounds as corrosion inhibitors for iron in acidic media: A quantum chemical calculation", *Corros. Sci.*, 50 (2008) 865-871.
28. J. Bhawsar, P. K. Jain and P. Jain, "Experimental and computational studies of Nicotiana tabacum leaves extract as green corrosion inhibitor for mild steel in acidic medium", *Alexandria Eng. J.*, 54 (2015) 769.
29. Z. Salarvand, M. Amirnasr, M. Talebian, K. Raeissi, S. Meghdadi, "Enhanced corrosion resistance of mild steel in 1 M HCl solution by trace amount of 2-phenyl-

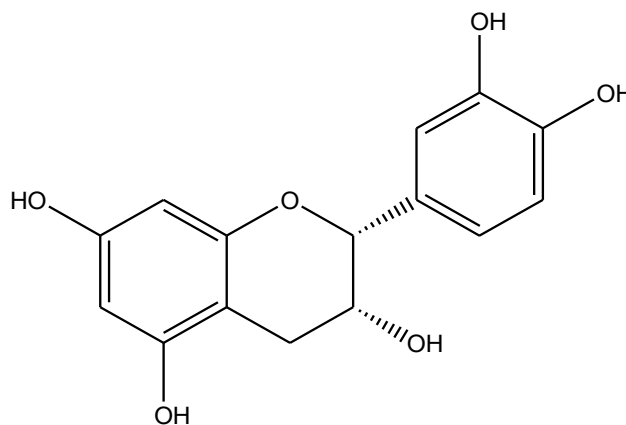
- benzothiazole derivatives: Experimental, quantum chemical calculations and molecular dynamics (MD) simulation studies”, *Corros. Sci.* 114 (2017) 133-145.
30. L. Liao, S. Mo, H. Luo, N. Li, “*Longan* seed and peel as environmentally friendly corrosion inhibitor for mild steel in acid solution: experimental and theoretical studies”, *J. Colloid and interface sci.*, (2016).
31. H. Lgaz, R. Salghi, S. Jodeh, B. Hammout, “Effect of clozapine on inhibition of mild steel corrosion in 1.0 M HCl medium”, *J. Mol. Liquids*, (2016).
32. P. Raja, A. Quraishi, A. Rahim, H. Osman, K. Awang, “*Neolamarckia cadamba* alkaloids as eco-friendly corrosion inhibitors for mild steel in 1 M HCl media”, *Corrosion Science* 69 (2013) 292–301.
33. S. Nofrizal, A. Rahim, B. Saad, P. Raja, M. Shah, and S. Yahya, “Elucidation of the Corrosion Inhibition of Mild Steel in 1.0 M HCl by Catechin Monomers from Commercial Green Tea Extracts”, *The Minerals, Metals & Materials Society*, ASM international, (2011).

## **Chapter 3**

### **Results and Discussion**

### 3.1 *Saraca ashoka* [J. Mol. Liq. 258 (2018) 89-97]

*Saraca ashoka* is a plant belonging to Legume family. It has been reported in literature that the seeds of *Saraca ashoka* contain Epicatechin [1] which is shown in Fig. 3.1. The seeds of *Saraca ashoka* were chosen to study its corrosion inhibition performance.



Epicatechin

Fig. 3.1: Chemical structure of Epicatechin.

#### 3.1.1 Weight loss studies

The corrosion inhibition efficiency ( $\eta$  %), corrosion rate (CR) and surface coverage ( $\Theta$ ) at various concentrations (25-100 mg/L) of *Saraca ashoka* extract as assessed by weight loss technique have been reported in Table 3.1.1. From Table 3.1.1, obviously increment in inhibition efficiency happens on expanding the inhibitor concentration. This is because when inhibitor adsorbs on the metal surface then a protective layer is formed on metal surface which reduces the corrosion reaction [2-3].

**Table 3.1.1:** The data of weight loss for mild steel in 0.5 M H<sub>2</sub>SO<sub>4</sub> without and with different concentrations of *Saraca ashoka* extract.

C mg/ L	298 K			308 K			318 K		
	CR (mm/ Y)	Θ	η%	CR (mm/Y )	Θ	η%	CR (mm/Y)	Θ	η%
0	26.11	-	-	41.46	-	-	62.88	-	-
25	7.33	0.7193	71.93	13.00	0.6868	68.68	22.10	0.6489	64.89
50	5.80	0.7779	77.79	11.50	0.7225	72.25	20.06	0.6814	68.14
75	4.54	0.8252	82.52	9.51	0.7706	77.06	16.94	0.7308	73.08
100	2.60	0.8998	89.98	7.94	0.8199	81.99	14.34	0.7721	77.21

### 3.1.2 Adsorption isotherm

The plots of  $C/\Theta$  vs.  $C$  for *Saraca ashoka* extract as indicated by Langmuir adsorption isotherm equation as discussed in chapter 2 are appeared in Fig.3.1.1. The estimation of  $K_{ads}$  were computed from the intercept of Fig.3.1.1 and detailed in Table 3.1.2.

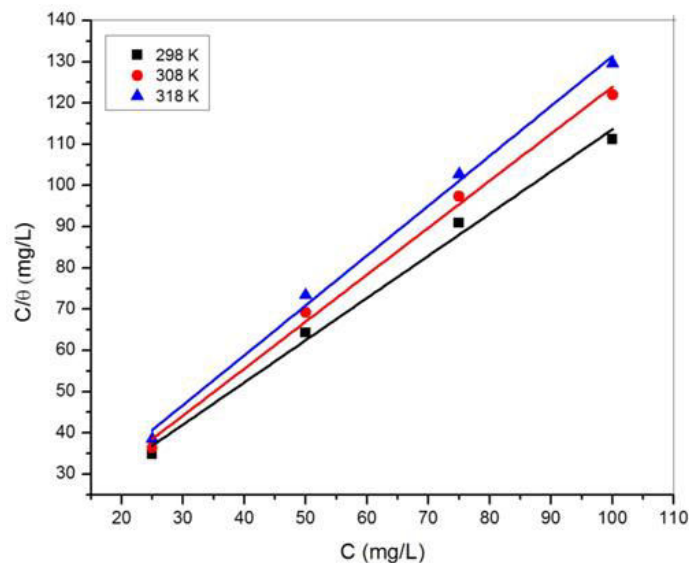


Fig.3.1.1: Langmuir adsorption isotherm for *Saraca ashoka* extract on mild steel in 0.5 M H<sub>2</sub>SO<sub>4</sub>.

Table 3.1.2: Adsorption parameters for mild steel in 0.5 M H<sub>2</sub>SO<sub>4</sub> at optimum concentration of *Saraca ashoka* inhibitor.

Temperature (K)	$K_{ads}$ (Lmg <sup>-1</sup> )	Slope	$R^2$
298	89.98	1.02	0.9899
308	45.52	1.13	0.9938
318	33.87	1.20	0.9946

### 3.1.3 Potentiodynamic polarization studies

Concentration impact of *Saraca ashoka* extract on the polarization character of mild steel in 0.5 M H<sub>2</sub>SO<sub>4</sub> was analysed and the Tafel plots were recorded for various inhibitor concentrations which are appeared in Fig.3.1.2. The parameters, including corrosion

potential ( $E_{\text{corr}}$ ), corrosion current density ( $I_{\text{corr}}$ ), anodic and cathodic Tafel slopes ( $\beta_a$  and  $\beta_c$ ) and inhibition efficiency ( $\eta$  %) ascertained by equation discussed in chapter 2, are reported in Table 3.1.3. It is clear that the maximum shift in the  $E_{\text{corr}}$  with respect to blank solution was 24 mV, which is within 85 mV, recommended that the contemplated inhibitor goes about as a mixed sort corrosion inhibitor [4-5]. The relatively unaffected anodic and cathodic Tafel slopes when including *Saraca ashoka* extract show that the anodic and cathodic reaction mechanisms are still controlled by charge transfer. It can be seen from Table 3.1.3 that with expanding concentration of *Saraca ashoka* extract, the corrosion current density diminishes and the maximum inhibition effectiveness is accomplished at the concentration of 100 mg/L.

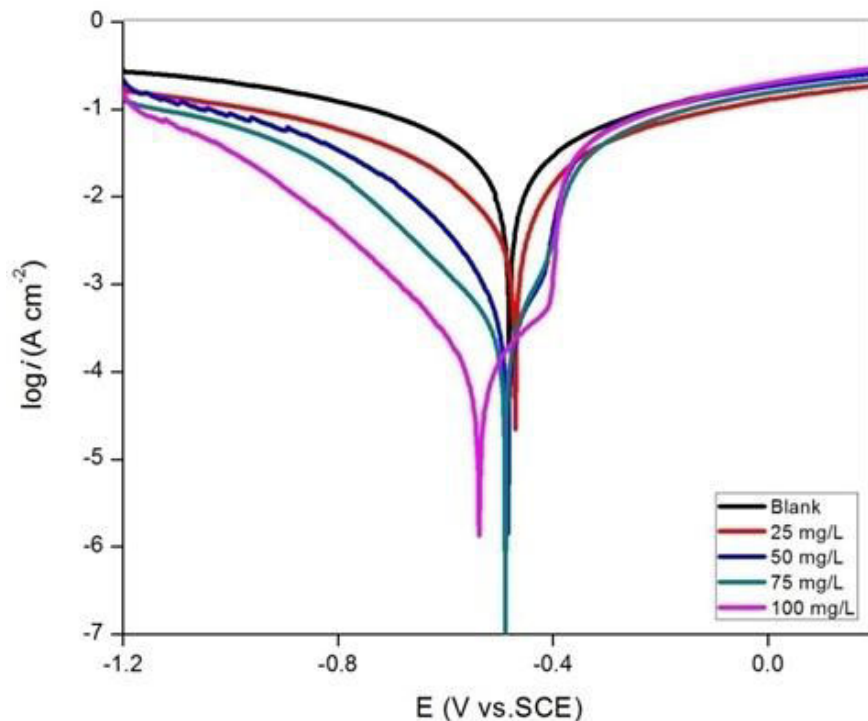


Fig.3.1.2: Tafel polarization curves for mild steel in 0.5 M H<sub>2</sub>SO<sub>4</sub> without and with different concentrations of *Saraca ashoka* extract.

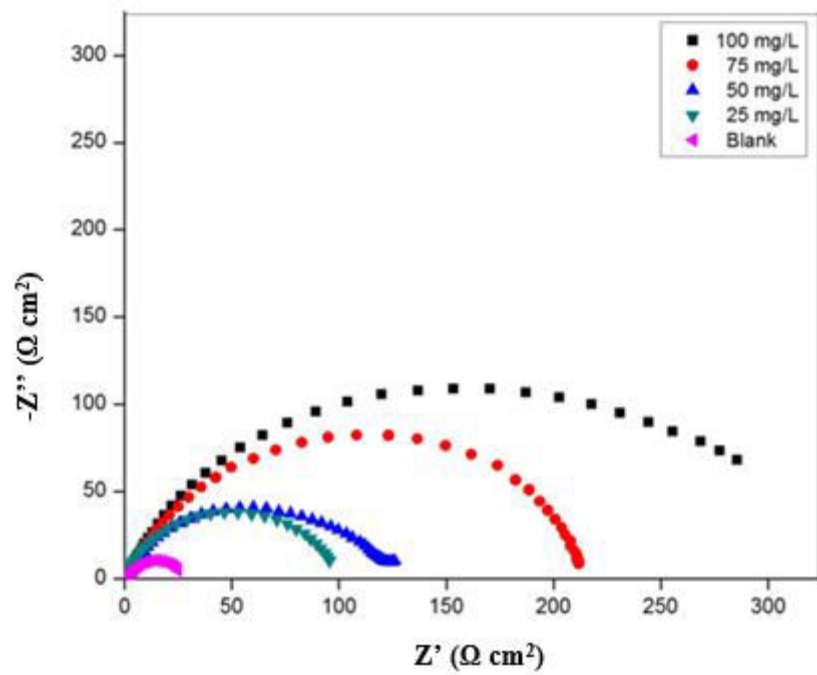


Table 3.1.3: Polarization parameters for mild steel in 0.5 M H<sub>2</sub>SO<sub>4</sub> without and with different concentrations of *Saraca ashoka* extract.

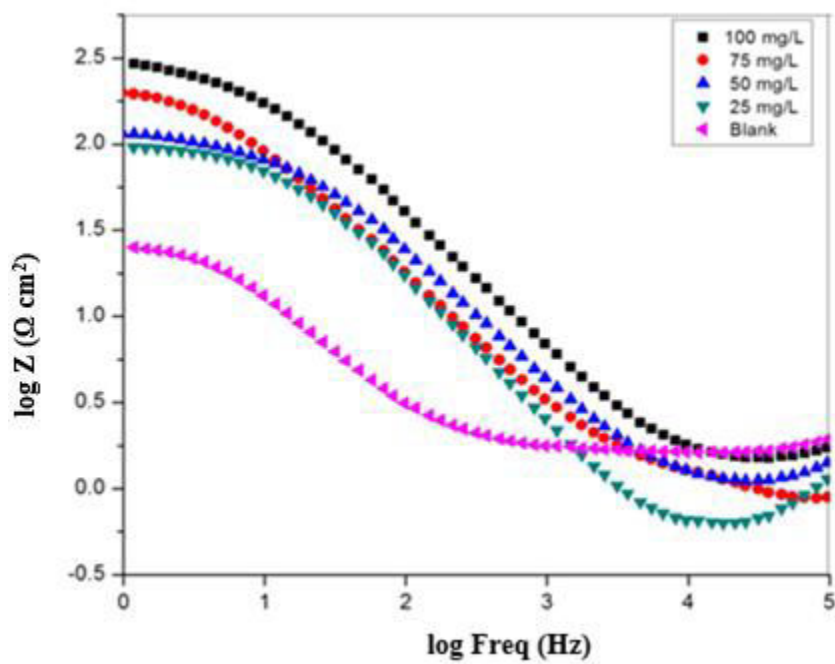
<b>Inhibitor concentration (mg/L)</b>	<b><math>E_{corr}</math> (V vs. SCE)</b>	<b><math>I_{corr}</math> (A cm<sup>-2</sup>)</b>	<b><math>\beta_a</math> (V/dec)</b>	<b><math>-\beta_c</math> (V/dec)</b>	<b>Efficiency (<math>\eta</math> %)</b>
0	-0.465	0.008909	141.66	164.25	0
25	-0.489	0.001851	91.44	122.91	79.22
50	-0.482	0.001254	79.15	106.23	86.01
75	-0.471	0.000857	51.43	104.25	90.37
100	-0.452	0.000402	57.44	117.86	95.48

### 3.1.4 Electrochemical impedance spectroscopy (EIS) studies

The EIS parameters for mild steel in the absence and presence of various concentrations of *Saraca ashoka* extract are appeared in Table 3.1.4 and the EIS curves (Nyquist and Bode plots) are shown in Fig.3.1.3. The EIS spectra of all tests were analyzed using the equivalent circuit shown in Fig. 2.2 as discussed in chapter 2. This circuit is a parallel combination of charge transfer resistance ( $R_{ct}$ ) and the constant phase element (CPE). This type of electrochemical equivalent circuit was reported previously to model the ion/acid interface [30 of thesis, page 63]. In Nyquist graph, due to the charge transfer resistance, a semicircle in each curve stands for a time constant. Expanding *Saraca ashoka* extract concentration increases the diameter of semicircle from 25 mg/L to 100 mg/L, which suggests an advancement of inhibition impact. The CPE value decreases on increasing the concentration of the inhibitor, indicating the decrease in local dielectric constant or an increase in the thickness of the electrical double layer, suggesting that the inhibitor molecules are adsorbed at metal/solution interface.



(a)



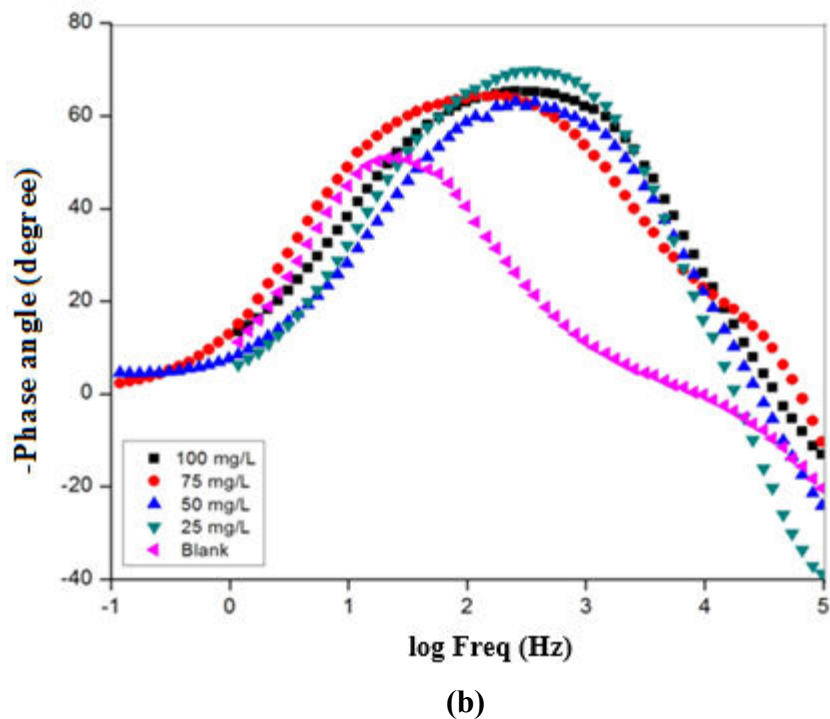


Fig.3.1.3: Nyquist (a) and Bode (b) plots for MS in 0.5 M H<sub>2</sub>SO<sub>4</sub> without and with various concentrations of *Saraca ashoka* extract at 298 K.

The single peak obtained in Bode plots (Fig. 3.1.3 b) for the inhibitor indicates that the electrochemical impedance measurements were fit well in one-time constant equivalent model with constant phase element (CPE). The magnitude of impedance is larger in the presence of inhibitor than in the absence of inhibitor and the value of impedance increases on increasing the concentration of inhibitor which means that the corrosion rate is reduced in the presence of inhibitor and continued to decreasing on increasing the concentration of inhibitors.

Table 3.1.4: EIS parameters for mild steel in 0.5 M H<sub>2</sub>SO<sub>4</sub> without and with different concentrations of *Saraca ashoka* extract.

Acid Solution	Concentration of inhibitor (mg/L)	$R_{ct}$ ( $\Omega$ cm <sup>2</sup> )	$CPE$ ( $\mu$ F cm <sup>-2</sup> )	Efficiency ( $\eta$ %)
0.5 M H <sub>2</sub> SO <sub>4</sub>	0	25.16	$1.3 \times 10^{-3}$	0
	25	102.66	$1.5 \times 10^{-4}$	75.48
	50	138.02	$1.0 \times 10^{-4}$	81.76
	75	220.14	$6.0 \times 10^{-5}$	88.56
	100	364.19	$4.9 \times 10^{-5}$	93.09

### 3.1.5 FTIR analysis

The obtained FTIR spectra of *Saraca ashoka* extract is shown in Fig. 3.1.4. In the FTIR spectra the stretching vibration of O-H causes the peak focused at 3379.40 cm<sup>-1</sup> and the peak at 1013.52 cm<sup>-1</sup> is credited to the stretching vibration of C-O. The aromatic ring framework vibration results in some bands at 1602.50 cm<sup>-1</sup>. The outcomes from FTIR spectroscopy demonstrates that the corrosion inhibition property of *Saraca ashoka* is because of the presence of O atoms and aromatic rings in the compounds which exist in extract.

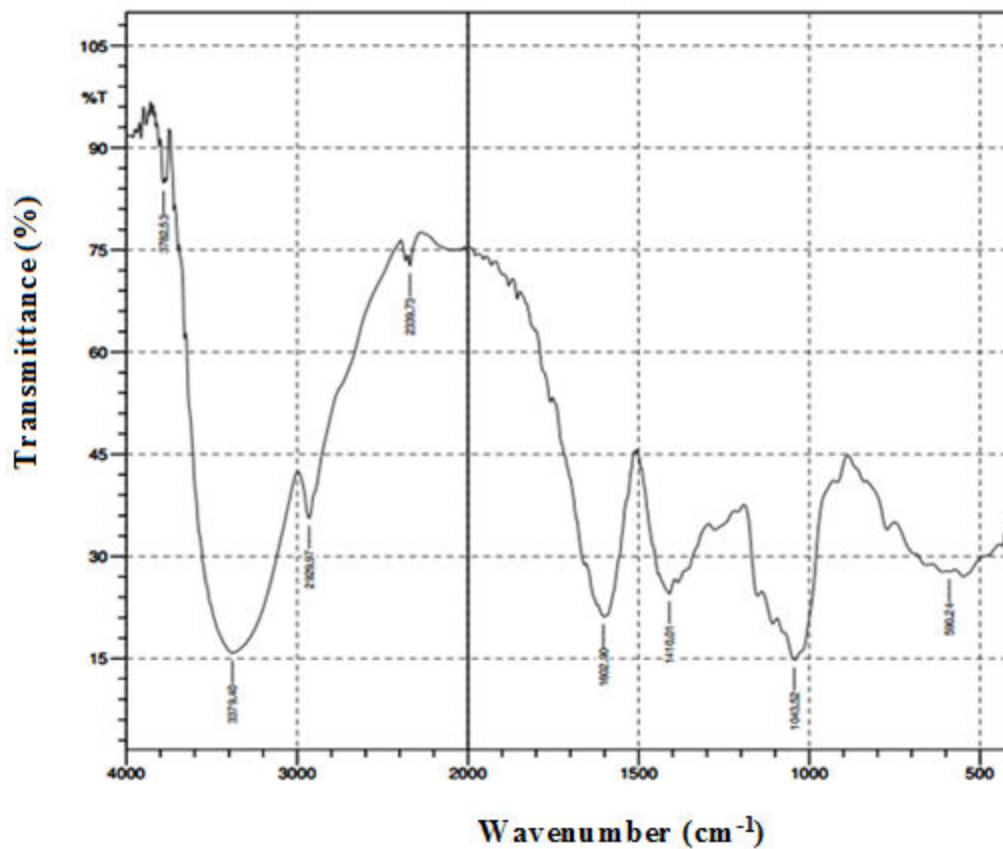


Fig.3.1.4: FTIR spectrum of *Saraca ashoka* extract.

### 3.1.6 UV-Visible spectroscopy

The UV spectra of *Saraca ashoka* extract before and after the corrosion test were contemplated and they have been appeared in Fig.3.1.5. The value of absorption maximum ( $\lambda_{max}$ ) or a change in the value of absorbance recommended the formation of a complex between the steel surface and inhibitor molecules.

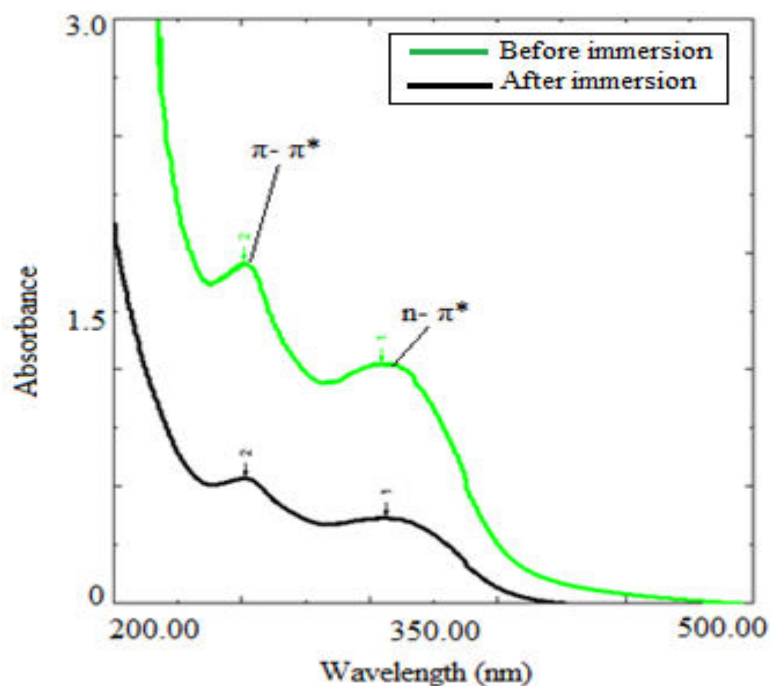


Fig.3.1.5: UV Spectra of *Saraca ashoka* extract before and after the corrosion test.

### 3.1.7 Surface studies

The SEM and AFM images of the mild steel immersed in 0.5 M H<sub>2</sub>SO<sub>4</sub> in the presence of *Saraca ashoka* extract are shown in Fig.3.1.6. These SEM and AFM micrographs were compared with the SEM and AFM images of the mild steel immersed in 0.5 M H<sub>2</sub>SO<sub>4</sub> without inhibitor. From the SEM image it is clear that the surface has astoundingly enhanced concerning its smoothness extensive lessening of corrosion rate. From AFM studies, the value of average surface roughness is 48.60 nm. The change in surface morphology is because of the arrangement of a decent defensive film of inhibitor on mild steel surface which is in charge of corrosion inhibition.

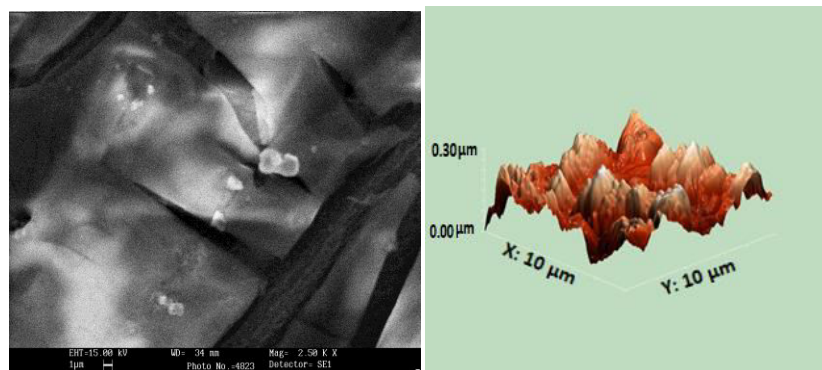


Fig.3.1.6: SEM and AFM images of mild steel immersed in 0.5 M H<sub>2</sub>SO<sub>4</sub> in the presence of *Saraca ashoka* extract.

### 3.1.8 Quantum chemical studies

The optimized structures of main constituents (Epicatechin) of *Saraca ashoka* extract are appeared in Fig. 3.1.7 and the corresponding quantum chemical parameters are reported in Table 3.1.5. The higher estimations of E<sub>HOMO</sub> and lower estimations of E<sub>LUMO</sub> recommend the power of inhibitor to get adsorbed on the mild steel surface.

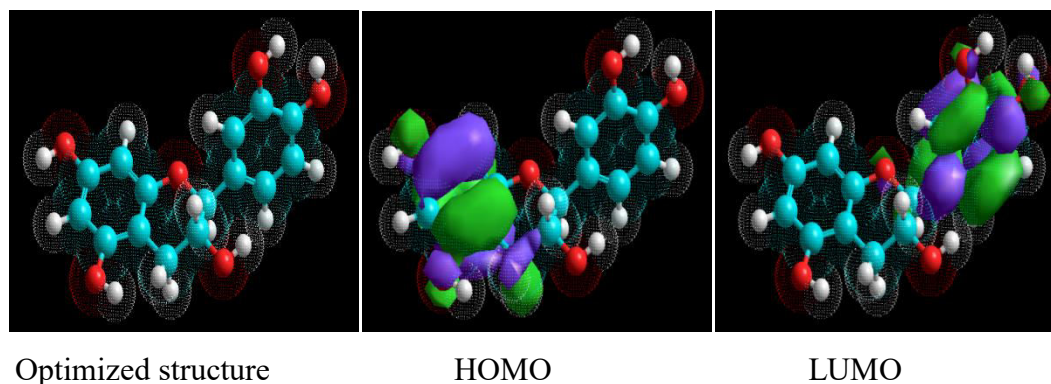


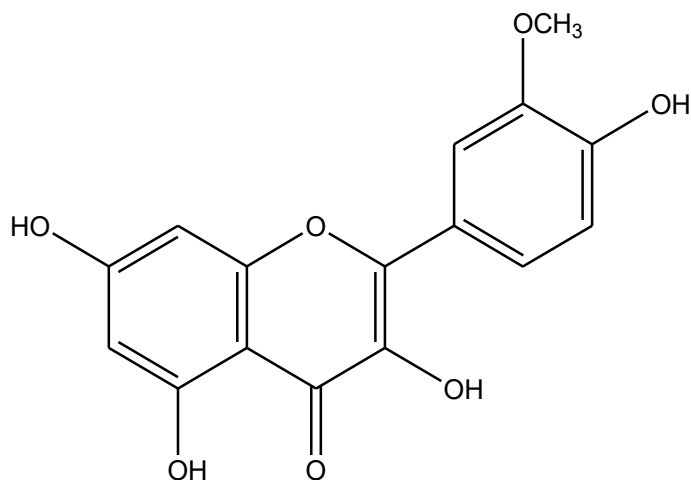
Fig.3.1.7: The optimized structure, HOMO and LUMO distribution for Epicatechin.

Table 3.1.5: Quantum chemical parameters of Epicatechin calculated with DFT method.

Molecule	E <sub>HOMO</sub> (eV)	E <sub>LUMO</sub> (eV)	ΔE (eV)
Epicatechin	-10.81	-0.13	10.67

### 3.2 *Cuscuta reflexa* [Bioelectrochem. 10.1016/j.bioelechem.2018.07.006]

*Cuscuta reflexa* is types of flowering vine in the family Piperaceae. It has been reported in literature that the stems of *Cuscuta reflexa* contain 3-methoxy-3, 4, 5, 7-tetrahydroxy flavone [6] which is shown in Fig. 3.2. The stems of *Cuscuta reflexa* were chosen to study its corrosion inhibition performance.



3-methoxy-3, 4, 5, 7-tetrahydroxy flavone

Fig. 3.2: Chemical structure of 3-methoxy-3, 4, 5, 7-tetrahydroxy flavone.

#### 3.2.1 Weight loss studies

The corrosion inhibition efficiency ( $\eta$  %), corrosion rate (CR), surface coverage ( $\Theta$ ) at various concentrations (100-500 mg/L) of *Cuscuta reflexa* extract as assessed by weight loss technique have been reported in Table 3.2.1. From Table 3.2.1, obviously increment in inhibition efficiency happens on expanding the inhibitor concentration. This is because when inhibitor adsorbs on the metal surface then a protective layer is formed on metal surface which reduces the corrosion reaction [2-3].



**Table 3.2.1:** The data of weight loss for mild steel in 0.5 M H<sub>2</sub>SO<sub>4</sub> without and with different concentrations of *Cuscuta reflexa* extract.

Conc. mg/L	298 K			308 K			318 K		
	CR (mm/Y)	Θ	η%	CR (mm/Y)	Θ	η%	CR (mm/Y)	Θ	η%
0	26.11	-	-	41.46	-	-	62.88	-	-
100	5.93	0.7726	77.26	10.57	0.7449	74.49	18.08	0.7087	70.87
200	4.54	0.8259	82.59	9.04	0.7829	78.29	14.93	0.7625	76.25
300	2.87	0.8898	88.98	6.67	0.8389	83.89	11.64	0.8148	81.48
400	1.90	0.9271	92.71	5.24	0.8736	87.36	9.92	0.8421	84.21
500	1.11	0.9573	95.73	3.33	0.9194	91.94	7.14	0.8864	88.64

### 3.2.2 Adsorption isotherm

The plots of  $C/\theta$  vs.  $C$  for *Cuscuta reflexa* extract as indicated by Langmuir adsorption isotherm equation as discussed in chapter 2 are appeared in Fig.3.2.1. The estimation of  $K_{ads}$  were computed from the intercept of Fig.3.2.1 and detailed in Table 3.2.2.

Table 3.2.2: Adsorption parameters for mild steel in 0.5 M H<sub>2</sub>SO<sub>4</sub> at optimum concentration of *Cuscuta reflexa* inhibitor.

Temperature (K)	$K_{ads}$ (Lmg <sup>-1</sup> )	Slope	$R^2$
298	44.83	0.97	0.9976
308	22.81	1.02	0.9950
318	15.60	1.05	0.9963

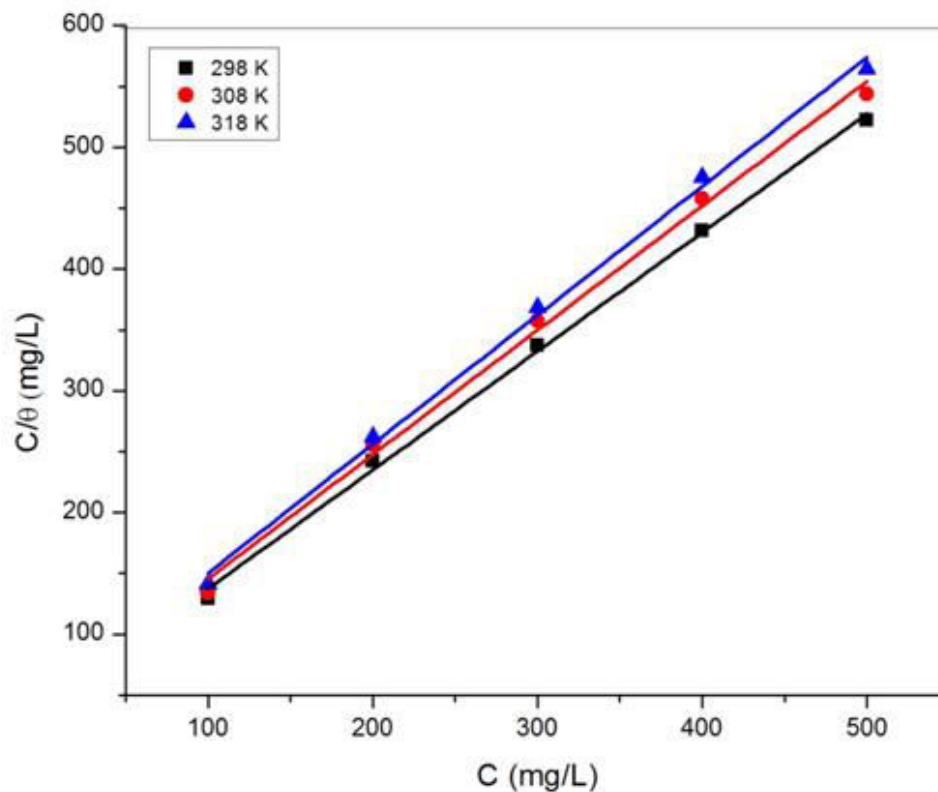


Fig.3.2.1: Langmuir adsorption isotherm for *Cuscuta reflexa* extract on mild steel in 0.5 M H<sub>2</sub>SO<sub>4</sub>.

### 3.2.3 Potentiodynamic polarization studies

Concentration impact of *Cuscuta reflexa* extract on the polarization character of mild steel in 0.5 M H<sub>2</sub>SO<sub>4</sub> was analysed and the Tafel plots were recorded for various inhibitor concentrations which are appeared in Fig.3.2.2. The parameters, including corrosion potential ( $E_{\text{corr}}$ ), corrosion current density ( $I_{\text{corr}}$ ), anodic and cathodic Tafel slopes ( $\beta_a$  and  $\beta_c$ ) and inhibition efficiency ( $\eta$  %) ascertained by equation discussed in chapter 2, are reported in Table 3.2.3.

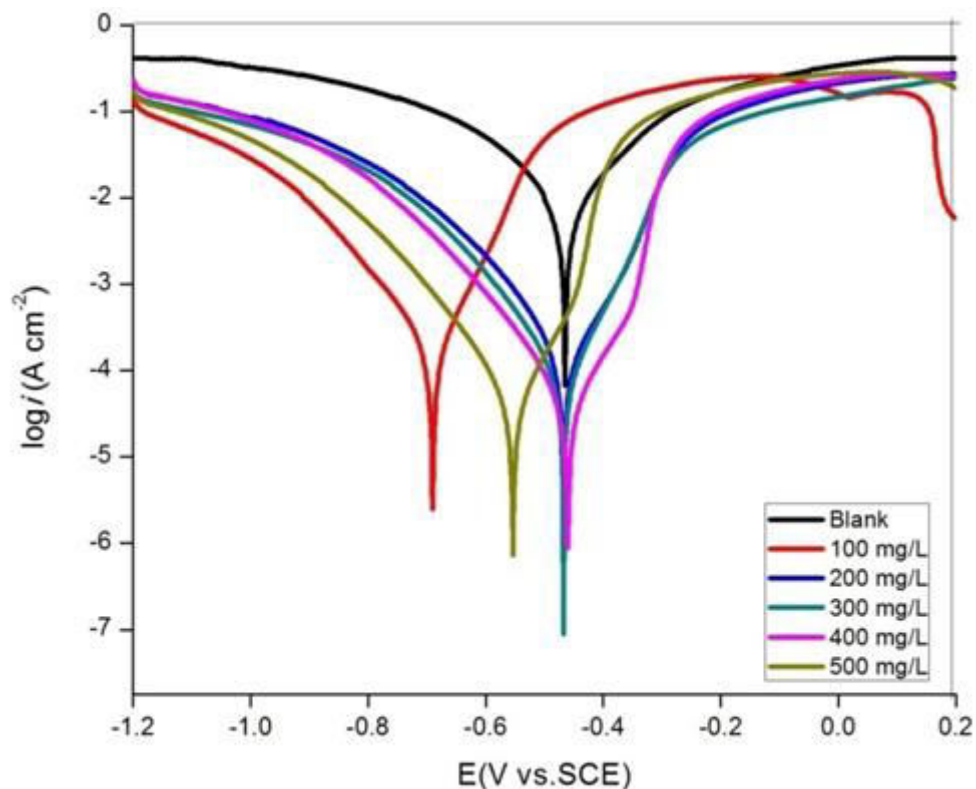


Fig.3.2.2: Tafel polarization curves for mild steel in 0.5 M  $\text{H}_2\text{SO}_4$  without and with different concentrations of *Cuscuta reflexa* extract.

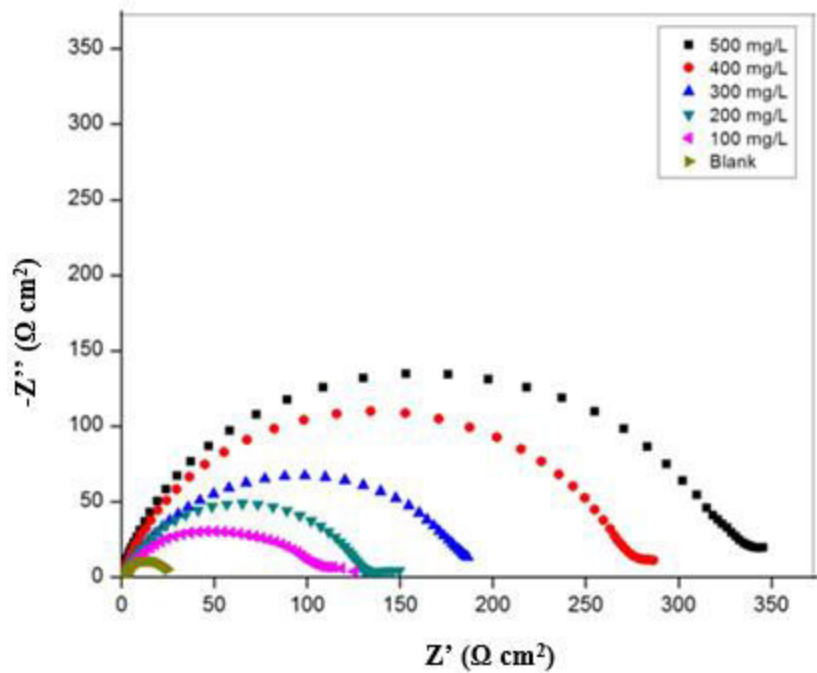
It is clear that the maximum shift in the  $E_{\text{corr}}$  with respect to blank solution was 79 mV, which is within 85 mV, recommended that the contemplated inhibitor goes about as a mixed sort corrosion inhibitor [4-5]. The relatively unaffected anodic and cathodic Tafel slopes when including *Cuscuta reflexa* extract show that the anodic and cathodic reaction mechanisms are still controlled by charge transfer. It can be seen from Table 3.2.3 that with expanding concentration of *Cuscuta reflexa* extract, the corrosion current density diminishes and the maximum inhibition effectiveness is accomplished at the concentration of 500 mg/L.

Table 3.2.3: Polarization parameters for mild steel in 0.5 M H<sub>2</sub>SO<sub>4</sub> without and with different concentrations of *Cuscuta reflexa* extract.

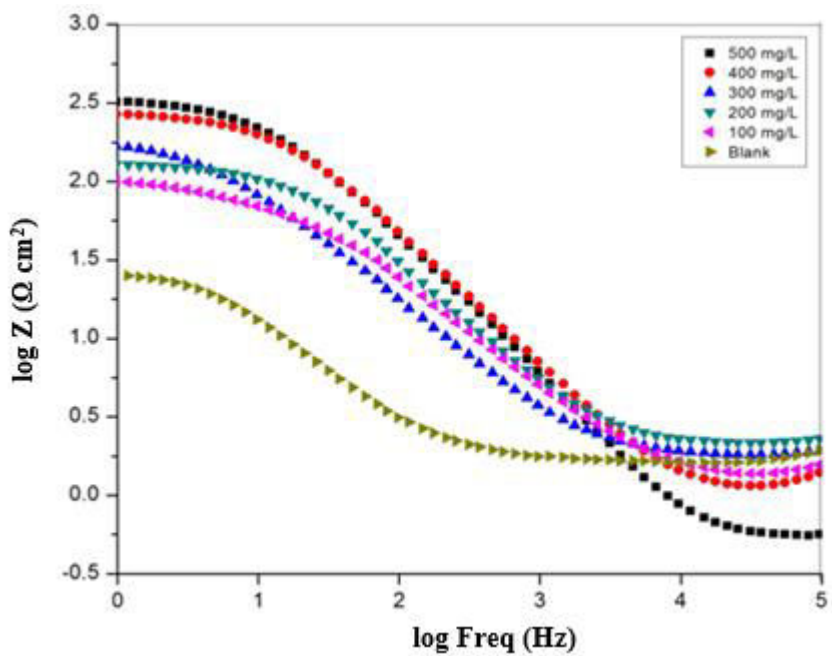
<b>Inhibitor concentration (mg/L)</b>	<b><math>E_{corr}</math> (V vs. SCE)</b>	<b><math>I_{corr}</math> (A cm<sup>-2</sup>)</b>	<b><math>\beta_a</math> (V/dec)</b>	<b><math>-\beta_c</math> (V/dec)</b>	<b>Efficiency (<math>\eta</math> %)</b>
0	-0.465	0.0008909	141.66	164.25	0
100	-0.490	0.0002125	71.13	125.77	76.14
200	-0.468	0.0001537	81.25	115.07	82.74
300	-0.468	0.0001074	73.43	109.98	87.94
400	-0.460	0.00008085	78.62	111.54	90.92
500	-0.544	0.00004028	67.79	110.90	95.47

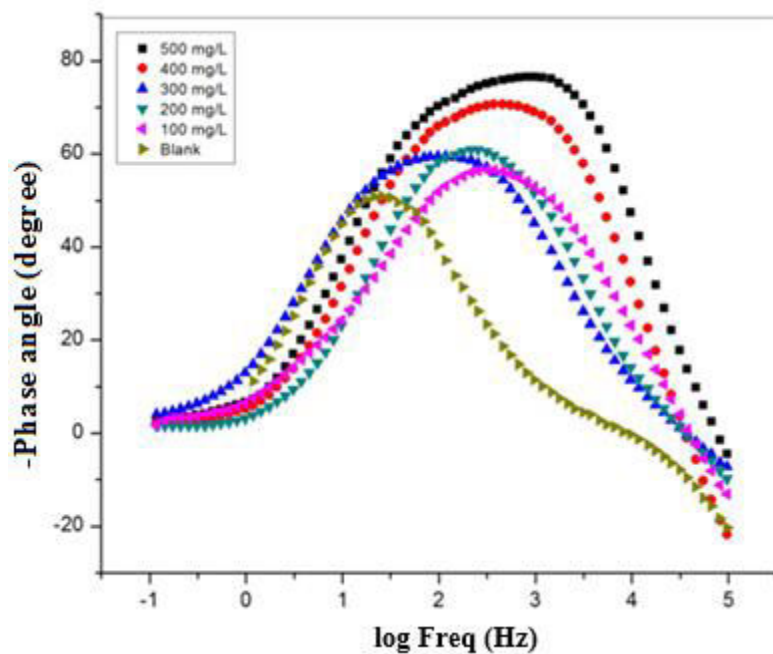
### 3.2.4 Electrochemical impedance spectroscopy (EIS) studies

The EIS parameters for mild steel in the absence and presence of various concentrations of *Cuscuta reflexa* extract are appeared in Table 3.2.4 and the EIS curves (Nyquist and Bode plots) are shown in Fig.3.2.3. In Nyquist graph, due to the charge transfer resistance, a semicircle in each curve stands for a time constant. Expanding *Cuscuta reflexa* extract concentration increases the diameter of semicircle from 100 mg/L to 500 mg/L, which suggests an advancement of inhibition impact.



(a)





(b)

Fig.3.2.3: Nyquist (a) and Bode (b) plots for MS in 0.5 M H<sub>2</sub>SO<sub>4</sub> without and with various concentrations of *Cuscuta reflexa* extract at 298 K.

Table 3.2.4: EIS parameters for mild steel in 0.5 M H<sub>2</sub>SO<sub>4</sub> without and with different concentrations of *Cuscuta reflexa* extract.

Acid Solution	Concentration of inhibitor (mg/L)	$R_{ct}$ ( $\Omega$ cm <sup>2</sup> )	$CPE$ ( $\mu$ F cm <sup>-2</sup> )	Efficiency ( $\eta$ %)
0.5 M H <sub>2</sub> SO <sub>4</sub>	0	25.164	$1.3 \times 10^{-3}$	0
	100	106.384	$1.0 \times 10^{-4}$	76.34
	200	137.358	$6.6 \times 10^{-5}$	81.67
	300	199.559	$4.6 \times 10^{-5}$	87.39
	400	285.091	$4.5 \times 10^{-5}$	91.17
	500	362.310	$4.4 \times 10^{-5}$	93.05

### 3.2.5 FTIR analysis

The obtained FTIR spectra of *Cuscuta reflexa* extract is shown in Fig. 3.2.4. In the FTIR spectra the stretching vibration of O-H causes the peak focused at  $3420.06\text{ cm}^{-1}$  and the peak at  $1645.33\text{ cm}^{-1}$  is credited to the stretching vibration of C=O. The aromatic ring framework vibration results in some bands at  $1402.66\text{ cm}^{-1}$ . The outcomes from FTIR spectroscopy demonstrates that the corrosion inhibition property of *Cuscuta reflexa* is because of the presence of O atoms and aromatic rings in the compounds which exist in extract.

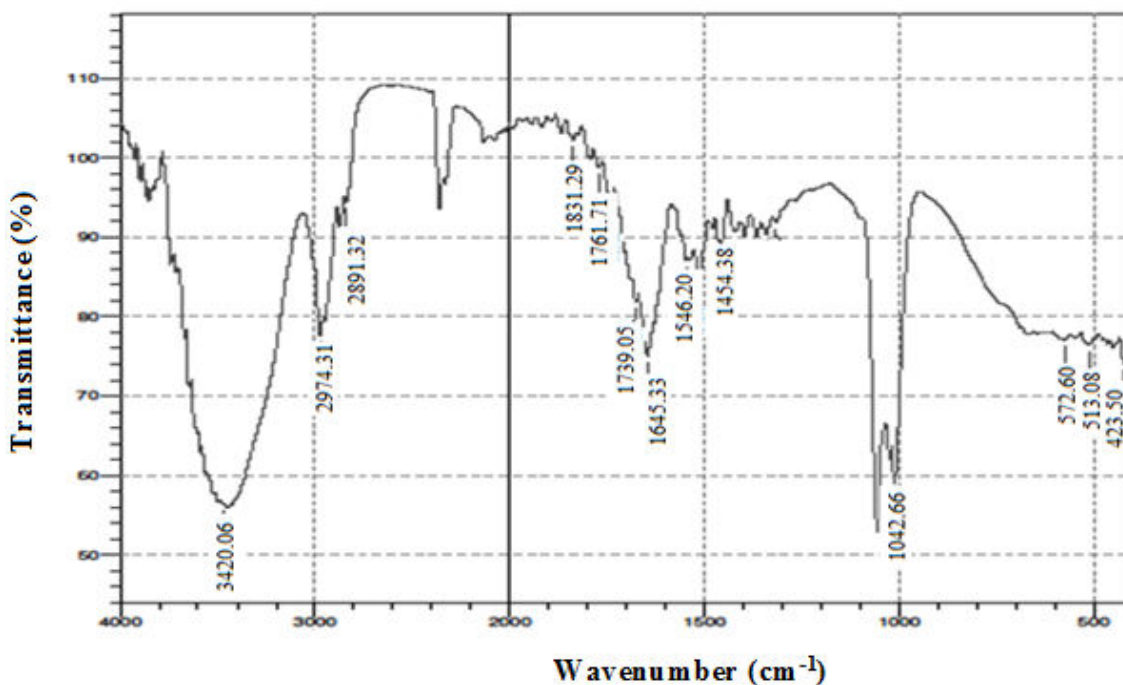


Fig.3.2.4: FTIR spectrum of *Cuscuta reflexa* extract.

### 3.2.6 UV-Visible spectroscopy

The UV spectra of *Cuscuta reflexa* extract before and after the corrosion test were contemplated and they have been appeared in Fig.3.2.5. The value of absorption maximum ( $\lambda_{max}$ ) or a change in the value of absorbance recommended the formation of a complex between the steel surface and inhibitor molecules.

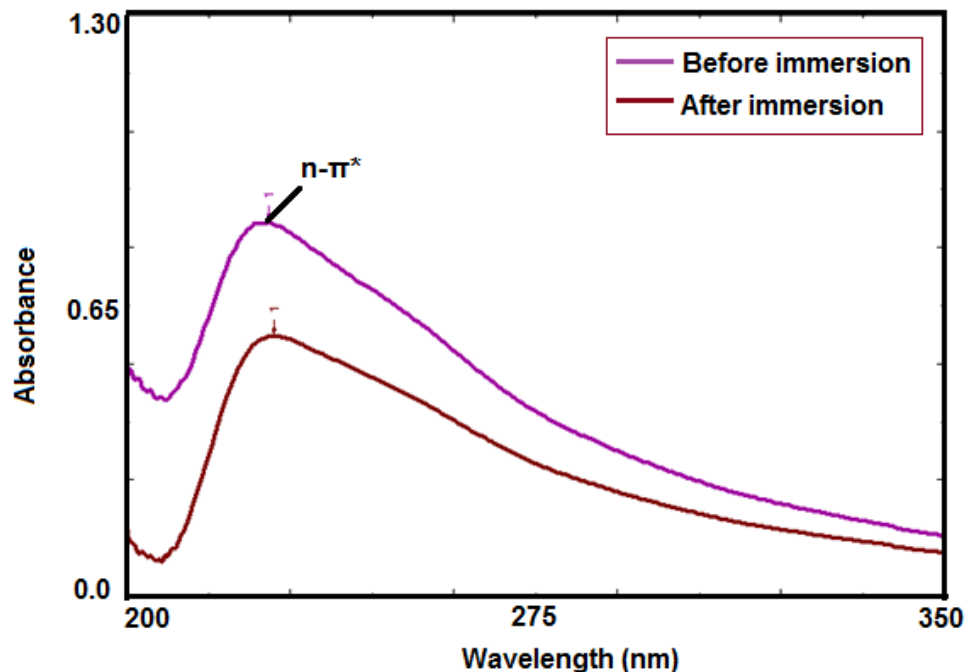


Fig.3.2.5: UV Spectra of *Cuscuta reflexa* extract before and after the corrosion test.

### 3.2.7 Surface studies

The SEM and AFM images of the mild steel immersed in 0.5 M H<sub>2</sub>SO<sub>4</sub> in the presence of *Cuscuta reflexa* extract are shown in Fig.3.2.6. These SEM and AFM micrographs were compared with the SEM and AFM images of the mild steel immersed in 0.5 M H<sub>2</sub>SO<sub>4</sub> without inhibitor. From the SEM image it is clear that the surface has astoundingly enhanced concerning its smoothness extensive lessening of corrosion rate. From AFM studies, the value of average surface roughness is 14.36 nm. The change in surface morphology is because of the arrangement of a decent defensive film of inhibitor on mild steel surface which is in charge of corrosion inhibition.



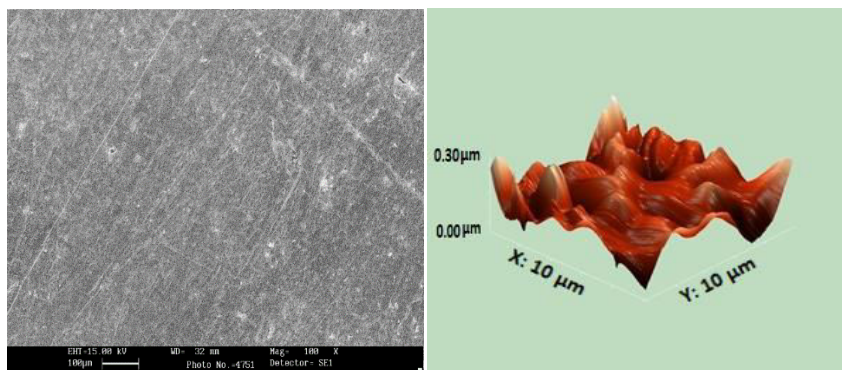


Fig.3.2.6: SEM and AFM images of mild steel immersed in 0.5 M H<sub>2</sub>SO<sub>4</sub> in the presence of *Cuscuta reflexa* extract.

### 3.2.8 Quantum chemical studies

The optimized structures of main constituents of *Cuscuta reflexa* extract are appeared in Fig. 3.2.7 and the corresponding quantum chemical parameters are reported in Table 3.2.5. The higher estimations of E<sub>HOMO</sub> and lower estimations of E<sub>LUMO</sub> recommend the power of inhibitor to get adsorbed on the mild steel surface.

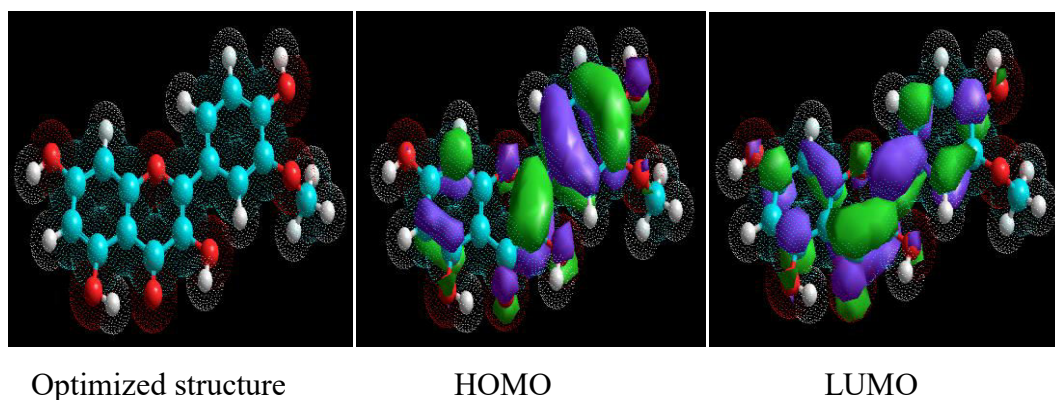


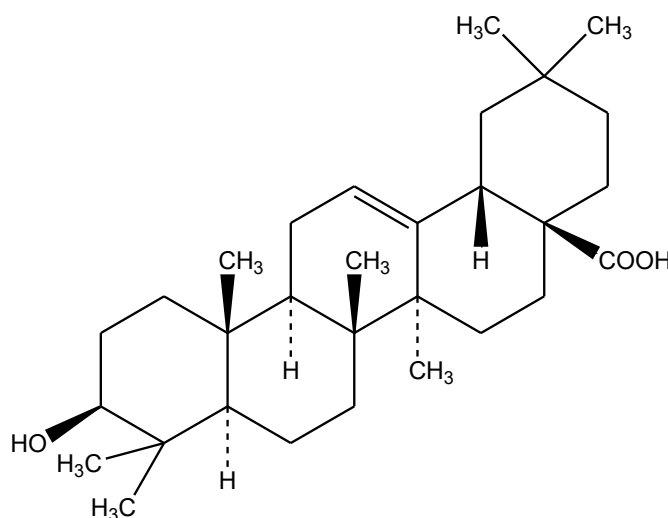
Fig.3.2.7: The optimized structure, HOMO and LUMO distribution for 3-methoxy-3, 4, 5, 7-tetrahydroxy flavone

Table 3.2.5: Quantum chemical parameters of 3-methoxy-3, 4, 5, 7-tetrahydroxy flavone calculated with DFT method.

<b>Molecule</b>	<b>E<sub>HOMO</sub> (eV)</b>	<b>E<sub>LUMO</sub> (eV)</b>	<b>ΔE (eV)</b>
<b>3-methoxy-3,4,5,7-tetrahydroxy</b>	-10.031	-3.278	6.353

### 3.3 *Achyranthes aspera* (J. Fail. Anal. And Preven., <http://doi.org/10.1007/s11668-018-0491-8>)

*Achyranthes aspera* is a species of plant in the Amaranthaceae family. It has been reported in literature that the roots of *Achyranthes aspera* contain Oleanolic acid [7] which is shown in Fig. 3.3. The roots of *Achyranthes aspera* were chosen to study its corrosion inhibition performance.



Oleanolic acid

Fig. 3.3: Chemical structure of Oleanolic acid.

#### 3.3.1 Weight loss studies

The corrosion inhibition efficiency ( $\eta$  %), corrosion rate (CR) and surface coverage ( $\Theta$ ) at various concentrations (100-500 mg/L) of *Achyranthes aspera* extract as assessed by weight loss technique have been reported in Table 3.3.1. From Table 3.3.1, obviously increment in inhibition efficiency happens on expanding the inhibitor concentration. This is because when inhibitor adsorbs on the metal surface then a protective layer is formed on metal surface which reduces the corrosion reaction [2-3].

**Table 3.3.1:** The data of weight loss for mild steel in 0.5 M H<sub>2</sub>SO<sub>4</sub> without and with different concentrations of *Achyranthes aspera* extract.

Conc. mg/L	298 K			308 K			318 K		
	CR (mm/ Y)	Θ	η%	CR (mm/Y)	Θ	η%	CR (mm/Y)	Θ	η%
0	26.11	-	-	41.46	-	-	62.88	-	-
100	6.35	0.7566	75.66	12.66	0.6946	69.46	23.05	0.6334	63.34
200	4.96	0.8099	80.99	10.38	0.7494	74.94	20.31	0.6769	67.69
300	4.31	0.8348	83.48	8.90	0.7852	78.52	17.43	0.7227	72.27
400	2.92	0.8880	88.80	7.69	0.8143	81.43	14.88	0.7632	76.32
500	2.36	0.9094	90.94	6.91	0.8333	83.33	14.70	0.7662	76.62

### 3.3.2 Adsorption isotherm

The plots of  $C/\Theta$  vs.  $C$  for *Achyranthes aspera* extract as indicated by Langmuir adsorption isotherm equation as discussed in chapter 2 are appeared in Fig.3.3.1. The estimation of  $K_{ads}$  were computed from the intercept of Fig.3.3.1 and detailed in Table 3.3.2.

Table 3.3.2: Adsorption parameters for mild steel in 0.5 M H<sub>2</sub>SO<sub>4</sub> at optimum concentration of *Achyranthes aspera* inhibitor.

Temperature (K)	$K_{ads}$ (Lmg <sup>-1</sup> )	Slope	$R^2$
298	20.07	1.03	0.9970
308	9.99	1.13	0.9990
318	6.55	1.21	0.9981

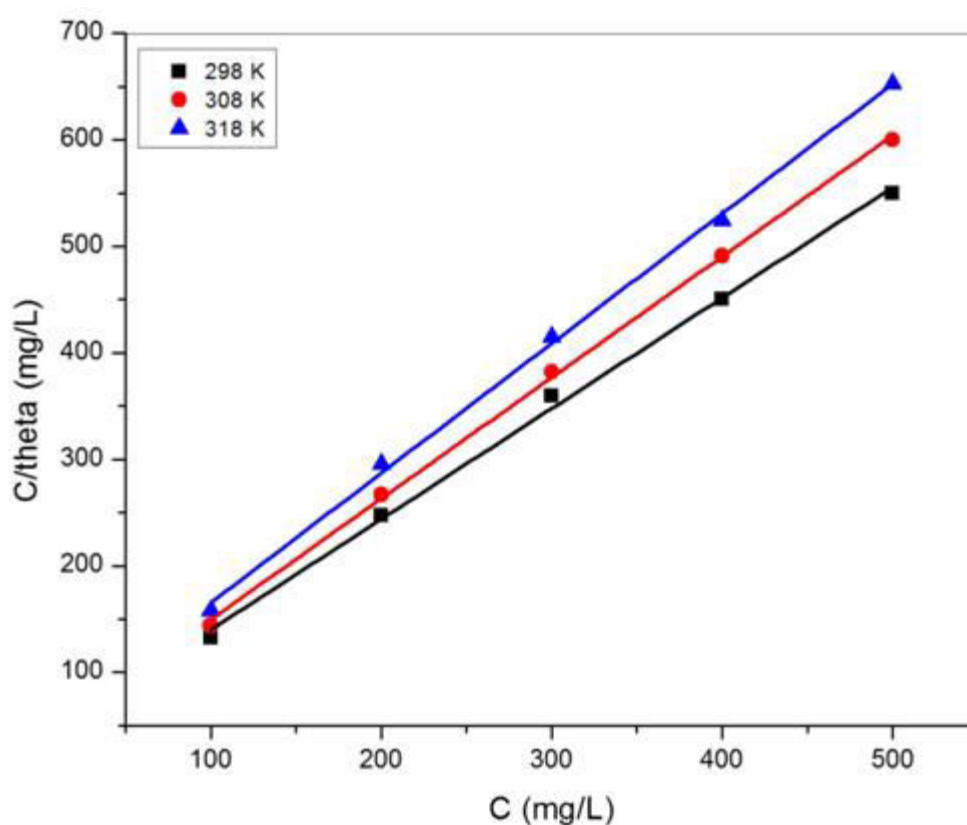


Fig.3.3.1: Langmuir adsorption isotherm for *Achyranthes aspera* extract on mild steel in 0.5 M H<sub>2</sub>SO<sub>4</sub>.

### 3.3.3 Potentiodynamic polarization studies

Concentration impact of *Achyranthes aspera* extract on the polarization character of mild steel in 0.5 M H<sub>2</sub>SO<sub>4</sub> was analysed and the Tafel plots were recorded for various inhibitor

concentrations which are appeared in Fig.3.3.2. The parameters, including corrosion potential ( $E_{\text{corr}}$ ), corrosion current density ( $I_{\text{corr}}$ ), anodic and cathodic Tafel slopes ( $\beta_a$  and  $\beta_c$ ) and inhibition efficiency ( $\eta$  %) ascertained by equation discussed in chapter 2, are reported in Table 3.3.3.

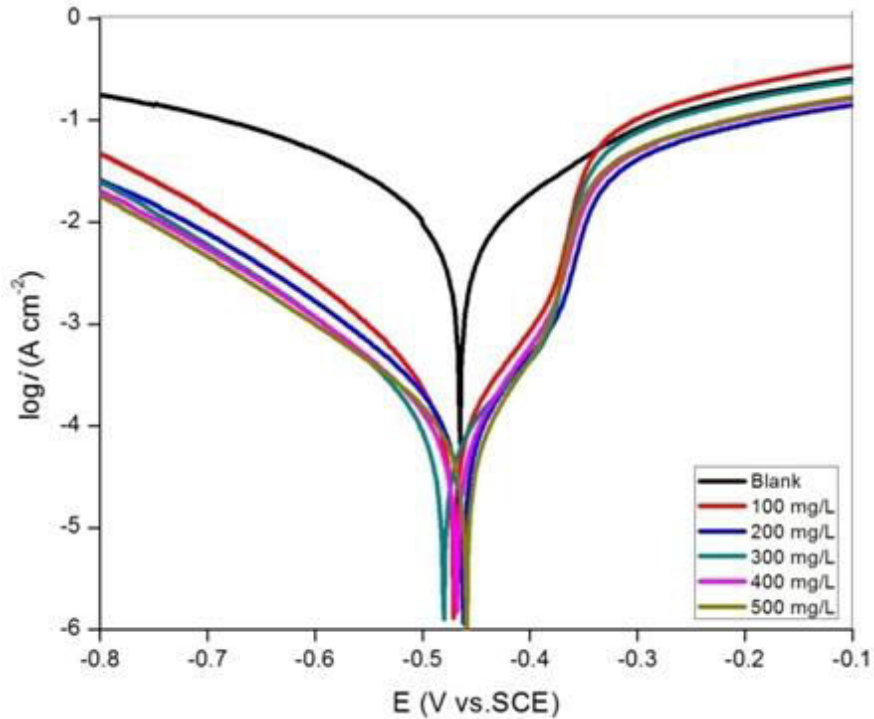


Fig.3.3.2: Tafel polarization curves for mild steel in 0.5 M H<sub>2</sub>SO<sub>4</sub> without and with different concentrations of *Achyranthes aspera* extract.

It is clear that the maximum shift in the  $E_{\text{corr}}$  with respect to blank solution was 15 mV, which is within 85 mV, recommended that the contemplated inhibitor goes about as a mixed sort corrosion inhibitor [4-5]. The relatively unaffected anodic and cathodic Tafel slopes when including *Achyranthes aspera* extract show that the anodic and cathodic reaction mechanisms are still controlled by charge transfer. It can be seen from Table 3.3.3 that with expanding concentration of *Achyranthes aspera* extract, the corrosion current

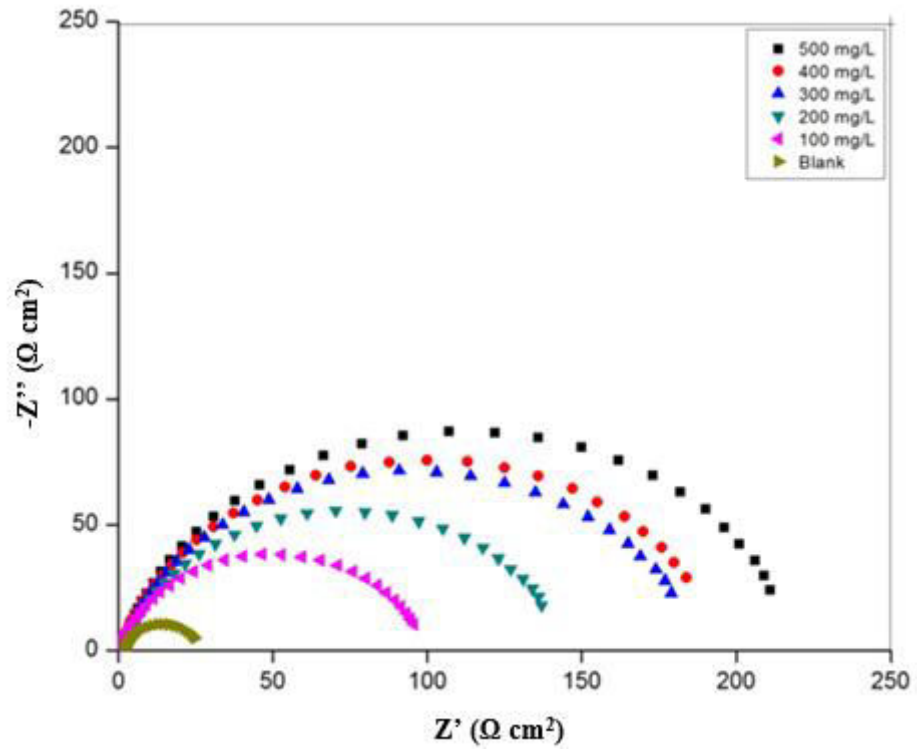
density diminishes and the maximum inhibition effectiveness is accomplished at the concentration of 500 mg/L.

Table 3.3.3: Polarization parameters for mild steel in 0.5 M H<sub>2</sub>SO<sub>4</sub> without and with different concentrations of *Achyranthes aspera* extract.

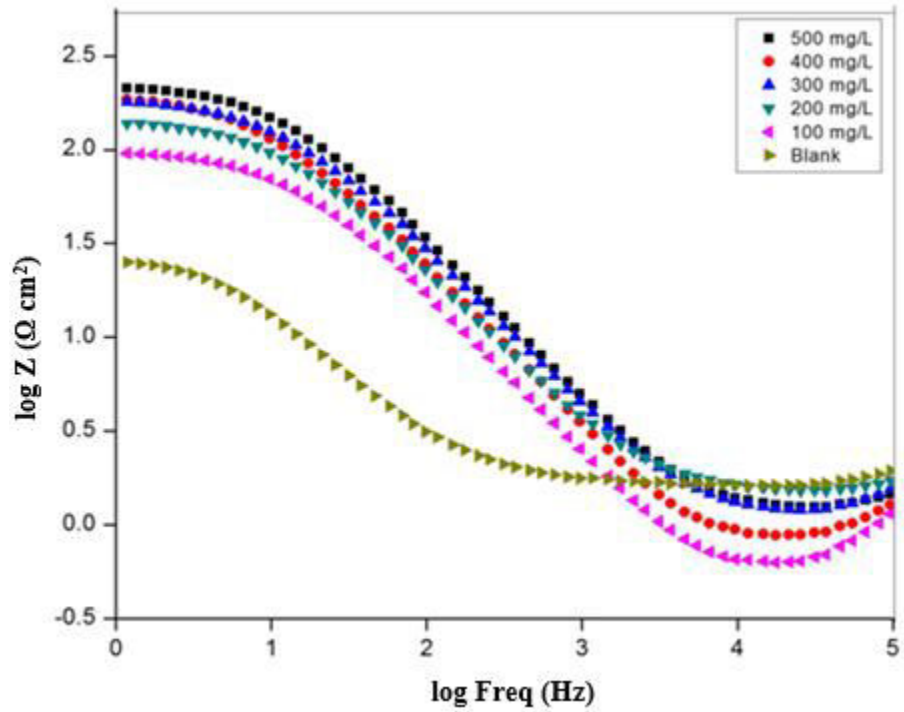
<b>Inhibitor concentration (mg/L)</b>	<b><math>E_{corr}</math> (V vs. SCE)</b>	<b><math>I_{corr}</math> (A cm<sup>-2</sup>)</b>	<b><math>\beta_a</math> (V/dec)</b>	<b><math>-\beta_c</math> (V/dec)</b>	<b>Efficiency (<math>\eta</math> %)</b>
0	-0.465	0.0008909	141.66	164.25	0
100	-0.471	0.0002431	36.29	109.41	72.71
200	-0.462	0.0001745	39.07	117.56	80.41
300	-0.480	0.0001441	42.43	114.01	83.82
400	-0.468	0.0001231	37.89	119.72	86.18
500	-0.459	0.00008205	29.88	129.52	90.79

### 3.3.4 Electrochemical impedance spectroscopy (EIS) studies

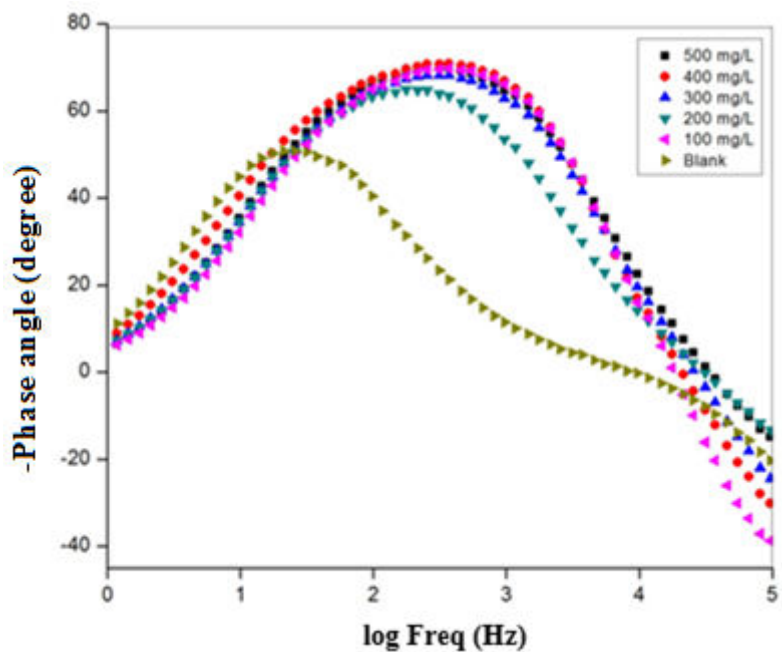
The EIS parameters for mild steel in the absence and presence of various concentrations of *Achyranthes aspera* extract are appeared in Table 3.3.4 and the EIS curves (Nyquist and Bode plots) are shown in Fig.3.3.3. In Nyquist graph, due to the charge transfer resistance, a semicircle in each curve stands for a time constant. Expanding *Achyranthes aspera* extract concentration increases the diameter of semicircle from 100 mg/L to 500 mg/L, which suggests an advancement of inhibition impact.



(a)







(b)

Fig.3.3.3: Nyquist (a) and Bode (b) plots for MS in 0.5 M H<sub>2</sub>SO<sub>4</sub> without and with various concentrations of *Achyranthes aspera* extract at 298 K.

Table 3.3.4: EIS parameters for mild steel in 0.5 M H<sub>2</sub>SO<sub>4</sub> without and with different concentrations of *Achyranthes aspera* extract.

Acid Solution	Concentration of inhibitor (mg/L)	$R_{ct}$ ( $\Omega$ cm <sup>2</sup> )	$CPE$ ( $\mu$ F cm <sup>-2</sup> )	Efficiency ( $\eta$ %)
0.5 M H <sub>2</sub> SO <sub>4</sub>	0	25.164	$1.3 \times 10^{-3}$	0
	100	101.55	$1.6 \times 10^{-4}$	75.22
	200	147.64	$1.1 \times 10^{-4}$	82.95
	300	194.43	$8.3 \times 10^{-5}$	87.05
	400	200.14	$7.9 \times 10^{-5}$	87.42
	500	224.34	$7.2 \times 10^{-5}$	88.78

### 3.3.5 FTIR analysis

The obtained FTIR spectra of *Achyranthes aspera* extract is shown in Fig. 3.3.4. In the FTIR spectra the stretching vibration of O-H causes the peak focused at  $3317.98\text{ cm}^{-1}$  and the peak at  $1639.55\text{ cm}^{-1}$  is credited to the stretching vibration of C=O. The aromatic ring framework vibration results in some bands at  $1408.08\text{ cm}^{-1}$ . The outcomes from FTIR spectroscopy demonstrates that the corrosion inhibition property of *Achyranthes aspera* is because of the presence of O atoms and aromatic rings in the compounds which exist in extract.

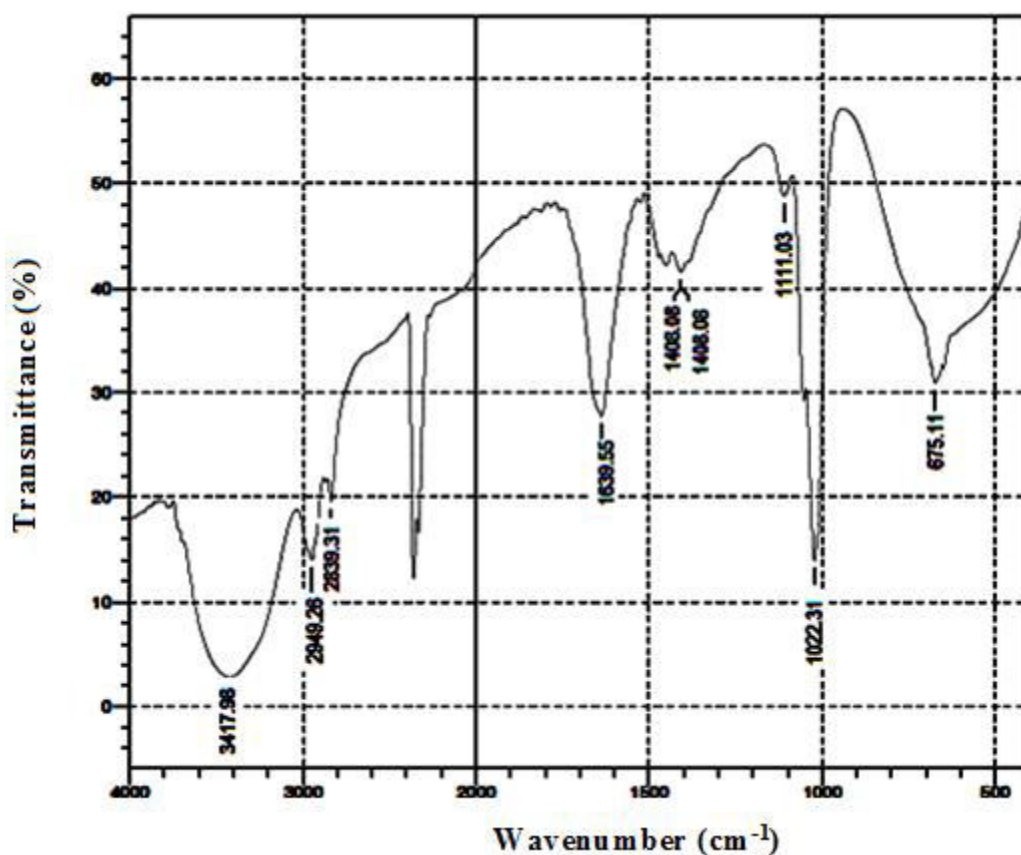


Fig.3.3.4: FTIR spectrum of *Achyranthes aspera* extract.

### 3.3.6 UV-Visible spectroscopy

The UV spectra of *Achyranthes aspera* extract before and after the corrosion test were contemplated and they have been appeared in Fig.3.3.5. The value of absorption maximum ( $\lambda_{max}$ ) or a change in the value of absorbance recommended the formation of a complex between the steel surface and inhibitor molecules.

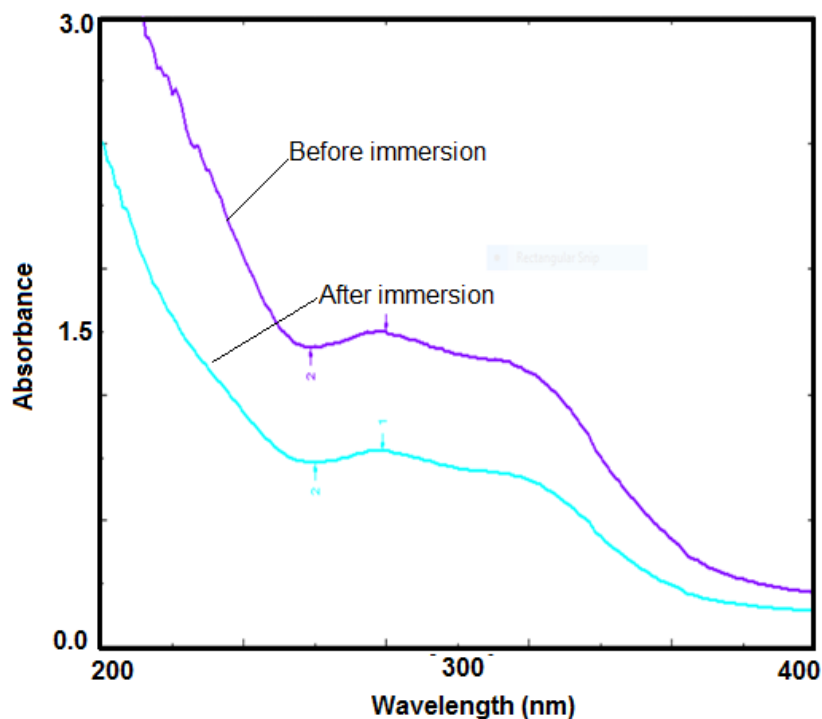


Fig.3.3.5: UV Spectra of *Achyranthes aspera* extract before and after the corrosion test.

### 3.3.7 Surface studies

The SEM and AFM images of the mild steel immersed in 0.5 M  $H_2SO_4$  in the presence of *Achyranthes aspera* extract are shown in Fig.3.3.6. These SEM and AFM micrographs were compared with the SEM and AFM images of the mild steel immersed in 0.5 M  $H_2SO_4$  without inhibitor. From the SEM image it is clear that the surface has astoundingly enhanced concerning its smoothness extensive lessening of corrosion rate. From AFM studies, the value of average surface roughness is 23.05 nm. The change in surface

morphology is because of the arrangement of a decent defensive film of inhibitor on mild steel surface which is in charge of corrosion inhibition.

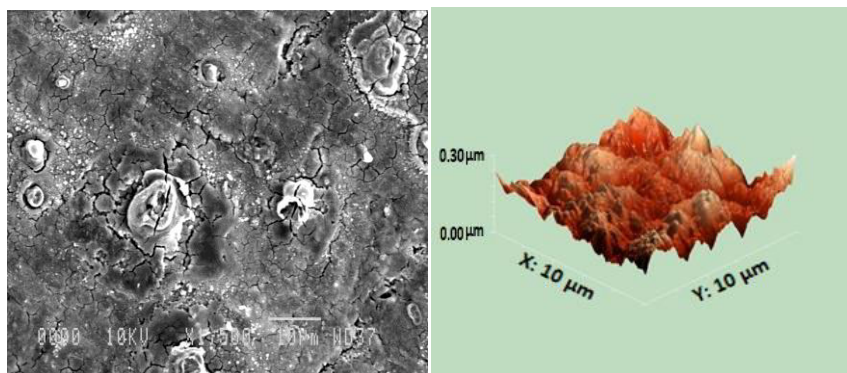
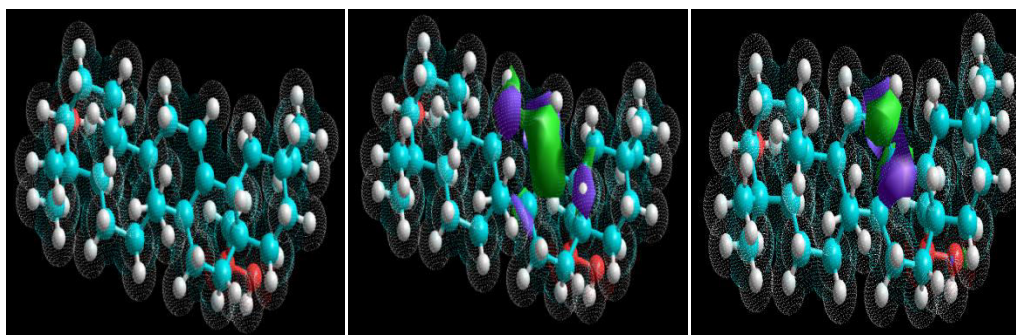


Fig.3.3.6: SEM and AFM images of mild steel immersed in 0.5 M H<sub>2</sub>SO<sub>4</sub> in the presence of *Achyranthes aspera* extract.

### 3.3.8 Quantum chemical studies

The optimized structures of main constituents of *Achyranthes aspera* extract are appeared in Fig. 3.3.7 and the corresponding quantum chemical parameters are reported in Table 3.3.5. The higher estimations of E<sub>HOMO</sub> and lower estimations of E<sub>LUMO</sub> recommend the power of inhibitor to get adsorbed on the mild steel surface.



Optimized structure

HOMO

LUMO

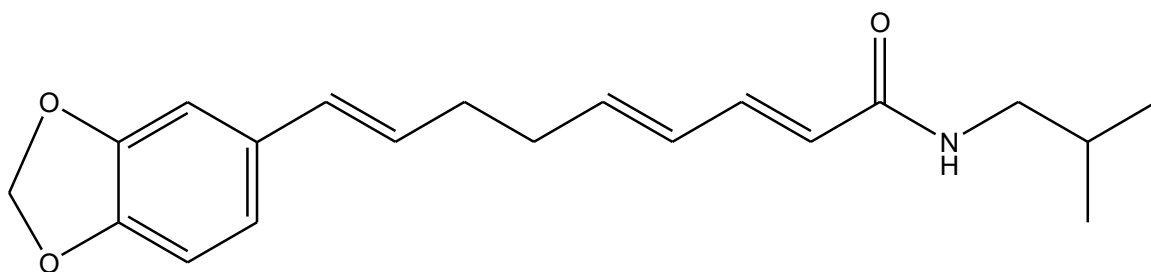
Fig.3.3.7: The optimized structure, HOMO and LUMO distribution for Oleanolic acid.

Table 3.3.5: Quantum chemical parameters of Oleanolic acid and methyl gallate calculated with DFT method.

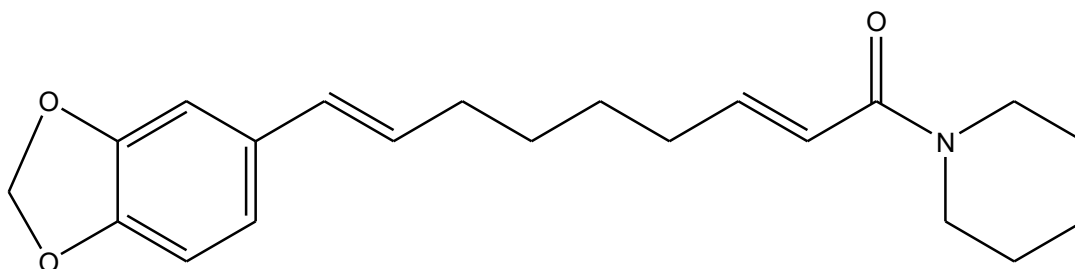
<b>Molecule</b>	<b>E<sub>HOMO</sub> (eV)</b>	<b>E<sub>LUMO</sub> (eV)</b>	<b>ΔE (eV)</b>
Oleanolic acid	-9.3505	0.9977	10.348

### 3.4 *Piper nigrum*

*Piper nigrum* is a plant belonging to Piperaceae family. It has been reported in literature that *Piper nigrum* extract contain Retrofractamide A and Dehydropiperonaline [8] which is shown in Fig. 3.4. The aerial parts of *Piper nigrum* were chosen to study its corrosion inhibition performance.



Retrofractamide A



Dehydropiperonaline

Fig. 3.4: Chemical structure of Retrofractamide A and Dehydropiperonaline.

#### 3.4.1 Weight loss studies

The corrosion inhibition efficiency ( $\eta$  %), corrosion rate (CR) and surface coverage ( $\Theta$ ) at various concentrations (100-500 mg/L) of *Piper nigrum* extract as assessed by weight loss technique have been reported in Table 3.4.1. From Table 3.4.1, obviously increment in inhibition efficiency happens on expanding the inhibitor concentration. This is because

when inhibitor adsorbs on the metal surface then a protective layer is formed on metal surface which reduces the corrosion reaction [2-3].

**Table 3.4.1:** The data of weight loss for mild steel in 0.5 M H<sub>2</sub>SO<sub>4</sub> without and with different concentrations of *Piper nigrum* extract.

C mg/ L	298 K			308 K			318 K		
	CR (mm/ Y)	Θ	η%	CR (mm/Y )	Θ	η%	CR (mm/Y)	Θ	η%
0	26.11	-	-	41.46	-	-	62.88	-	-
100	6.95	0.7335	73.35	12.24	0.7046	70.46	20.91	0.6674	66.74
200	5.28	0.7975	79.75	11.08	0.7326	73.26	19.80	0.6851	68.51
300	3.94	0.8490	84.90	9.46	0.7718	77.18	17.80	0.7168	71.68
400	3.29	0.8738	87.38	7.93	0.8087	80.87	16.09	0.7441	74.41
500	2.27	0.9129	91.29	7.04	0.8299	82.99	14.79	0.7647	76.47

### 3.4.2 Adsorption isotherm

The plots of  $C/\Theta$  vs.  $C$  for *Piper nigrum* extract as indicated by Langmuir adsorption isotherm equation as discussed in chapter 2 are appeared in Fig.3.4.1. The estimation of  $K_{ads}$  were computed from the intercept of Fig.3.4.1 and detailed in Table 3.4.2.

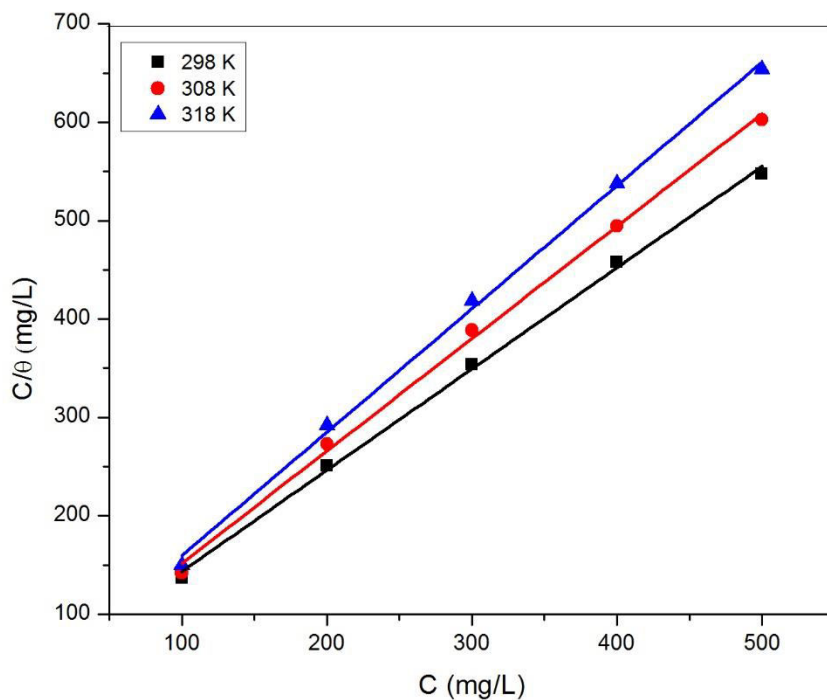


Fig.3.4.1: Langmuir adsorption isotherm for *Piper nigrum* extract on mild steel in 0.5 M  $H_2SO_4$ .

Table 3.4.2: Adsorption parameters for mild steel in 0.5 M  $H_2SO_4$  at optimum concentration of *Piper nigrum* inhibitor.

Temperature (K)	$K_{ads}$ ( $Lmg^{-1}$ )	Slope	$R^2$
298	20.96	1.02	0.9978
308	09.75	1.12	0.9875
318	06.49	1.25	0.9977



### 3.4.3 Potentiodynamic polarization studies

Concentration impact of *Piper nigrum* extract on the polarization character of mild steel in 0.5 M H<sub>2</sub>SO<sub>4</sub> was analysed and the Tafel plots were recorded for various inhibitor concentrations which are appeared in Fig.3.4.2. The parameters, including corrosion potential ( $E_{\text{corr}}$ ), corrosion current density ( $I_{\text{corr}}$ ), anodic and cathodic Tafel slopes ( $\beta_a$  and  $\beta_c$ ) and inhibition efficiency ( $\eta$  %) ascertained by equation discussed in chapter 2, are reported in Table 3.4.3.

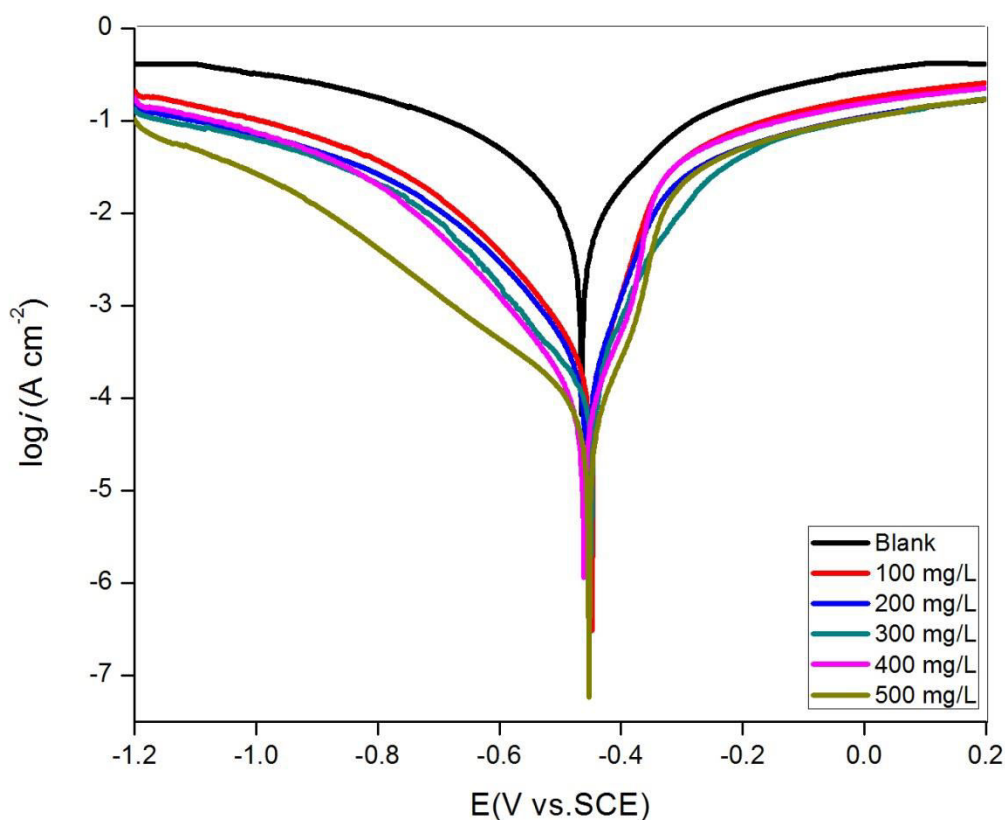


Fig.3.4.2: Tafel polarization curves for mild steel in 0.5 M H<sub>2</sub>SO<sub>4</sub> without and with different concentrations of *Piper nigrum* extract.

Table 3.4.3: Polarization parameters for mild steel in 0.5 M H<sub>2</sub>SO<sub>4</sub> without and with different concentrations of *Piper nigrum* extract.

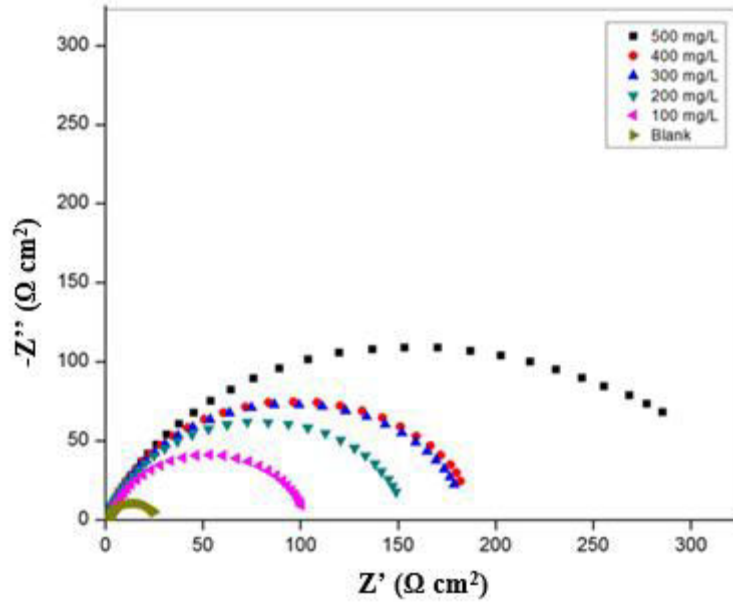
<b>Inhibitor concentration (mg/L)</b>	<b><math>E_{corr}</math> (V vs. SCE)</b>	<b><math>I_{corr}</math> (A cm<sup>-2</sup>)</b>	<b><math>\beta_a</math> (V/dec)</b>	<b><math>-\beta_c</math> (V/dec)</b>	<b>Efficiency (<math>\eta</math> %)</b>
0	-0.465	0.0008909	141.66	164.25	0
100	-0.531	0.0002585	71.68	127.00	70.98
200	-0.501	0.0001456	67.37	112.27	83.65
300	-0.472	0.0001163	48.09	116.48	86.94
400	-0.488	0.0000574	43.52	119.65	93.54
500	-0.461	0.0000516	34.40	121.05	94.20

It is clear that the maximum shift in the  $E_{corr}$  with respect to blank solution was 36 mV, which is within 85 mV, recommended that the contemplated inhibitor goes about as a mixed sort corrosion inhibitor [4-5]. The relatively unaffected anodic and cathodic Tafel slopes when including *Piper nigrum* extract show that the anodic and cathodic reaction mechanisms are still controlled by charge transfer. It can be seen from Table 3.4.3 that with expanding concentration of *Piper nigrum* extract, the corrosion current density diminishes and the maximum inhibition effectiveness is accomplished at the concentration of 500 mg/L.

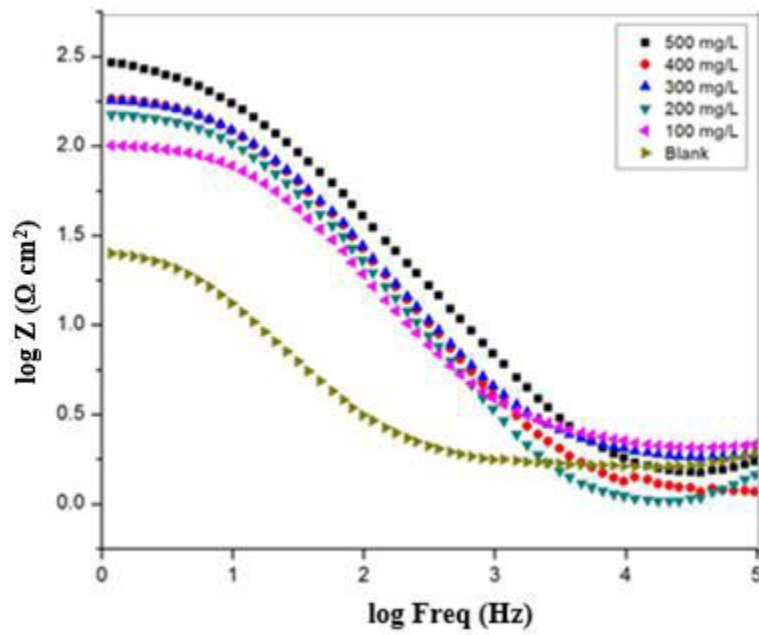
### 3.4.4 Electrochemical impedance spectroscopy (EIS) studies

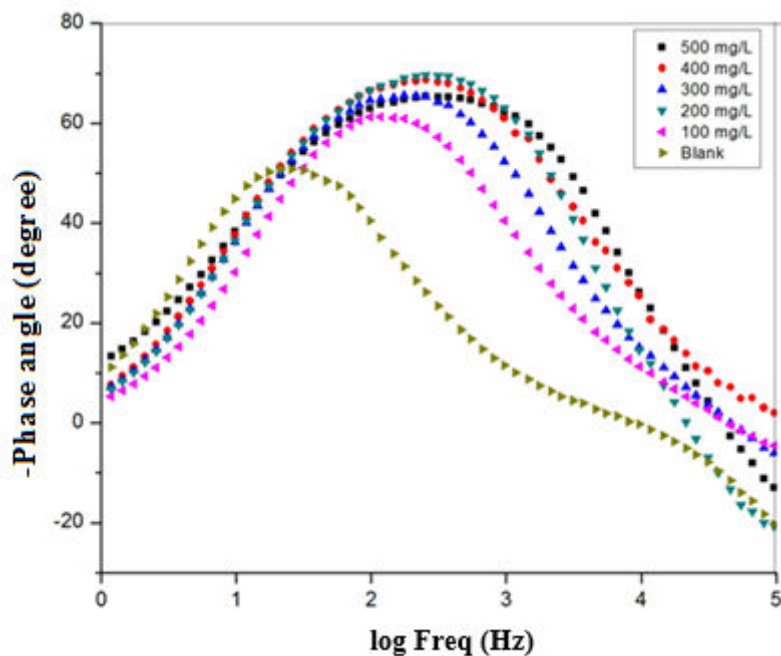
The EIS parameters for mild steel in the absence and presence of various concentrations of *Piper nigrum* extract are appeared in Table 3.4.4 and the EIS curves (Nyquist and Bode plots) are shown in Fig.3.4.3. In Nyquist graph, due to the charge transfer resistance, a semicircle in each curve stands for a time constant. Expanding *Piper nigrum* extract

concentration increases the diameter of semicircle from 100 mg/L to 500 mg/L, which suggests an advancement of inhibition impact.



(a)





(b)

Fig.3.4.3: Nyquist (a) and Bode (b) plots for MS in 0.5 M H<sub>2</sub>SO<sub>4</sub> without and with various concentrations of *Piper nigrum* extract at 298 K.

Table 3.4.4: EIS parameters for mild steel in 0.5 M H<sub>2</sub>SO<sub>4</sub> without and with different concentrations of *Piper nigrum* extract.

Acid Solution	Inhibitor conc. (mg/L)	$R_{ct}$ ( $\Omega$ cm <sup>2</sup> )	$CPE$ ( $\mu$ F cm <sup>-2</sup> )	Efficiency ( $\eta$ %)
0.5 M H <sub>2</sub> SO <sub>4</sub>	0	25.164	$1.3 \times 10^{-3}$	0
	100	102.930	$1.3 \times 10^{-4}$	75.55
	200	156.758	$1.0 \times 10^{-4}$	83.94
	300	190.458	$8.5 \times 10^{-5}$	86.78
	400	195.329	$1.0 \times 10^{-4}$	87.11
	500	366.223	$6.5 \times 10^{-5}$	93.12

### 3.4.5 FTIR analysis

The obtained FTIR spectra of *Piper nigrum* extract is shown in Fig. 3.4.4. In the FTIR spectra the stretching vibration of O-H causes the peak focused at  $3447\text{ cm}^{-1}$  and the peak at  $1022.31\text{ cm}^{-1}$  is credited to the stretching vibration of C-O. The aromatic ring framework vibration results in some bands at  $1637.12\text{ cm}^{-1}$ . The outcomes from FTIR spectroscopy demonstrates that the corrosion inhibition property of *Piper nigrum* is because of the presence of O atoms and aromatic rings in the compounds which exist in extract.

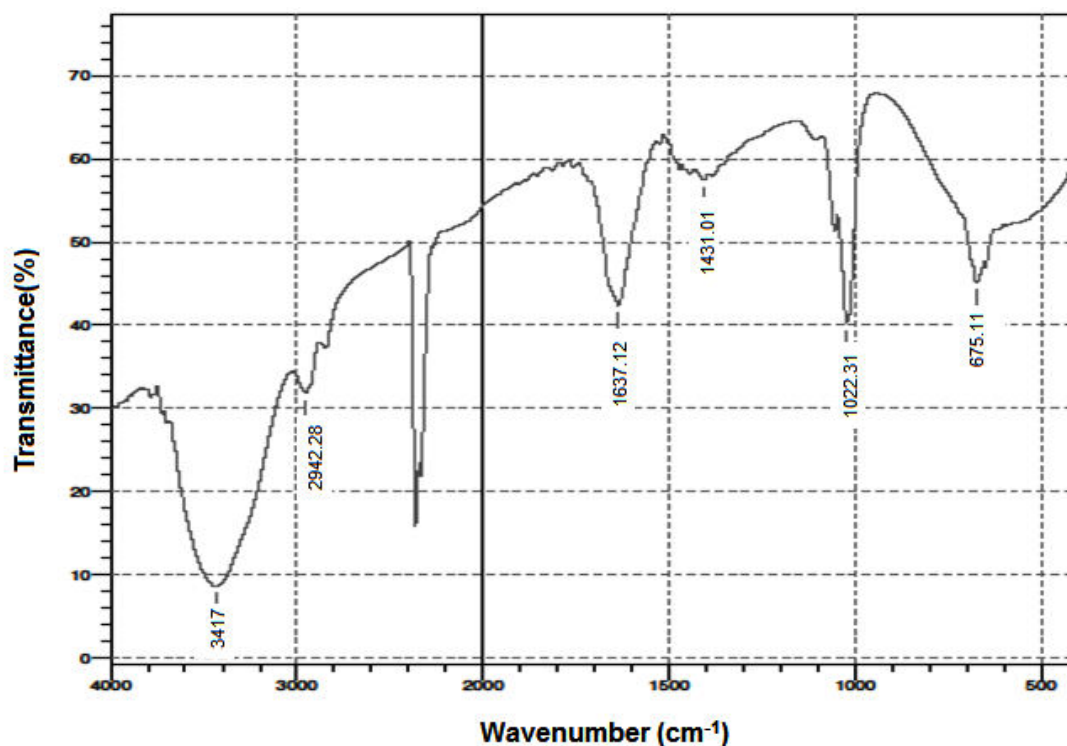


Fig.3.4.4: FTIR spectrum of *Piper nigrum* extract.

### 3.4.6 UV-Visible spectroscopy

The UV spectra of *Piper nigrum* extract before and after the corrosion test were contemplated and they have been appeared in Fig.3.4.5. The value of absorption maximum ( $\lambda_{max}$ ) or a change in the value of absorbance recommended the formation of a complex between the steel surface and inhibitor molecules.

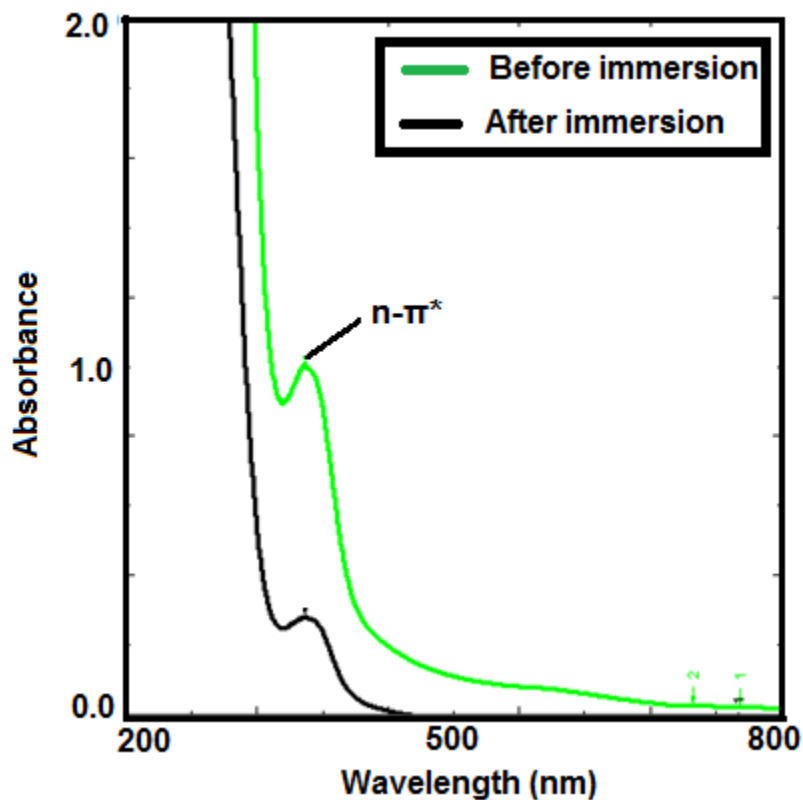


Fig.3.4.5: UV Spectra of *Piper nigrum* extract before and after the corrosion test.

### 3.4.7 Surface studies

The SEM and AFM images of the mild steel immersed in 0.5 M H<sub>2</sub>SO<sub>4</sub> in the presence of *Piper nigrum* extract are shown in Fig.3.4.6. These SEM and AFM micrographs were compared with the SEM and AFM images of the mild steel immersed in 0.5 M H<sub>2</sub>SO<sub>4</sub> without inhibitor. From the SEM image it is clear that the surface has astoundingly enhanced concerning its smoothness extensive lessening of corrosion rate. From AFM studies, the value of average surface roughness is 17.98 nm. The change in surface morphology is because of the arrangement of a decent defensive film of inhibitor on mild steel surface which is in charge of corrosion inhibition.

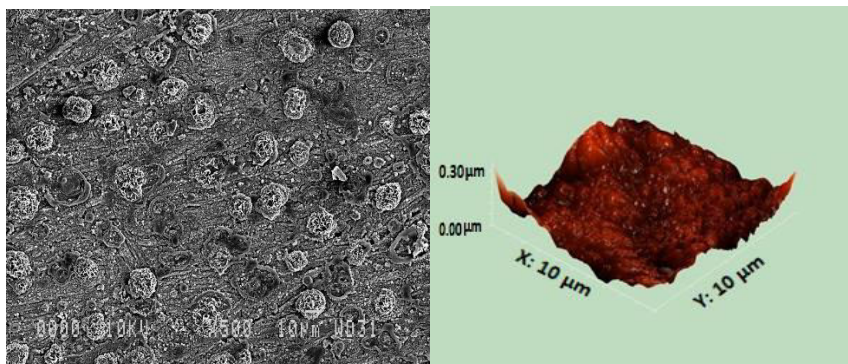
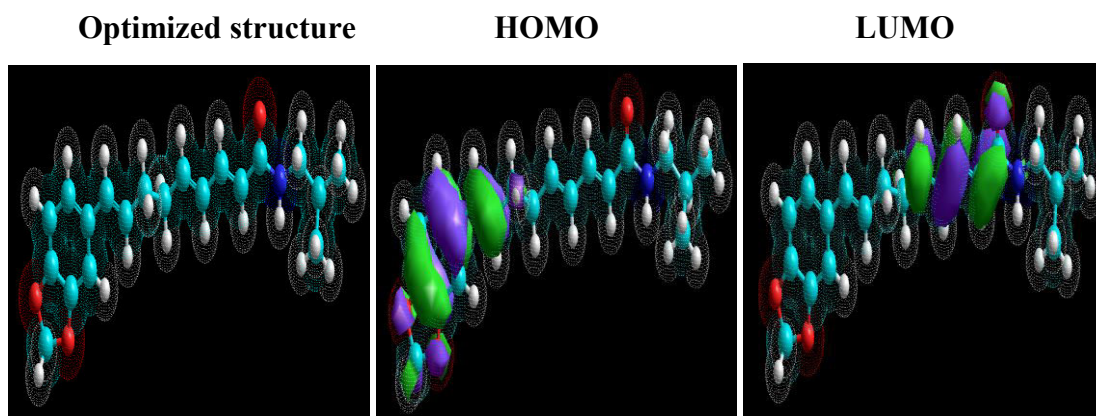


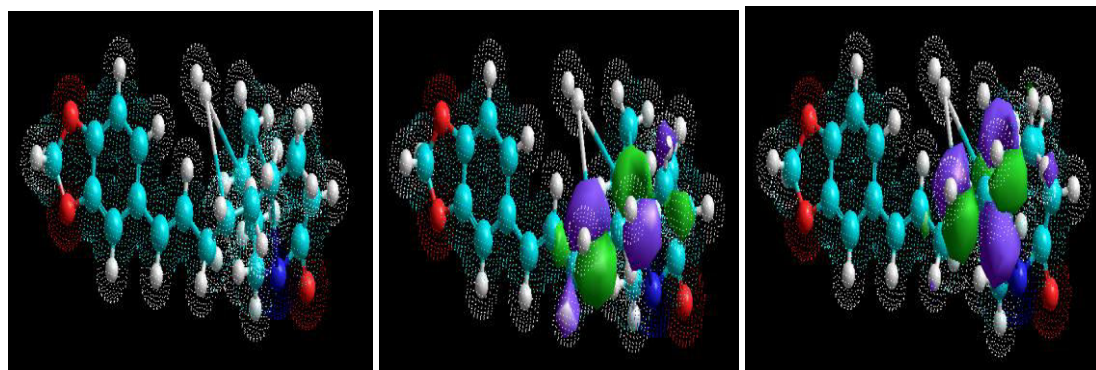
Fig.3.4.6: SEM and AFM images of mild steel immersed in 0.5 M H<sub>2</sub>SO<sub>4</sub> in the presence of *Piper nigrum* extract.

### 3.4.8 Quantum chemical studies

The optimized structures of main constituents (Retrofractamide A and Piperonaline) of *Piper nigrum* extract are appeared in Fig. 3.4.7 and the corresponding quantum chemical parameters are reported in Table 3.4.5. The higher estimations of E<sub>HOMO</sub> and lower estimations of E<sub>LUMO</sub> recommend the power of inhibitor to get adsorbed on the mild steel surface.



**Retrofractamide A**



### Dehydropiperonaline

Fig.3.4.7: The optimized structure, HOMO and LUMO distribution for Retrofractamide A and Dehydropiperonaline.

Table 3.4.5: Quantum chemical parameters of Retrofractamide A and Dehydropiperonaline calculated with DFT method.

Molecule	$E_{\text{HOMO}}$ (eV)	$E_{\text{LUMO}}$ (eV)	$\Delta E$ (eV)
Retrofractamide A	-8.7633	-0.5146	8.2487
Dehydropiperonaline	-6.7856	-1.2467	5.5389



### 3.5 *Trachyspermum ammi*

*Trachyspermum ammi* is a plant belonging to Apiaceae family. It has been reported in literature that the fruits of *Trachyspermum ammi* contain Thymol and  $\alpha$  Terpineol [9] which is shown in Fig. 3.5. The fruits of *Trachyspermum ammi* were chosen to study its corrosion inhibition performance.

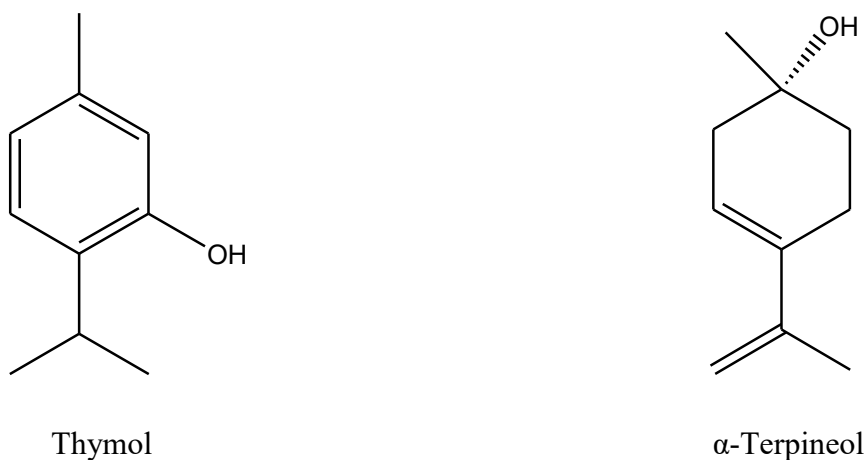


Fig. 3.5: Chemical structure of Thymol and  $\alpha$  Terpineol.

#### 3.5.1 Weight loss studies

The corrosion inhibition efficiency ( $\eta$  %), corrosion rate (CR) and surface coverage ( $\Theta$ ) at various concentrations (100-500 mg/L) of *Trachyspermum ammi* extract as assessed by weight loss technique have been reported in Table 3.5.1. From Table 3.5.1, obviously increment in inhibition efficiency happens on expanding the inhibitor concentration. This is because when inhibitor adsorbs on the metal surface then a protective layer is formed on metal surface which reduces the corrosion reaction [2-3].

**Table 3.5.1:** The data of weight loss for mild steel in 0.5 M H<sub>2</sub>SO<sub>4</sub> without and with different concentrations of *Trachyspermum ammi* extract.

C mg/ L	298 K			308 K			318 K		
	CR (mm/ Y)	Θ	η%	CR (mm/Y )	Θ	η%	CR (mm/Y)	Θ	η%
0	26.11	-	-	41.46	-	-	62.88	-	-
100	7.37	0.7125	71.25	13.40	0.6767	67.67	24.16	0.6157	61.57
200	5.61	0.7850	78.50	11.08	0.7326	73.26	21.65	0.6556	65.56
300	4.68	0.8206	82.06	9.36	0.7740	77.40	18.31	0.7087	70.87
400	3.43	0.8685	86.85	8.44	0.7964	79.64	15.86	0.7477	74.77
500	2.22	0.9147	91.47	6.40	0.8456	84.56	14.09	0.7758	77.58

### 3.5.2 Adsorption isotherm

The plots of  $C/\Theta$  vs.  $C$  for *Trachyspermum ammi* extract as indicated by Langmuir adsorption isotherm equation as discussed in chapter 2 are appeared in Fig.3.5.1. The estimation of  $K_{ads}$  were computed from the intercept of Fig.3.5.1 and detailed in Table 3.5.2.

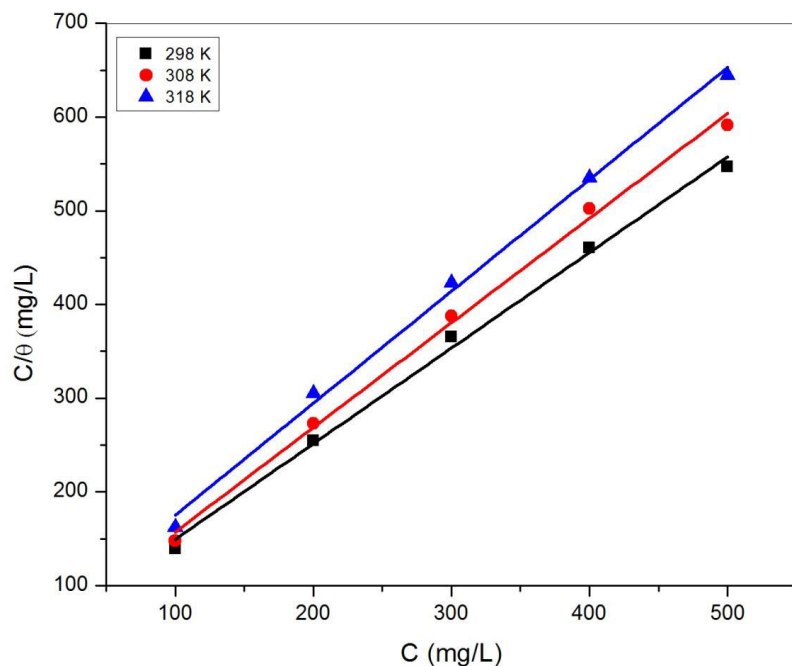


Fig.3.5.1: Langmuir adsorption isotherm for *Trachyspermum ammi* extract on mild steel in 0.5 M H<sub>2</sub>SO<sub>4</sub>.

Table 3.5.2: Adsorption parameters for mild steel in 0.5 M H<sub>2</sub>SO<sub>4</sub> at optimum concentration of *Trachyspermum ammi* inhibitor.

Temperature (K)	$K_{ads}$ (Lmg <sup>-1</sup> )	Slope	$R^2$
298	21.44	1.02	0.9948
308	10.95	1.11	0.9955
318	06.92	1.19	0.9959

### 3.5.3 Potentiodynamic polarization studies

Concentration impact of *Trachyspermum ammi* extract on the polarization character of mild steel in 0.5 M H<sub>2</sub>SO<sub>4</sub> was analysed and the Tafel plots were recorded for various inhibitor concentrations which are appeared in Fig.3.5.2. The parameters, including corrosion potential ( $E_{\text{corr}}$ ), corrosion current density ( $I_{\text{corr}}$ ), anodic and cathodic Tafel slopes ( $\beta_a$  and  $\beta_c$ ) and inhibition efficiency ( $\eta$  %) ascertained by equation discussed in chapter 2, are reported in Table 3.5.3.

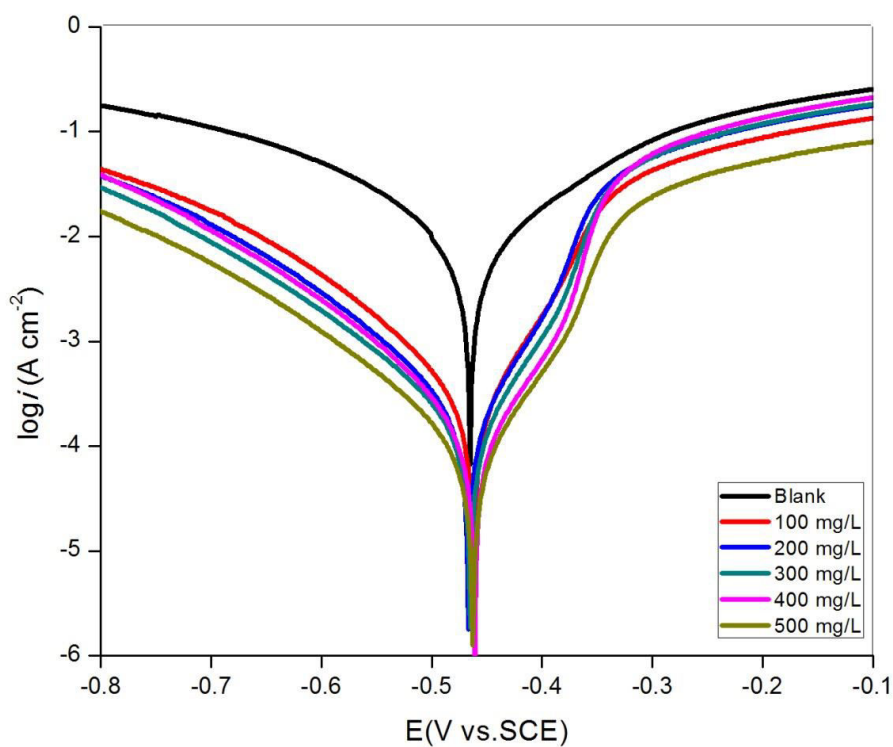


Fig.3.5.2: Tafel polarization curves for mild steel in 0.5 M H<sub>2</sub>SO<sub>4</sub> without and with different concentrations of *Trachyspermum ammi* extract.

Table 3.5.3: Polarization parameters for mild steel in 0.5 M H<sub>2</sub>SO<sub>4</sub> without and with different concentrations of *Trachyspermum ammi* extract.

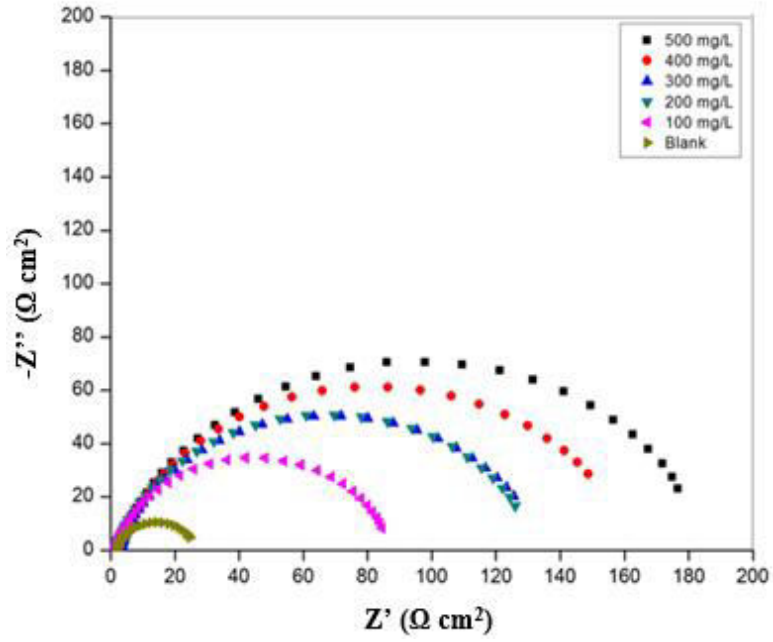
<b>Inhibitor concentration (mg/L)</b>	<b><math>E_{corr}</math> (V vs. SCE)</b>	<b><math>I_{corr}</math> (A cm<sup>-2</sup>)</b>	<b><math>\beta_a</math> (V/dec)</b>	<b><math>-\beta_c</math> (V/dec)</b>	<b>Efficiency (<math>\eta</math> %)</b>
0	-0.465	0.0008909	141.663	164.257	0
100	-0.462	0.0002070	50.170	113.662	76.76
200	-0.467	0.0001365	41.80	115.035	84.67
300	-0.465	0.00009946	39.875	121.580	88.83
400	-0.461	0.00007449	34.920	112.574	91.63
500	-0.463	0.00006282	45.339	121.359	92.94

It is clear that the maximum shift in the  $E_{corr}$  with respect to blank solution was 2 mV, which is within 85 mV, recommended that the contemplated inhibitor goes about as a mixed sort corrosion inhibitor [4-5]. The relatively unaffected anodic and cathodic Tafel slopes when including *Trachyspermum ammi* extract show that the anodic and cathodic reaction mechanisms are still controlled by charge transfer. It can be seen from Table 3.5.3 that with expanding concentration of *Trachyspermum ammi* extract, the corrosion current density diminishes and the maximum inhibition effectiveness is accomplished at the concentration of 500 mg/L.

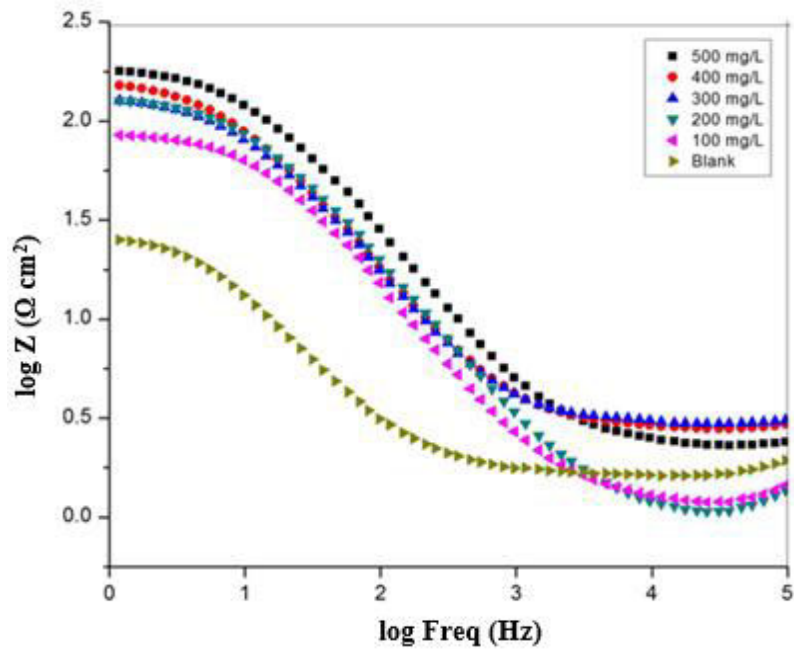
### 3.5.4 Electrochemical impedance spectroscopy (EIS) studies

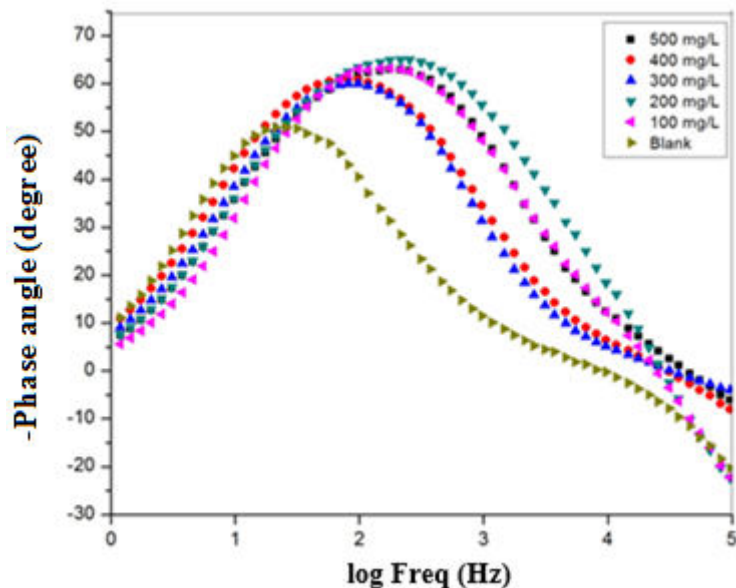
The EIS parameters for mild steel in the absence and presence of various concentrations of *Trachyspermum ammi* extract are appeared in Table 3.5.4 and the EIS curves (Nyquist and Bode plots) are shown in Fig.3.5.3. In Nyquist graph, due to the charge transfer resistance, a semicircle in each curve stands for a time constant. Expanding *Trachyspermum ammi*

extract concentration increases the diameter of semicircle from 100 mg/L to 500 mg/L, which suggests an advancement of inhibition impact.



(a)





(b)

Fig.3.5.3: Nyquist (a) and Bode (b) plots for MS in 0.5 M H<sub>2</sub>SO<sub>4</sub> without and with various concentrations of *Trachyspermum ammi* extract at 298 K.

Table 3.5.4: EIS parameters for mild steel in 0.5 M H<sub>2</sub>SO<sub>4</sub> without and with different concentrations of *Trachyspermum ammi* extract.

Acid Solution	Inhibitor conc. (mg/L)	$R_{ct}$ ( $\Omega$ cm <sup>2</sup> )	$CPE$ ( $\mu$ F cm <sup>-2</sup> )	Efficiency ( $\eta$ %)
0.5 M H <sub>2</sub> SO <sub>4</sub>	0	25.164	$1.3 \times 10^{-3}$	0
	100	88.08	$1.5 \times 10^{-4}$	71.43
	200	129.41	$1.5 \times 10^{-4}$	80.55
	300	137.84	$1.7 \times 10^{-4}$	81.74
	400	164.93	$1.7 \times 10^{-4}$	84.75
	500	190.52	$1.0 \times 10^{-4}$	86.79

### 3.5.5 FTIR analysis

The obtained FTIR spectra of *Trachyspermum ammi* extract is shown in Fig. 3.5.4. In the FTIR spectra the stretching vibration of O-H causes the peak focused at  $3377.47\text{ cm}^{-1}$  and the peak at  $1076.32\text{ cm}^{-1}$  is credited to the stretching vibration of C-O. The aromatic ring framework vibration results in some bands at  $1649.19\text{ cm}^{-1}$ . The outcomes from FTIR spectroscopy demonstrates that the corrosion inhibition property of *Trachyspermum ammi* is because of the presence of O atoms and aromatic rings in the compounds which exist in extract.

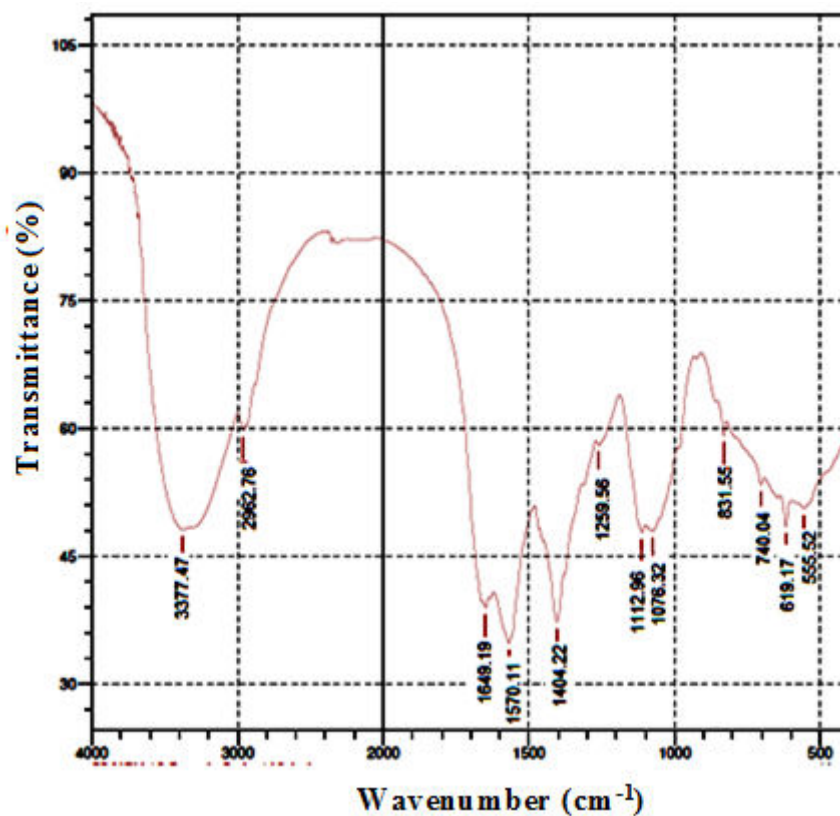


Fig.3.5.4: FTIR spectrum of *Trachyspermum ammi* extract.

### 3.5.6 UV-Visible spectroscopy

The UV spectra of *Trachyspermum ammi* extract before and after the corrosion test were contemplated and they have been appeared in Fig.3.5.5. The value of absorption maximum



( $\lambda_{max}$ ) or a change in the value of absorbance recommended the formation of a complex between the steel surface and inhibitor molecules.

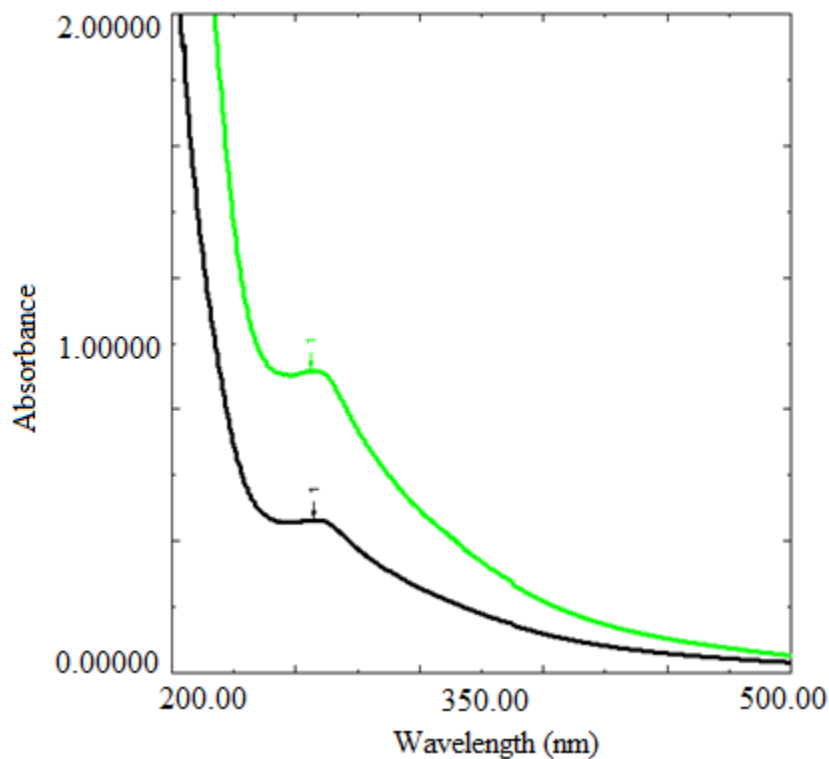


Fig.3.5.5: UV Spectra of *Trachyspermum ammi* extract before and after the corrosion test.

### 3.5.7 Surface studies

The SEM and AFM images of the mild steel immersed in 0.5 M H<sub>2</sub>SO<sub>4</sub> in the presence of *Trachyspermum ammi* extract are shown in Fig.3.5.6. These SEM and AFM micrographs were compared with the SEM and AFM images of the mild steel immersed in 0.5 M H<sub>2</sub>SO<sub>4</sub> without inhibitor. From the SEM image it is clear that the surface has astoundingly enhanced concerning its smoothness extensive lessening of corrosion rate. From AFM studies, the value of average surface roughness is 16.67 nm. The change in surface morphology is because of the arrangement of a decent defensive film of inhibitor on mild steel surface which is in charge of corrosion inhibition.

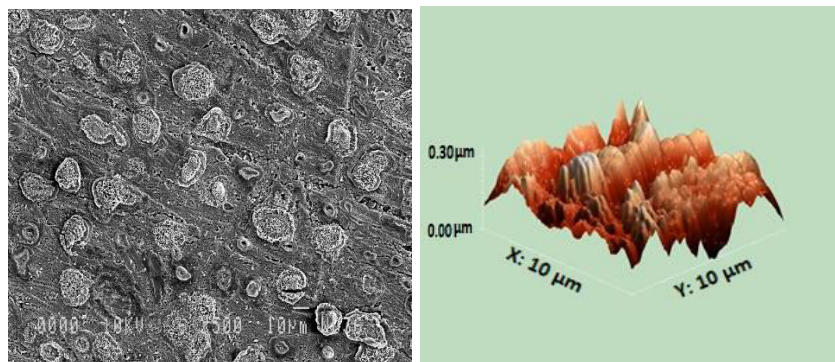
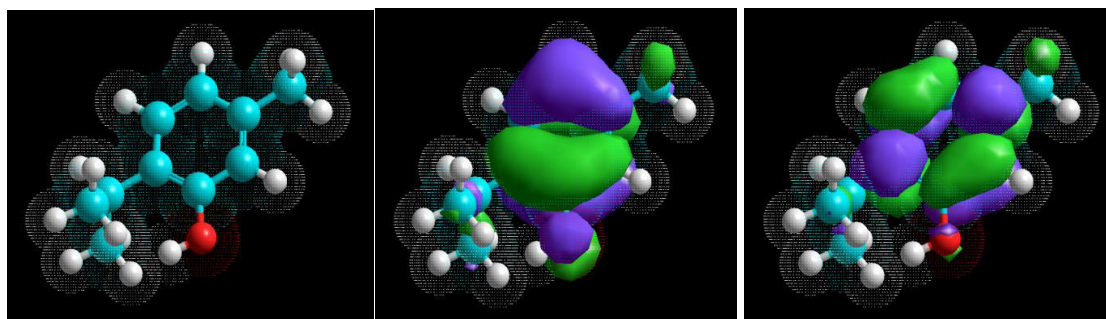


Fig.3.5.6: SEM and AFM images of mild steel immersed in 0.5 M H<sub>2</sub>SO<sub>4</sub> in the presence of *Trachyspermum ammi* extract.

### 3.5.8 Quantum chemical studies

The optimized structures of main constituents (Thymol and  $\alpha$  Terpineol) of *Trachyspermum ammi* extract are appeared in Fig. 3.5.7 and the corresponding quantum chemical parameters are reported in Table 3.5.5. The higher estimations of E<sub>HOMO</sub> and lower estimations of E<sub>LUMO</sub> recommend the power of inhibitor to get adsorbed on the mild steel surface.

(a)- Thymol



Optimized geometry

HOMO

LUMO

(b)-  $\alpha$ -Terpineol

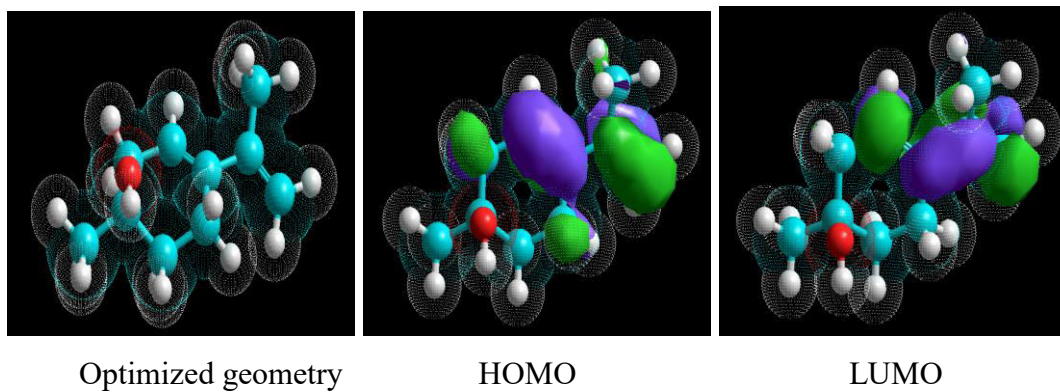


Fig.3.5.7: The optimized structure, HOMO and LUMO distribution for Thymol and  $\alpha$  Terpineol.

Table 3.5.5: Quantum chemical parameters of Thymol and  $\alpha$  Terpineol calculated with DFT method.

Molecule	$E_{\text{HOMO}}$ (eV)	$E_{\text{LUMO}}$ (eV)	$\Delta E$ (eV)
Thymol	-9.009	-0.1748	8.8342
$\alpha$ -Terpineol	-9.016	0.4923	9.5083

### 3.6 *Syzygium aromaticum* [Surface reviews and Letters, doi: 10.1142/S0218625X18502001]

Cloves are the aromatic flower buds of a tree in the family Myrtaceae. It has been reported in literature that this plant contains Eugenol and Eugenol acetate [10] which is shown in Fig. 3.6. The buds of *Syzygium aromaticum* were chosen to study its corrosion inhibition performance.

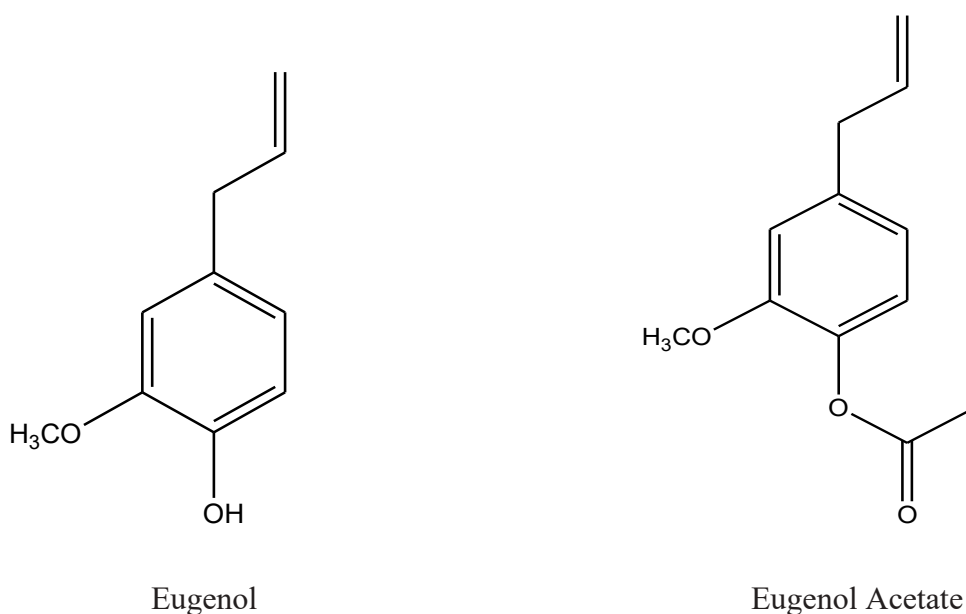


Fig. 3.6: Chemical structures of Eugenol and Eugenol acetate.

#### 3.6.1 Weight loss studies

The corrosion inhibition efficiency ( $\eta$  %), corrosion rate (CR) and surface coverage ( $\Theta$ ) at various concentrations (100-500 mg/L) of *Syzygium aromaticum* extract as assessed by weight loss technique have been reported in Table 3.6.1. From Table 3.6.1, obviously increment in inhibition efficiency happens on expanding the inhibitor concentration. This is because when inhibitor adsorbs on the metal surface then a protective layer is formed on metal surface which reduces the corrosion reaction [2-3].

**Table 3.6.1:** The data of weight loss for mild steel in 0.5 M H<sub>2</sub>SO<sub>4</sub> without and with different concentrations of *Syzygium aromaticum* extract.

Conc. mg/L	298 K			308 K			318 K		
	CR (mm/ Y)	Θ	η%	CR (mm/ Y)	Θ	η%	CR (mm /Y)	Θ	η%
0	26.11	-	-	41.46	-	-	62.88	-	-
100	6.53	0.7513	75.13	11.45	0.7237	72.37	20.03	0.6831	68.31
200	4.77	0.8170	81.70	9.78	0.7639	76.39	17.48	0.7219	72.19
300	3.61	0.8614	86.14	7.55	0.8176	81.76	14.42	0.7706	77.06
400	2.87	0.8916	89.16	5.65	0.8635	86.35	11.64	0.8148	81.48
500	1.76	0.9325	93.25	4.31	0.8959	89.59	9.22	0.8532	85.32

### 3.6.2 Adsorption isotherm

The plots of  $C/\Theta$  vs.  $C$  for *Syzygium aromaticum* extract as indicated by Langmuir adsorption isotherm equation as discussed in chapter 2 are appeared in Fig.3.6.1. The estimation of  $K_{ads}$  were computed from the intercept of Fig.3.6.1 and detailed in Table 3.6.2.

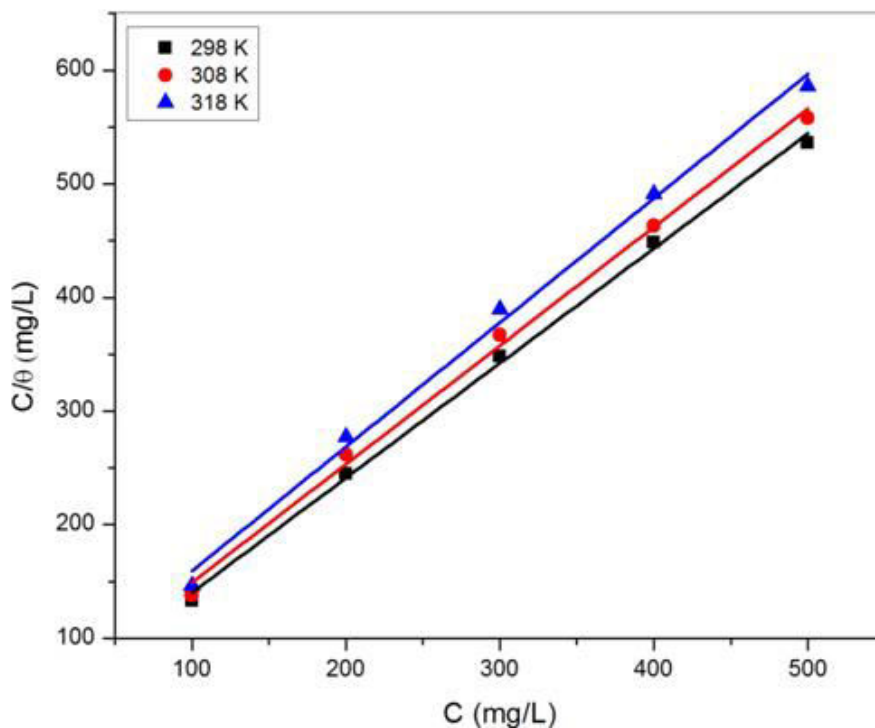


Fig.3.6.1: Langmuir adsorption isotherm for *Syzygium aromaticum* extract on mild steel in 0.5 M H<sub>2</sub>SO<sub>4</sub>.

Table 3.6.2: Adsorption parameters for mild steel in 0.5 M H<sub>2</sub>SO<sub>4</sub> at optimum concentration of *Syzygium aromaticum* inhibitor.

Temperature (K)	$K_{ads}$ (Lmg <sup>-1</sup> )	Slope	$R^2$
298	27.62	1.01	0.9974
308	17.21	1.04	0.9957
318	11.62	1.09	0.9945

### 3.6.3 Potentiodynamic polarization studies

Concentration impact of *Syzygium aromaticum* extract on the polarization character of mild steel in 0.5 M H<sub>2</sub>SO<sub>4</sub> was analysed and the Tafel plots were recorded for various inhibitor concentrations which are appeared in Fig.3.6.2. The parameters, including corrosion potential ( $E_{\text{corr}}$ ), corrosion current density ( $I_{\text{corr}}$ ), anodic and cathodic Tafel slopes ( $\beta_a$  and  $\beta_c$ ) and inhibition efficiency ( $\eta$  %) ascertained by equation discussed in chapter 2, are reported in Table 3.6.3. It is clear that the maximum shift in the  $E_{\text{corr}}$  with respect to blank solution was 69 mV, which is within 85 mV, recommended that the contemplated inhibitor goes about as a mixed sort corrosion inhibitor [4-5]. The relatively unaffected anodic and cathodic Tafel slopes when including *Syzygium aromaticum* extract show that the anodic and cathodic reaction mechanisms are still controlled by charge transfer.

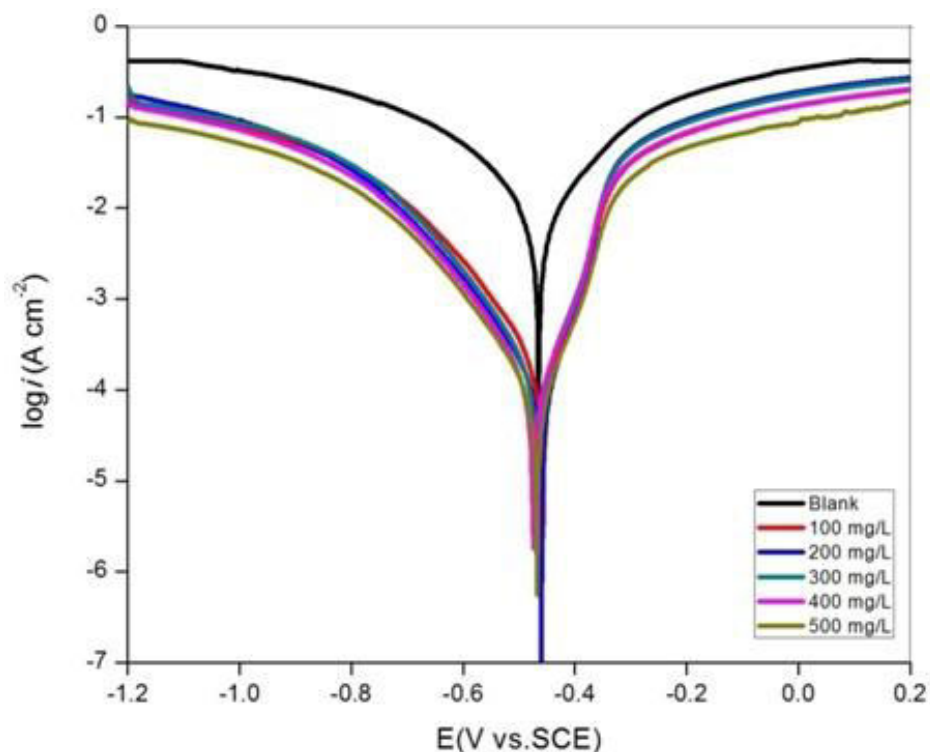


Fig.3.6.2: Tafel polarization curves for mild steel in 0.5 M H<sub>2</sub>SO<sub>4</sub> without and with different concentrations of *Syzygium aromaticum* extract.

It can be seen from Table 3.6.3 that with expanding concentration of *Syzygium aromaticum* extract, the corrosion current density diminishes and the maximum inhibition effectiveness is accomplished at the concentration of 500 mg/L.

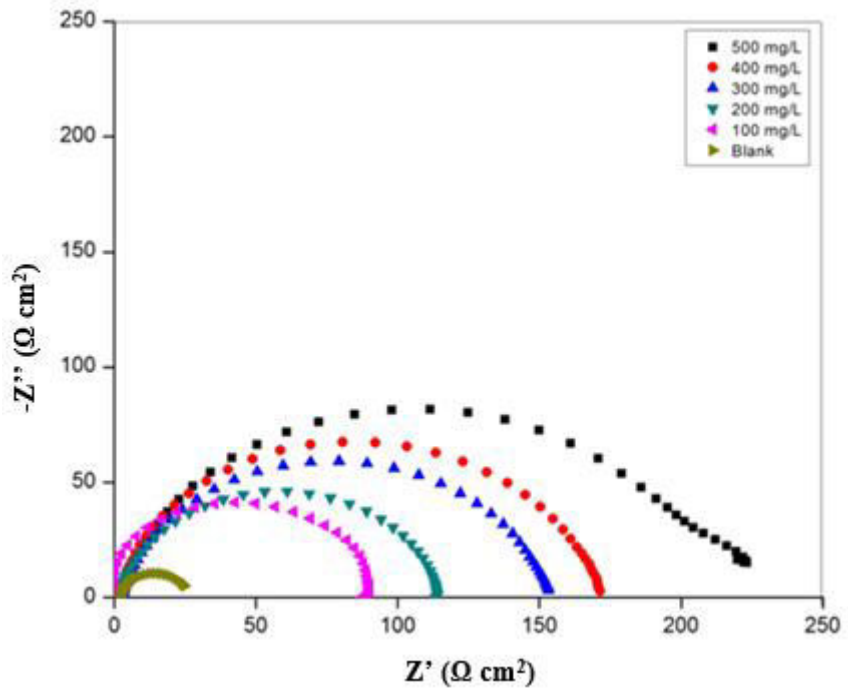
Table 3.6.3: Polarization parameters for mild steel in 0.5 M H<sub>2</sub>SO<sub>4</sub> without and with different concentrations of *Syzygium aromaticum* extract.

<b>Inhibitor concentration (mg/L)</b>	<b><math>E_{corr}</math> (V vs. SCE)</b>	<b><math>I_{corr}</math> (A cm<sup>-2</sup>)</b>	<b><math>\beta_a</math> (V/dec)</b>	<b><math>-\beta_c</math> (V/dec)</b>	<b>Efficiency (<math>\eta</math> %)</b>
0	-0.465	0.0008909	141.663	164.257	0
100	-0.454	0.0002487	48.56	117.05	72.08
200	-0.471	0.0002061	69.01	117.45	76.86
300	-0.460	0.0001569	48.19	117.08	83.29
400	-0.456	0.0001083	45.94	114.61	87.84
500	-0.534	0.00006702	49.97	106.21	92.48

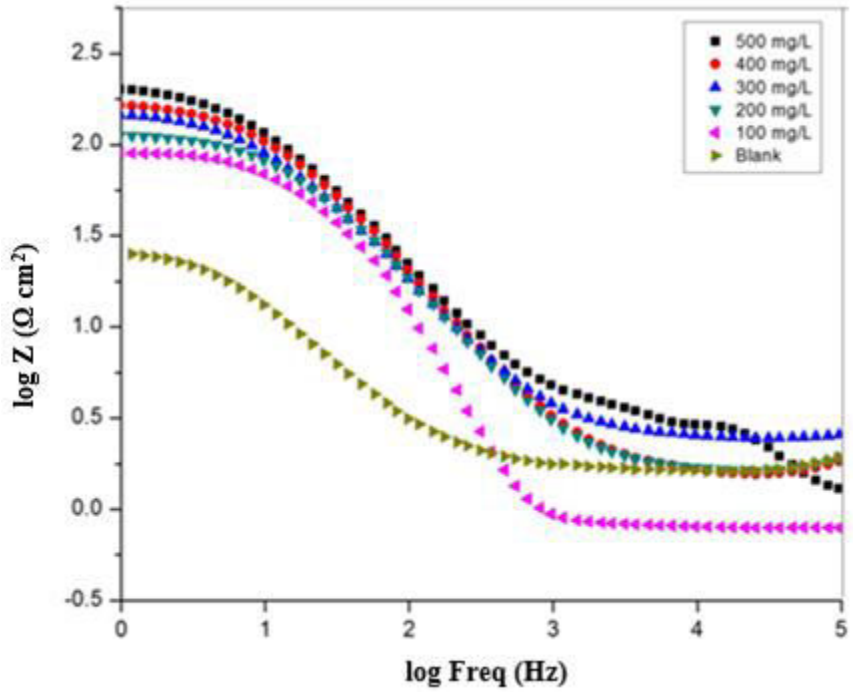
### 3.6.4 Electrochemical impedance spectroscopy (EIS) studies

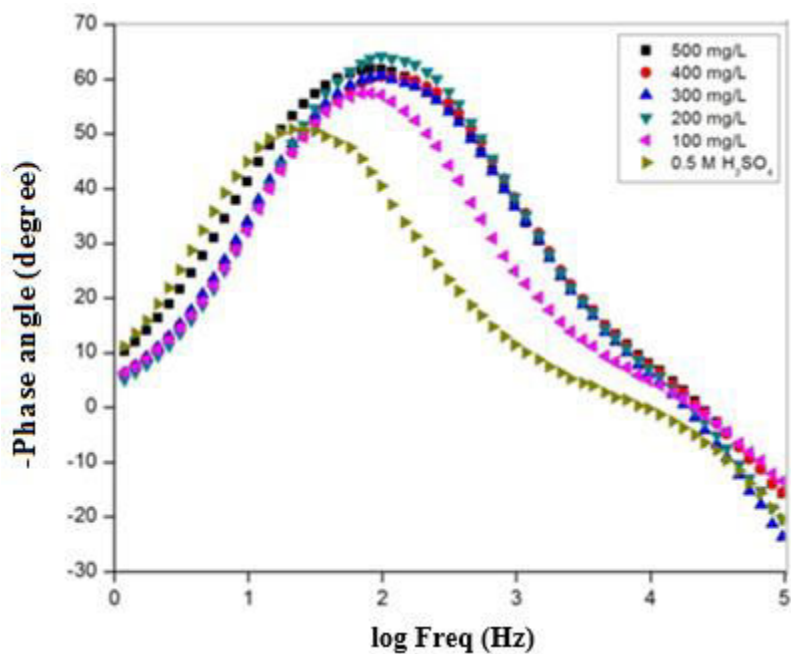
The EIS parameters for mild steel in the absence and presence of various concentrations of *Syzygium aromaticum* extract are appeared in Table 3.6.4 and the EIS curves (Nyquist and Bode plots) are shown in Fig.3.6.3. In Nyquist graph, due to the charge transfer resistance, a semicircle in each curve stands for a time constant. Expanding *Syzygium aromaticum* extract concentration increases the diameter of semicircle from 100 mg/L to 500 mg/L, which suggests an advancement of inhibition impact.





(a)





(b)

Fig.3.6.3: Nyquist (a) and Bode (b) plots for MS in 0.5 M H<sub>2</sub>SO<sub>4</sub> without and with various concentrations of *Syzygium aromaticum* extract at 298 K.

Table 3.6.4: EIS parameters for mild steel in 0.5 M H<sub>2</sub>SO<sub>4</sub> without and with different concentrations of *Syzygium aromaticum* extract.

Acid Solution	Concentration of inhibitor (mg/L)	$R_{ct}$ ( $\Omega$ cm <sup>2</sup> )	$CPE$ ( $\mu$ F cm <sup>-2</sup> )	Efficiency ( $\eta$ %)
0.5 M H <sub>2</sub> SO <sub>4</sub>	0	25.164	$1.3 \times 10^{-3}$	0
	100	90.86	$1.5 \times 10^{-4}$	72.30
	200	114.19	$1.4 \times 10^{-4}$	77.96
	300	155.49	$1.4 \times 10^{-4}$	83.63
	400	174.23	$1.4 \times 10^{-4}$	85.55
	500	237.73	$1.2 \times 10^{-4}$	89.41

### 3.6.5 FTIR analysis

The obtained FTIR spectra of *Syzygium aromaticum* extract is shown in Fig. 3.6.4. In the FTIR spectra the stretching vibration of O-H causes the peak focused at  $3406.40\text{ cm}^{-1}$  and the peak at  $1602.90\text{ cm}^{-1}$  is credited to the stretching vibration of C=O. The aromatic ring framework vibration results in some bands at  $1406.15\text{ cm}^{-1}$ . The outcomes from FTIR spectroscopy demonstrates that the corrosion inhibition property of *Syzygium aromaticum* is because of the presence of O atoms and aromatic rings in the compounds which exist in extract.

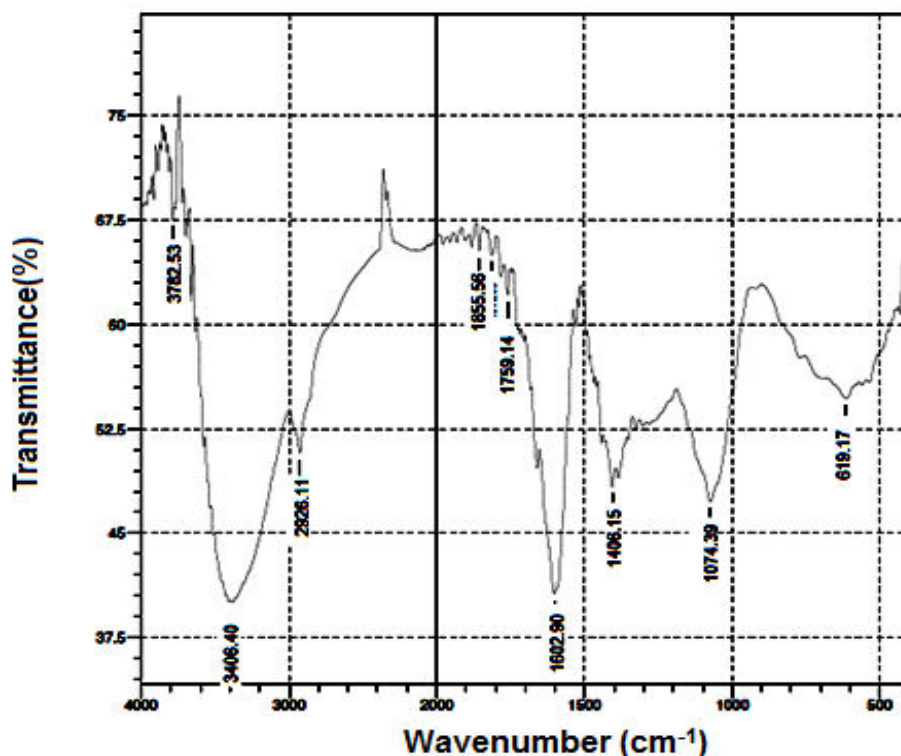


Fig.3.6.4: FTIR spectrum of *Syzygium aromaticum* extract.

### 3.6.6 UV-Visible spectroscopy

The UV spectra of *Syzygium aromaticum* extract before and after the corrosion test were contemplated and they have been appeared in Fig.3.6.5. The value of absorption maximum

( $\lambda_{max}$ ) or a change in the value of absorbance recommended the formation of a complex between the steel surface and inhibitor molecules.

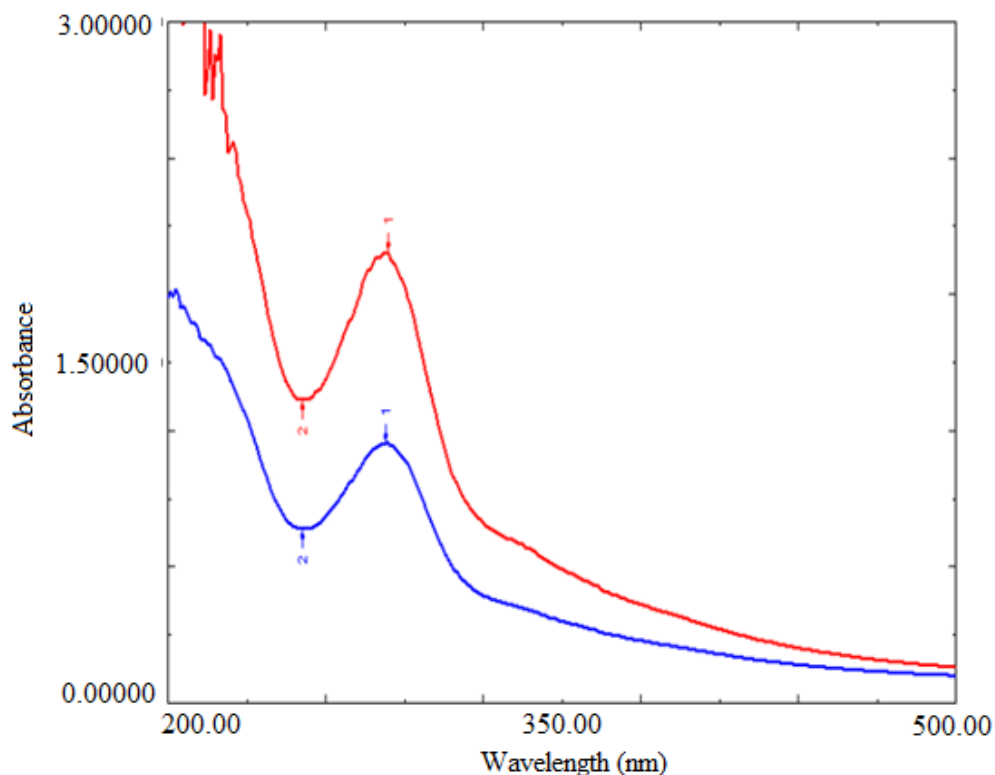


Fig.3.6.5: UV Spectra of *Syzygium aromaticum* extract before and after the corrosion test.

### 3.6.7 Surface studies

The SEM and AFM images of the mild steel immersed in 0.5 M H<sub>2</sub>SO<sub>4</sub> in the presence of *Syzygium aromaticum* extract are shown in Fig.3.6.6. These SEM and AFM micrographs were compared with the SEM and AFM images of the mild steel immersed in 0.5 M H<sub>2</sub>SO<sub>4</sub> without inhibitor. From the SEM image it is clear that the surface has astoundingly enhanced concerning its smoothness extensive lessening of corrosion rate. From AFM studies, the value of average surface roughness is 20.35 nm. The change in surface

morphology is because of the arrangement of a decent defensive film of inhibitor on mild steel surface which is in charge of corrosion inhibition.

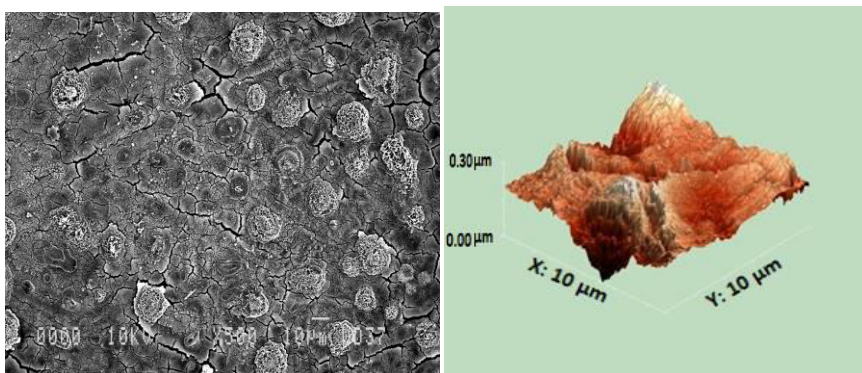
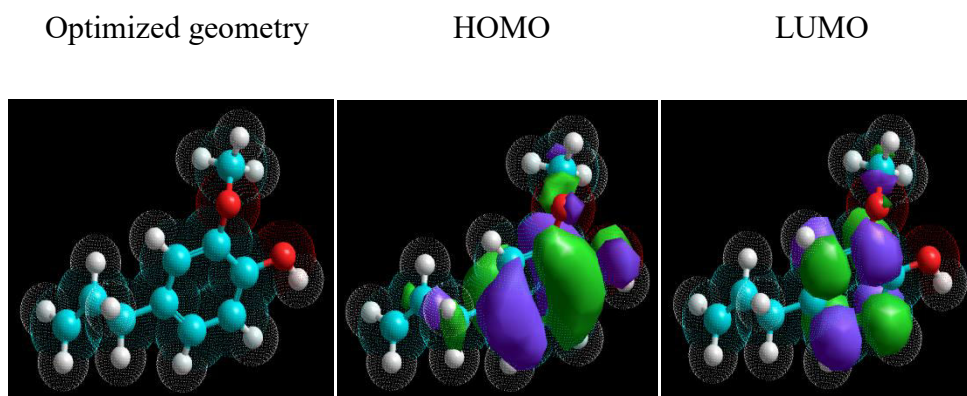


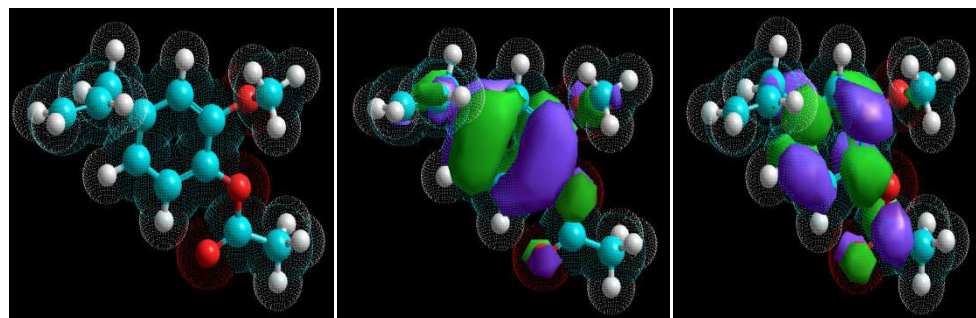
Fig.3.6.6: SEM and AFM images of mild steel immersed in 0.5 M H<sub>2</sub>SO<sub>4</sub> in the presence of *Syzygium aromaticum* extract.

### 3.6.8 Quantum chemical studies

The optimized structures of main constituents of *Syzygium aromaticum* extract are appeared in Fig. 3.6.7 and the corresponding quantum chemical parameters are reported in Table 3.6.5. The higher estimations of E<sub>HOMO</sub> and lower estimations of E<sub>LUMO</sub> recommend the power of inhibitor to get adsorbed on the mild steel surface.



(a)



(b)

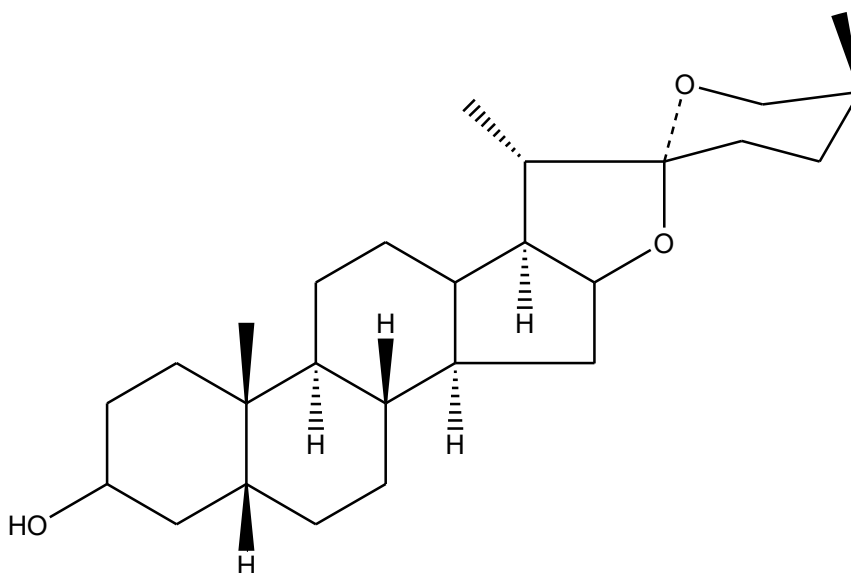
Fig.3.6.7: The optimized structure, HOMO and LUMO distribution for Eugenol (a) and Eugenol acetate (b).

Table 3.6.5: Quantum chemical parameters of Eugenol and Eugenol acetate calculated with DFT method.

Molecule	$E_{\text{HOMO}}$ (eV)	$E_{\text{LUMO}}$ (eV)	$\Delta E$ (eV)
Eugenol	-8.7320	-0.5329	8.1991
Eugenol acetate	-9.1590	0.0567	9.2157

### 3.7 *Asparagus racemosus* [J. Mater. Sci. 53 (2018) 8523-8535]

*Asparagus racemosus* is a species of Liliaceae family common throughout Nepal, Sri Lanka and India. It has been reported in literature that this plant contains Sarsasapogenin [11] which is shown in Fig. 3.7. The fruits of *Asparagus racemosus* were chosen to study its corrosion inhibition performance.



Sarsasapogenin

Fig. 3.7: Chemical structure of Sarsasapogenin.

#### 3.7.1 Weight loss studies

The corrosion inhibition efficiency ( $\eta$  %), corrosion rate (CR), surface coverage ( $\Theta$ ) at various concentrations (25-100 mg/L) of *Asparagus racemosus* extract as assessed by weight loss technique have been reported in Table 3.7.1. From Table 3.7.1, obviously increment in inhibition efficiency happens on expanding the inhibitor concentration. This is because when inhibitor adsorbs on the metal surface then a protective layer is formed on metal surface which reduces the corrosion reaction [2-3].

**Table 3.7.1:** The data of weight loss for mild steel in 0.5 M H<sub>2</sub>SO<sub>4</sub> without and with different concentrations of *Asparagus racemosus* extract.

Conc. mg/L	298 K			308 K			318 K		
	CR (mm/Y)	Θ	η%	CR (mm/ Y)	Θ	η%	CR (mm/ Y)	Θ	η%
0	26.11	-	-	41.46	-	-	62.88	-	-
25	8.39	0.6783	67.83	15.30	0.6308	63.08	25.97	0.5870	58.70
50	6.07	0.7678	76.78	12.52	0.6979	69.79	23.18	0.6312	63.12
75	4.59	0.8247	82.47	9.27	0.7762	77.62	18.55	0.7050	70.50
100	2.92	0.8885	88.85	6.95	0.8322	83.22	13.91	0.7787	77.87

### 3.7.2 Adsorption isotherm

The plots of  $C/\Theta$  vs.  $C$  for *Asparagus racemosus* extract as indicated by Langmuir adsorption isotherm equation as discussed in chapter 2 are appeared in Fig.3.7.1. The estimation of  $K_{ads}$  were computed from the intercept of Fig.3.7.1 and detailed in Table 3.7.2.



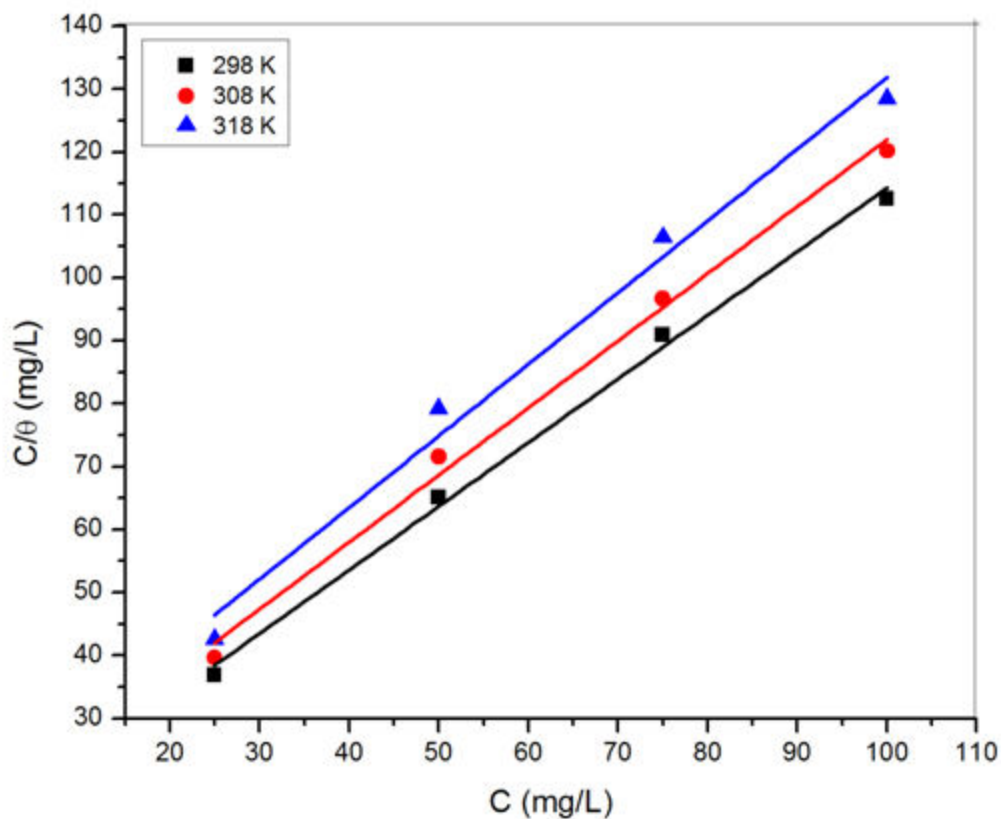


Fig.3.7.1: Langmuir adsorption isotherm for *Asparagus racemosus* extract on mild steel in 0.5 M H<sub>2</sub>SO<sub>4</sub>.

Table 3.7.2: Adsorption parameters for mild steel in 0.5 M H<sub>2</sub>SO<sub>4</sub> at optimum concentration of *Asparagus racemosus* inhibitor.

Temperature (K)	$K_{ads}$ (Lmg <sup>-1</sup> )	Slope	$R^2$
298	79.68	1.01	0.9947
308	49.59	1.06	0.9918
318	35.18	1.13	0.9801

### 3.7.3 Potentiodynamic polarization studies

Concentration impact of *Asparagus racemosus* extract on the polarization character of mild steel in 0.5 M H<sub>2</sub>SO<sub>4</sub> was analysed and the Tafel plots were recorded for various inhibitor concentrations which are appeared in Fig.3.7.2. The parameters, including corrosion potential ( $E_{\text{corr}}$ ), corrosion current density ( $I_{\text{corr}}$ ), anodic and cathodic Tafel slopes ( $\beta_a$  and  $\beta_c$ ) and inhibition efficiency ( $\eta$  %) ascertained by equation discussed in chapter 2, are reported in Table 3.7.3. It is clear that the maximum shift in the  $E_{\text{corr}}$  with respect to blank solution was 23 mV, which is within 85 mV, recommended that the contemplated inhibitor goes about as a mixed sort corrosion inhibitor [4-5].

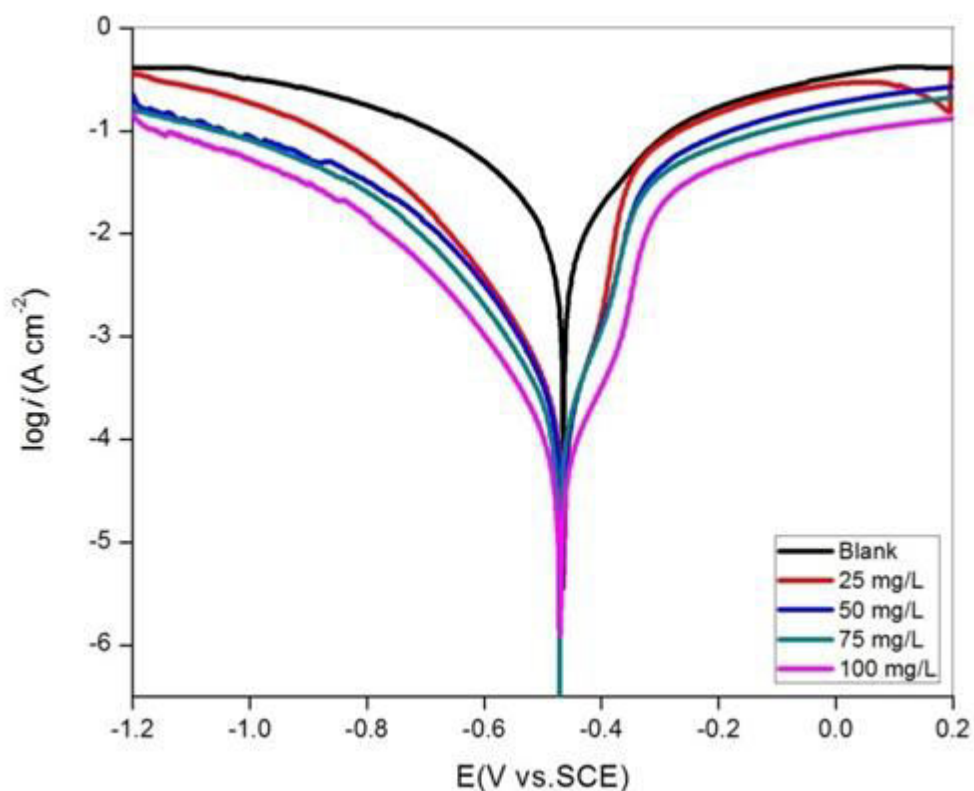


Fig.3.7.2: Tafel polarization curves for mild steel in 0.5 M H<sub>2</sub>SO<sub>4</sub> without and with different concentrations of *Asparagus racemosus* extract.

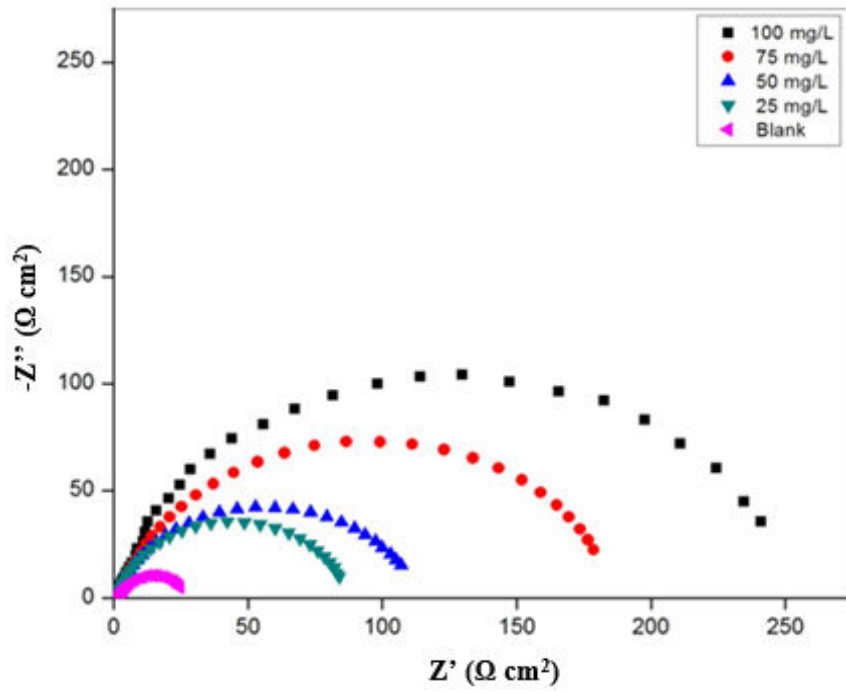
The relatively unaffected anodic and cathodic Tafel slopes when including *Asparagus racemosus* extract show that the anodic and cathodic reaction mechanisms are still controlled by charge transfer. It can be seen from Table 3.7.3 that with expanding concentration of *Asparagus racemosus* extract, the corrosion current density diminishes and the maximum inhibition effectiveness is accomplished at the concentration of 100 mg/L.

Table 3.7.3: Polarization parameters for mild steel in 0.5 M H<sub>2</sub>SO<sub>4</sub> without and with different concentrations of *Asparagus racemosus* extract.

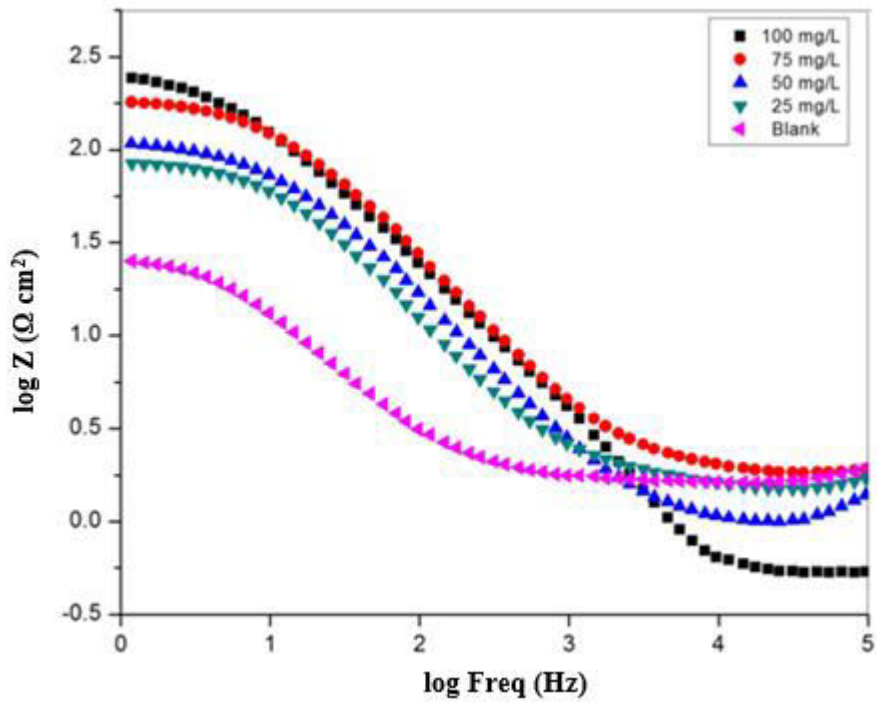
<b>Inhibitor concentration (mg/L)</b>	<b><math>E_{corr}</math> (V vs. SCE)</b>	<b><math>I_{corr}</math> (A cm<sup>-2</sup>)</b>	<b><math>\beta_a</math> (V/dec)</b>	<b><math>-\beta_c</math> (V/dec)</b>	<b>Efficiency (<math>\eta</math> %)</b>
0	-0.465	0.0008909	141.66	164.257	0
25	-0.466	0.0002371	46.72	110.75	73.38
50	-0.465	0.0001744	36.17	108.74	80.42
75	-0.488	0.0001219	43.52	119.65	86.31
100	-0.470	0.00006012	64.27	115.13	93.25

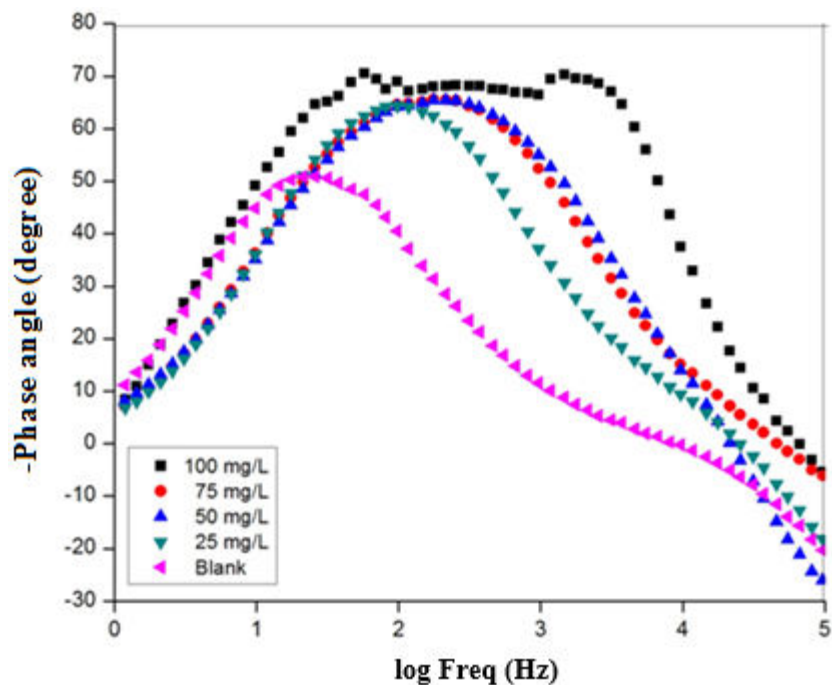
### 3.7.4 Electrochemical impedance spectroscopy (EIS) studies

The EIS parameters for mild steel in the absence and presence of various concentrations of *Asparagus racemosus* extract are appeared in Table 3.7.4 and the EIS curves (Nyquist and Bode plots) are shown in Fig.3.7.3. In Nyquist graph, due to the charge transfer resistance, a semicircle in each curve stands for a time constant. Expanding *Asparagus racemosus* extract concentration increases the diameter of semicircle from 25 mg/L to 100 mg/L, which suggests an advancement of inhibition impact.



(a)





(b)

Fig.3.7.3: Nyquist (a) and Bode (b) plots for MS in 0.5 M H<sub>2</sub>SO<sub>4</sub> without and with various concentrations of *Asparagus racemosus* extract at 298 K.

Table 3.7.4: EIS parameters for mild steel in 0.5 M H<sub>2</sub>SO<sub>4</sub> without and with different concentrations of *Asparagus racemosus* extract.

Acid Solution	Concentration of inhibitor (mg/L)	$R_{ct}$ ( $\Omega$ cm <sup>2</sup> )	$CPE$ ( $\mu$ F cm <sup>-2</sup> )	Efficiency ( $\eta$ %)
0.5 M H <sub>2</sub> SO <sub>4</sub>	0	25.16	$1.3 \times 10^{-3}$	0
	25	87.62	$1.9 \times 10^{-4}$	71.28
	50	119.16	$1.4 \times 10^{-4}$	78.88
	75	193.78	$1.0 \times 10^{-4}$	87.01
	100	266.64	$9.4 \times 10^{-5}$	90.56

### 3.7.5 FTIR analysis

The obtained FTIR spectra of *Asparagus racemosus* extract is shown in Fig. 3.7.4. In the FTIR spectra the stretching vibration of O-H causes the peak focused at  $3454\text{ cm}^{-1}$  and the peak at  $1012\text{ cm}^{-1}$  is credited to the stretching vibration of C-O. The outcomes from FTIR spectroscopy demonstrates that the corrosion inhibition property of *Asparagus racemosus* is because of the presence of O atoms and aromatic rings in the compounds which exist in extract.

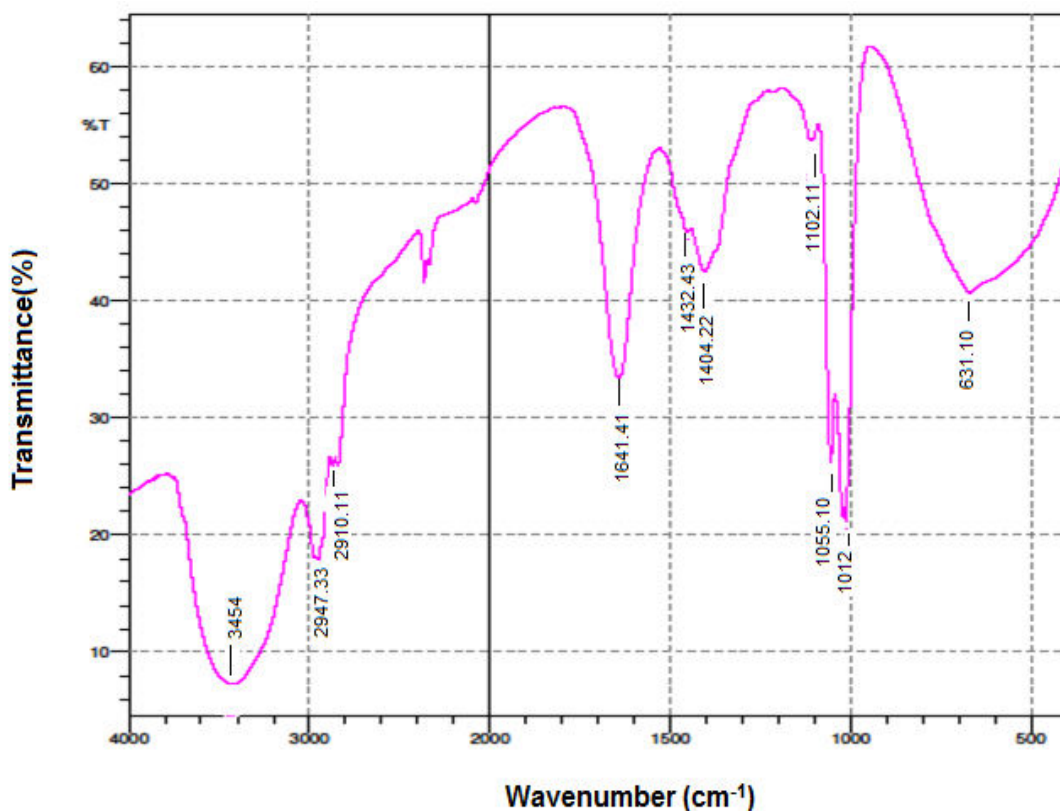


Fig.3.7.4: FTIR spectrum of *Asparagus racemosus* extract.

### 3.7.6 UV-Visible spectroscopy

The UV spectra of *Asparagus racemosus* extract before and after the corrosion test were contemplated and they have been appeared in Fig.3.7.5. The value of absorption maximum

( $\lambda_{max}$ ) or a change in the value of absorbance recommended the formation of a complex between the steel surface and inhibitor molecules.

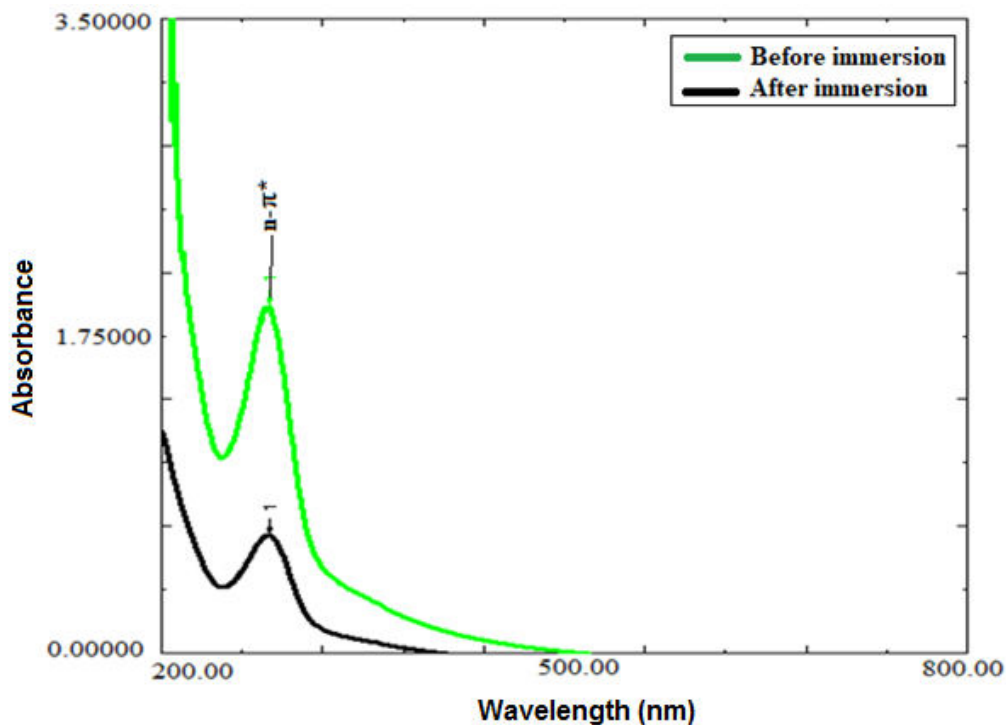


Fig.3.7.5: UV Spectra of *Asparagus racemosus* extract before and after the corrosion test.

### 3.7.7 Surface studies

The SEM and AFM images of the mild steel immersed in 0.5 M H<sub>2</sub>SO<sub>4</sub> in the presence of *Asparagus racemosus* extract are shown in Fig.3.7.6. These SEM and AFM micrographs were compared with the SEM and AFM images of the mild steel immersed in 0.5 M H<sub>2</sub>SO<sub>4</sub> without inhibitor. From the SEM image it is clear that the surface has astoundingly enhanced concerning its smoothness extensive lessening of corrosion rate. From AFM studies, the value of average surface roughness is 11.90 nm. The change in surface morphology is because of the arrangement of a decent defensive film of inhibitor on mild steel surface which is in charge of corrosion inhibition.

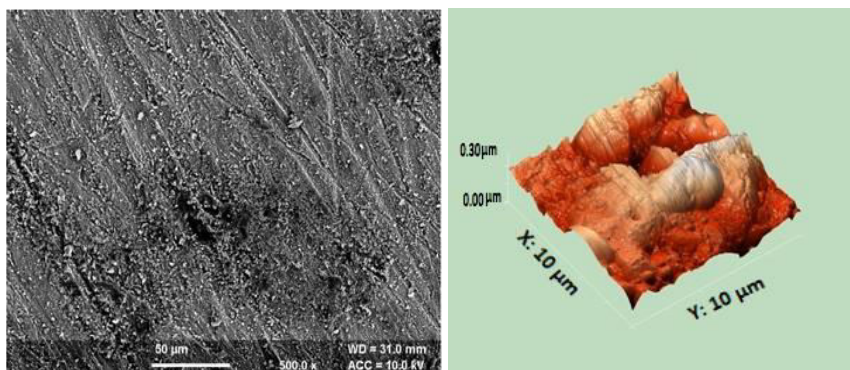


Fig.3.7.6: SEM and AFM images of mild steel immersed in 0.5 M H<sub>2</sub>SO<sub>4</sub> in the presence of *Asparagus racemosus* extract.

### 3.7.8 Quantum chemical studies

The optimized structures of main constituents of *Asparagus racemosus* extract are appeared in Fig. 3.7.7 and the corresponding quantum chemical parameters are reported in Table 3.7.5.

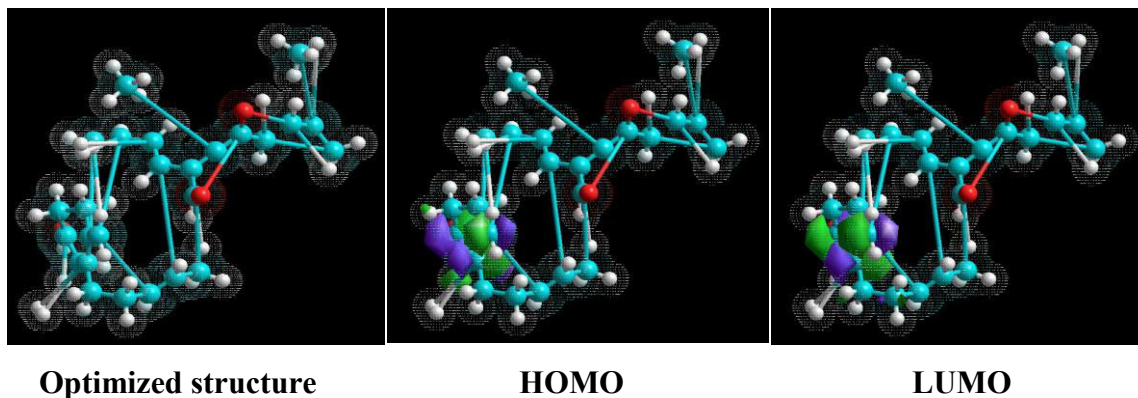


Fig.3.7.7: The optimized structure, HOMO and LUMO distribution for Sarsasapogenin

The higher estimations of  $E_{\text{HOMO}}$  and lower estimations of  $E_{\text{LUMO}}$  recommend the power of inhibitor to get adsorbed on the mild steel surface.



Table 3.7.5: Quantum chemical parameters of Sarsasapogenin calculated with DFT method.

<b>Molecule</b>	<b>E<sub>HOMO</sub> (eV)</b>	<b>E<sub>LUMO</sub> (eV)</b>	<b>ΔE (eV)</b>
<b>Sarsasapogenin</b>	-0.2487	-0.0297	0.2784

## References

1. S. Sasmal, S. Majumdar, M. Gupta, A. Mukherjee and P. Mukherjee, "Pharmacognostical, phytochemical and pharmacological evaluation for the antipyretic effect of the seeds of *Saraca ashoka* Roxb", *Asi. Pacif. J. Tro. Biomed.*, 2 (2012), 782-786.
2. A. Yurt, V. Butun and B. Duran, "Effect of the molecular weight and structure of some novel water-soluble triblock copolymers on the electrochemical behavior of mild steel", *Mater. Chem. Phys.*, 105 (2017) 114-121.
3. A. Khadraoui, A. Khelifa, M. Hadjmeliiani, R. Mehdaoui, K. Hachama, A. Tidu, Z. Azari, I. Obot and A. Zarrouk, "Extraction, characterization and anti-corrosion activity of *Mentha pulegium* oil: Weight loss, electrochemical, thermodynamic and surface studies", *J. Mol. Liq.*, 216 (2016) 724-731.
4. E. Ferreira, C. Giacomelli, F. Giacomelli and A. Spinelli, "Evaluation of the inhibitor effect of l-ascorbic acid on the corrosion of mild steel", *Mater chem. Phys.* 83 (2004) 129-134.
5. G. Ji, P. Dwivedi, S. Sundaram and R. Prakash, "Aqueous extract of *Argemone mexicana* roots for effective protection of mild steel in an HCl environment", *Res. Chem. Intermed.* 42 (2016) 439-459.
6. D. Pal, M. Mandal, D. Senthilkumar and A. Padhiari, "Antibacterial activity of *Cuscuta reflexa* stem and *Corchorus olitorius* seed", *Fitoter.* 77 (2006) 589-591.
7. H. Mukherjee, D. Ojha, P. Bag, H. Chandel, S. Bhattacharya, T. Chatterjee, P. Mukherjee, S. Chakraborti and D. Chattopadhyay, "Anti-herpes virus activities of *Achyranthes aspera*: an Indian ethnomedicine, and its triterpene acid", *Microbiol. Res.*, 168 (2013) 238-244.
8. A. Ahmad, A. Hussain, M. Mujeeb, S. Khan and A. Bhandari, "Quantification of total phenol, flavanoid content and pharmacognostical evaluation including HPTLC fingerprinting for the standardization of *Piper nigrum* Linn fruits", *Asi. Pacif. J. Tro. Biomed.*, 5 (2015), 101-107.

9. H. Asif, S. Sultana and Akhtar, "A panoramic view on phytochemical, nutritional, ethnobotanical uses and pharmacological values of *Trachyspermum ammi* Linn", *Asi. Pacif. J. Tro. Biomed.*, 4 (2014), S545-S553..
10. E. Arung, E. Mastubara, I. Kusuma, E. Sukaton, K. Shimizu and R. Kondo, "Inhibitory components from the buds of clove (*Syzygium aromaticum*) on melanin formation in B16 melanoma cells", *Fitoter.*, 82 (2011) 198-202.
11. D. Mandal, S. Banerjee, N. Mondal, A. Chakravarty and N. Sahu, "Steroidal saponins from the fruits of *Asparagus racemosus*", *Phytochem.*, 67 (2006) 1316-1321.

**Chapter 4**  
**Summary and Conclusions**

## **4.1 Summary and Conclusions**

### **4.1.1 Summary**

The present study aimed at investigation of corrosion restraint effectiveness of some inhibitors for mild steel in 0.5 M sulfuric acid solution.

In potentiodynamic polarization studies, a minor shift in  $E_{\text{corr}}$  values in presence of inhibitors as compared to absence of inhibitors suggests the mixed nature of all inhibitors. The polarization results showed that the current density decreased in the presence of inhibitors indicating that these inhibitors adsorbed on the metal surface and hence the inhibition efficiency increases with the increase in inhibitor concentrations.

In EIS study an increase in  $R_{\text{ct}}$  value is observed with increasing the inhibitors concentration, suggesting that the charge transfer process is retarded due to decrease in the uncovered surface available for corrosion reaction. The single peak obtained in Bode plots for inhibitors indicated that the electrochemical impedance measurements were fit well in one-time constant equivalent model with constant phase element (CPE).

FTIR spectral analysis showed the presence of hetero atoms in the extract. The SEM and AFM microphotographs show the badly damaged surface obtained when the metal was kept immersed in 0.5 M  $\text{H}_2\text{SO}_4$  solution without inhibitor indicated significant corrosion. However, in the presence of inhibitors the surface has remarkably improved with respect to its smoothness indicating considerable reduction of corrosion rate.

### **4.1.2 Conclusion**

The efficiency of all studied inhibitors at 100 mg/L inhibitor concentration is reported in Table 4.1.

Table 4.1: Efficiency of all the studied inhibitors at 100 mg/L inhibitor concentration.

S. No.	Inhibitor	Inhibitor concentration (mg/L)	Efficiency (%)
1.	<i>Saraca ashoka</i>	100	95.48
2.	<i>Cuscuta reflexa</i>	100	76.14
3.	<i>Achyranthes aspera</i>	100	72.71
4.	<i>Piper nigrum</i>	100	70.91
5.	<i>Trachyspermum ammi</i>	100	76.76
6.	<i>Syzygium aromaticum</i>	100	72.03
7.	<i>Asparagus racemosus</i>	100	93.25

- The percentage inhibition efficiency of all inhibitors expanded with expanded concentration.
- The results obtained from UV, FTIR, SEM and AFM showed adsorption of inhibitor molecules on the surface of mild steel.
- The theoretical parameters obtained by DFT calculations are in good agreement with the experimental results.

#### 4.2 Scope for future work

- The inhibitors studied here are good inhibitors for protection of the mild steel in 0.5 M sulfuric acid solution. They may be tried for other metals in acid solutions.
- The inhibitors may be applied for corrosion inhibition of other metals in various other media.

### List of Publications:

1. Use of *Saraca ashoka* extract as green corrosion inhibitor for mild steel in 0.5 M H<sub>2</sub>SO<sub>4</sub>, *J. Mol. Liq.*, 258 (2018) 89-97.
2. Investigation of Corrosion Inhibition Effect and adsorption Activities of *Cuscuta reflexa* extract as green corrosion inhibitor for mild steel in 0.5 M H<sub>2</sub>SO<sub>4</sub>, *Bioelectrochemistry*, 124 (2018) 156-164.
3. Investigation of Corrosion Inhibition Effect and adsorption Activities of *Achyranthes aspera* extract as green corrosion inhibitor for mild steel in 0.5 M H<sub>2</sub>SO<sub>4</sub>, *J. Fail Anal. and Preven.* <https://doi.org/10.1007/s11668-018-0491-8>.
4. Investigation of Corrosion inhibition effect and adsorption activities of *Syzygium aromaticum* extract for mild steel in 0.5 M H<sub>2</sub>SO<sub>4</sub>, *Surf. Reviews and Lett.*, <https://doi.org/10.1142/S0218625X18502001>.
5. Use of *Asparagus racemosus* extract as green corrosion inhibitor for mild steel in 0.5 M H<sub>2</sub>SO<sub>4</sub>, *J. Mater. Sci.*, <https://doi.org/10.1007/s10853-018-2123-9>.